Developing methods to image non-fluorescent anticancer cylinders in cancer cell lines

By

Zahra Khan

A thesis submitted to the University of Birmingham for the degree of DOCTOR OF PHILOSOPHY

Research and Training Centre in Physical Sciences for Health
School of Chemistry
University of Birmingham
June 2014

Abstract

In this thesis, biological and imaging studies have been carried out on a supramolecular helicate (iron cylinder) and indirect methods to image this non-fluorescent compound have been developed. The iron cylinder has been investigated as a quencher of nuclear Hoechst fluorescence in a range of cancer cell lines. Flow cytometry and epifluorescence data has shown quenching occurring in a concentration-dependent manner at both the population and cellular level. These results provide evidence for the cylinder being able to interact in close proximity to the DNA within 20 minutes of administration. Using luciferase-expressing breast cancer cells, the iron cylinder has been shown to directly affect light emission in a concentration-dependent manner, an inhibition that has not previously been investigated providing further opportunities for imaging by monitoring the inhibition of luminescent enzymes. Furthermore, iron cylinder has been shown to quench GFP fluorescence using fluorimetry and confocal microscopy providing novel possibilities supporting the imaging of non-fluorescent compounds indirectly through the use of fluorescent stains. This thesis has also pioneered the first *in vivo* research relating to the iron cylinder in the model organism, zebrafish, and findings indicate a large therapeutic window over which the cylinder can bring about its effects.

This thesis is dedicated to my mum for her constant support and unconditional love. I love you dearly.

First and foremost I offer my sincerest gratitude to my supervisors, Professor Michael John Hannon and Dr Nik Hodges, who have supported me throughout my phD with their patience and knowledge whilst allowing me the room to work in my own way. I attribute my degree to their encouragement and effort and without them this thesis, too, would not have been completed or written. One simply could not wish for better or friendlier supervisors. I would also like to thank Professor Ferenc Mueller and Dr Yavor Hadzhiev for the opportunity to collaborate with them.

A good support network is essential to complete a phD and I was fortunate to have the support of my colleagues in Biosciences, PSIBS and Chemistry. Many thanks to Farhat and Shrikant who have always guided me and provided excellent advice on lab related issues. I thank all the past and present members of the Hannon group for being extremely knowledgeable about everything, helpful, and friendly - best of luck to all.

Lorna is the most creative person I know and I admire her positive outlook on life. I'll always remember the crazy things we've done like the day we cancelled all our experiments to save the injured bird and our teddybear tea parties. I'll never forget the confused looks we got, they were priceless!

I must also express my thanks to Imran for all the silliness and childish fun we've had. Movie marathons, creating 'the clucky' and rainbow hunting are just some of those moments which allowed me to escape from the pressures of the 'real world' and for that I am truly grateful. I still get a laugh when I reminisce about the times we've shared.

Thank you to my friend Margaret who I met many years ago when I started my undergraduate degree in Biosciences. Despite the distance, we've remained close and I value our friendship. In recent times, her advice and her parents' prayers have given me and my family great strength.

These past several years have not been an easy ride, both academically and personally. I especially thank my mum for her support and encouragement. My hard-working mother has sacrificed her life for my sister and myself and provided unconditional love and care. I would not have made it this far without her and this achievement is hers as much as it is mine. For having faith in me and my intellect at times when I didn't have faith in myself. I thank her for inspiring confidence in me at every stage of my career. For her positive attitude and belief in silver linings which kept me afloat during my darkest times. She really is an extraordinary woman and words would not do justice to how much she means to me.

My sister, Sara, is the most beautiful and vivacious girl I know. She has been my rock throughout life. I love her dearly and thank her for all her advice and support. I was continually amazed by her patience during the ups and downs of my research but I always knew that I could count on her when times were rough. A vivid memory from my childhood is of Sara wrapping me in a blanket, holding my hand and telling me that everything would be ok. 25 years later and she's still that protective of her little sister. Whatever life throws at us, I know we'll be fine as long as we've got each other.

In recent times, I faced my hardest challenge when someone close to my heart was diagnosed with cancer. I was so used to dealing with cancer in a lab environment that I remained ignorant to the challenges faced by sufferers of this terrible disease. Within moments of receiving the diagnosis, every aspect of life from jobs and relationships to ambitions and dreams are shattered. Reassessing priorities is just one side that patients and their families have to deal with. The greater challenge is coping with surgery and the side/ after effects of chemo/ radiotherapy. Cancer sufferers are truly inspiring individuals and incredibly brave people. I can now fully appreciate the importance of furthering cancer research and I pray that all sufferers and their families remain strong during their darkest times.

Contents

List of Figures

CHAPTER 1

Introduction

1.1 DNA (Deoxyribonucleic Acid)

The self-assembled helical structure of DNA was proposed by James Watson and Francis Crick in 1953. DNA is composed of a string of nucleotides which in turn are made up of 3 subunits: a ribose sugar (deoxyribose for DNA or ribose for RNA), a nitrogen base and a phosphate group.[1] Two types of nitrogenous bases can be present in the DNA/RNA and these are purines and pyrimidines. Pyrimidines are single 6-membered rings and include uracil, cytosine and thymine while purines are composed of a fused 5 and 6-membered heterocyclic ring and include adenine and guanine. Thymine is present only in DNA, while uracil takes its place in RNA (Figure 1.1).[1]

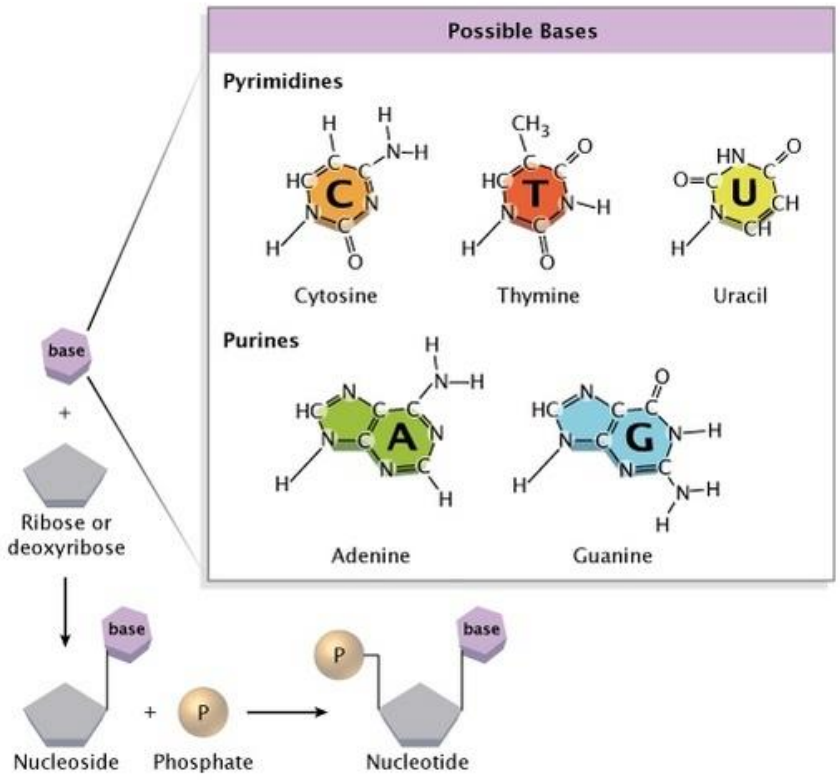

Figure 1.1. *The composition of a nucleotide: a sugar, a phosphate group and a nitrogenous base. Taken from ref 2.*

In the Watson-Crick B-DNA duplex, two sugar-phosphate backbones run in antiparallel directions with one going from 5’ to 3’ and the complementary strand running from 3’, to 5’. The strands twist together to form the double helical structure of the DNA molecule which is stabilized by hydrogen bonding occurring between bases. Two hydrogen bonds are formed between adenine which pairs with thymine and three form between cytosine which pairs with guanine (Figure 1.2). Further hydrogen bonding is possible from the exposed outer edges of the bases and proteins and other molecules important in DNA expression and replication can easily access the DNA via these hydrogen bonds.[3] The structure is further stabilized by π-stacking interactions with bases above and below in the helix, and interactions of the hydrophilic sugar-phosphate backbone of the polyanion with the solvent and counter cations such as Na^+, K^+, Mg^{2+}.

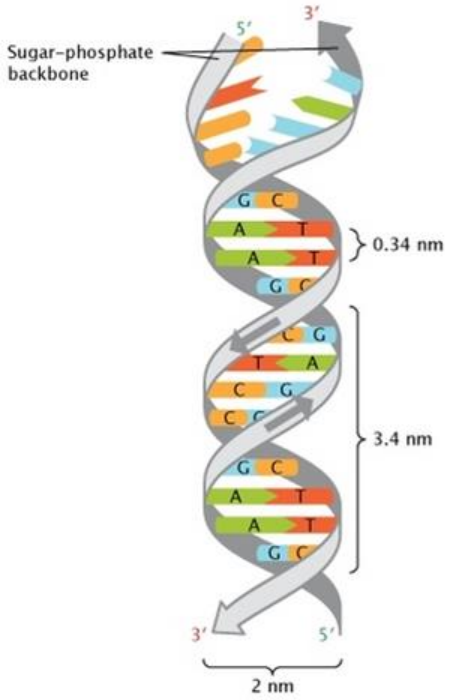

Figure 1.2. *The DNA double helix. Taken from ref 2.*

When the two strands of the DNA molecule twist together to form the helix, the exact dimensions and geometries can lead to different conformations. The most common form that occurs in living organisms is right-handed B-DNA in which the major groove of DNA is formed where the sugar-phosphate backbones are far apart on one side of the double helix and the minor groove forms where they are closer together.[2] Two other conformations known as A-DNA and Z-DNA also exist (Figure 1.3). The A-DNA occurs rarely in living organisms and is a shorter, wider form of DNA. When the first X-ray crystal structure of DNA was identified in 1979, it was seen in the left-handed Z-DNA conformation which is a transient form of the molecule later found to be stabilized by negative supercoiling.[2,4] Strong binding of specific proteins to the Z form of DNA have indicated it has a crucial role in protection against viruses.[2]

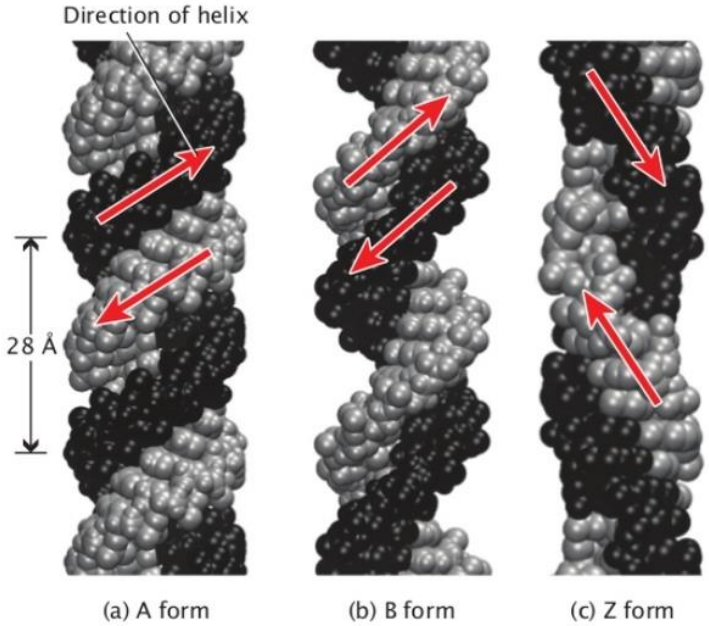

Figure 1.3. *A-DNA, B-DNA and Z-DNA conformations of the double-stranded helix. Taken from ref 2.*

Some unusual DNA structures such as G-quadruplexes are formed during biological processes including replication and transcription (Figure 1.4). These 4-stranded DNA structures are formed from hydrogen-bonded guanine bases in guanine-rich regions of DNA sequences. Repeated sequences of nucleotides known as telomeres cap the end of chromosomes protecting them from degradation. During replication of DNA, the strands of the double helix become shorter and upon telomere loss the cell undergoes death.[5] Maintenance of telomere length through overexpression of the telomerase enzyme leads to a continually replicating cell causing cancer. In the presence of cations, G-quadruplex structures may form in telomeric regions of DNA, thereby inhibiting the action of telomerase enzymes. Furthermore, the promoter region of the proto-oncogene, c-myc has been linked to many cancers. The presence of G-quadruplexes in these regions can prevent binding of proteins linked to cancer development.[6]

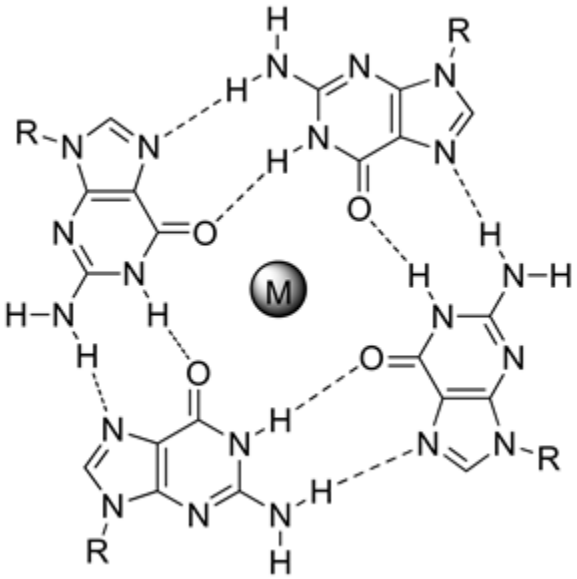

Figure 1.4. *Guanine base positions in a G-quadruplex with a centrally located cation. Hydrogen bonding is indicated by the dotted lines. Taken from ref 7.*

1.2 DNA-Binding Agents

The process of transcription is crucial for protein synthesis and in order to occur it requires numerous interactions between DNA and proteins. There has been much research focussed on identifying and developing small molecules that can inhibit this process and to understand the mechanism involved by which they interact with DNA. Covalent or non-covalent binding of small molecules to DNA helices can occur. A non-covalent interaction with the DNA molecule is often reversible whereas production of an adduct leading to a permanent alteration at the DNA site occurs as a result of covalent binding. There are 4 main types of non-covalent ligand interactions with DNA. These include electrostatic interactions with the sugar-phosphate backbone, intercalation, major groove interactions and minor groove interactions.[8]

Non-covalent intercalation is the process by which small molecules can insert between base pairs of DNA which lengthens the DNA and reduces the twist of the helix. This causes unwinding of the DNA which inhibits the enzyme topoisomerase that normally regulates DNA winding and unwinding. Replication and transcription are inhibited leading to cellular death.[9] Intercalators need to be at least partially planar and the interaction is often mediated by some additional hydrogen bonds.[10]

Due to poor specificity of most intercalators resulting in severe side effects, very few reach clinical drug status. However, new molecular structures are sometimes discovered which show a preference to specific sequences and these are very useful in the design of novel compounds.[10] One such example is that of the antimalarial drug, Cryptolepine

(Figure 1.5). This indoloquinoline alkaloid intercalates into DNA at guanine-cytosine rich sequences and cytosine-cytosine sites.[11] It is believed to interfere with the binding of the transcription factor, NF-KB to DNA and thereby inhibiting NF-KB mediated gene expression.[12]

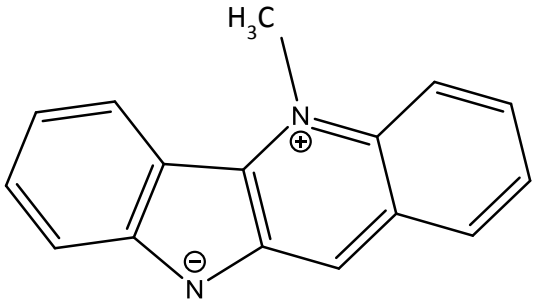

Figure 1.5. *The structure of the antimalarial drug, Cryptolepine.*

DNA minor groove binders have received much attention over the past years as opposed to major groove binders largely due to the discovery of natural small molecules.[8] Examples include distamycin and netropsin (Figure 1.6) which form hydrophobic interactions and hydrogen bonds with AT-rich areas in the minor groove of DNA. The readily used bisbenzimidazole Hoechst dyes (Figure 1.7) also bind to the minor grooves of DNA with specificity to AT regions causing the minor groove to become wider. In mammalian cells, Hoechst causes DNA strand breaks, induces protein- DNA crosslinking and arrest of the cell cycle in the G2 phase.[13]

A

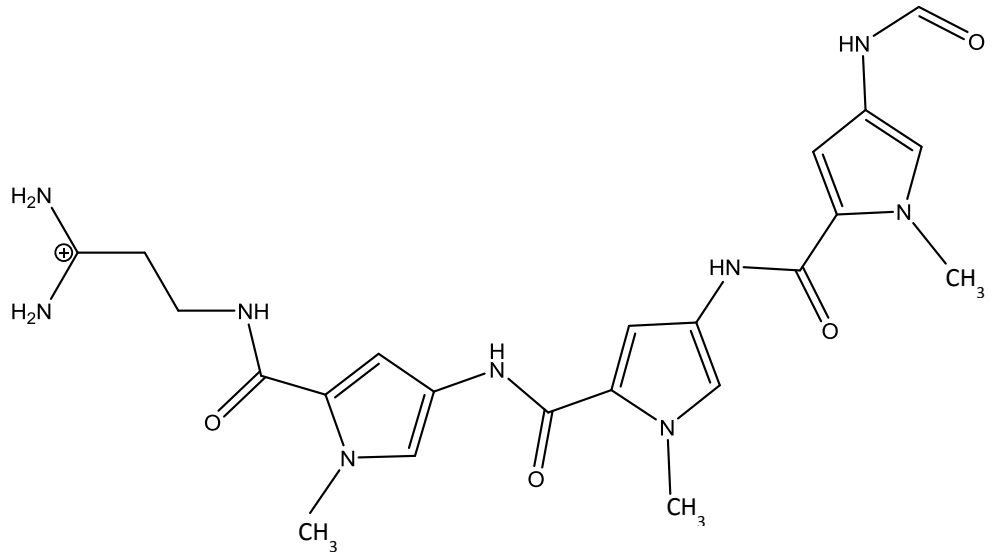

B

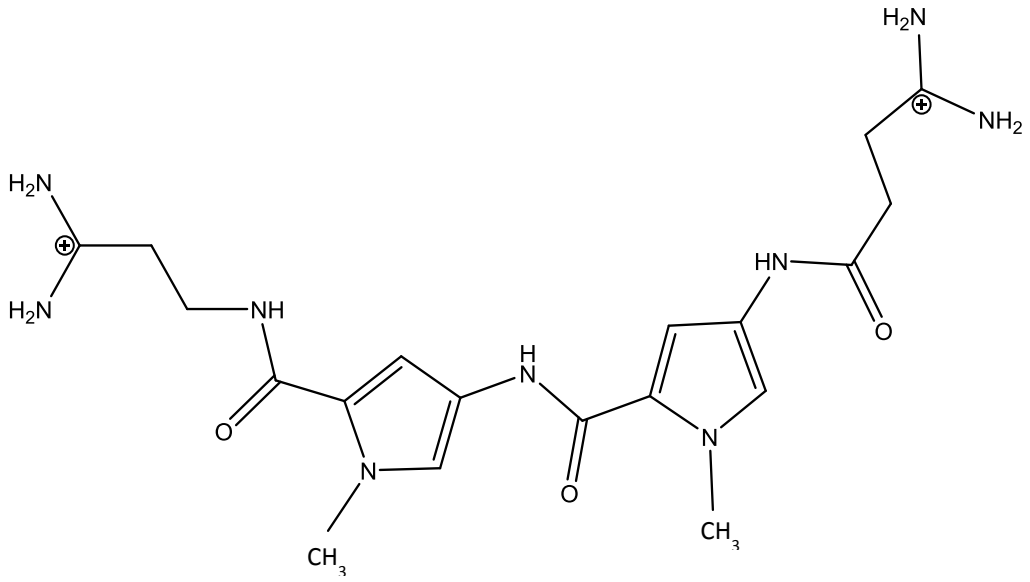

Figure 1.6. *The structure of* ***(A)*** *Distamycin and* ***(B)*** *Netropsin.*

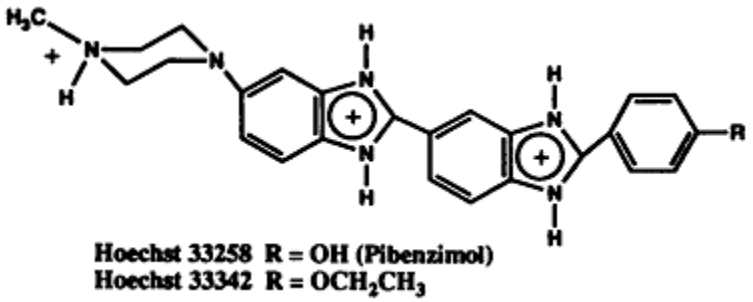

Figure 1.7. *The structure of Hoechst dyes. Taken from ref 13.*

The anti-tumor drug, azinomycin B (Figure 1.8) forms interstrand crosslinks with the DNA helix and transfers alkyl groups at guanine residues in duplex DNA. Bis-alkylation of N7 positions of guanine residues in the major groove are caused by 2 electrophilic sites on azinomycin B. Another anti-cancer drug, ditercalinium is a dimer which binds via the major groove through bis-intercalation between base pairs (Figure 1.9). This non-alkylating compound is derived from the natural product, ellipticine. Upon interaction, the DNA duplex becomes bent in the direction of the major groove and X-ray crystallography has identified widening of the major and minor groove in addition to unwinding of the DNA helix.[8]

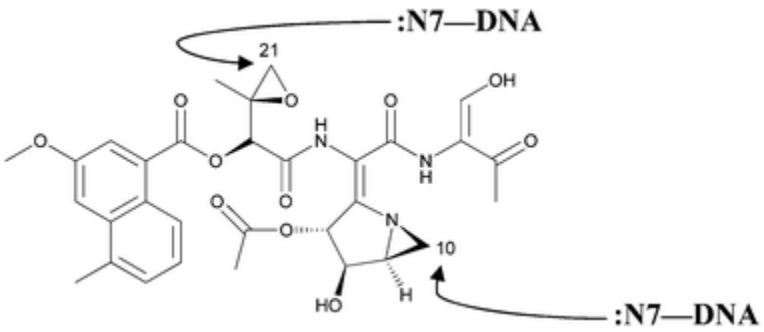

Figure 1.8. *Electrophilic sites of the major groove binder, Azinomycin B. Taken from ref 8.*

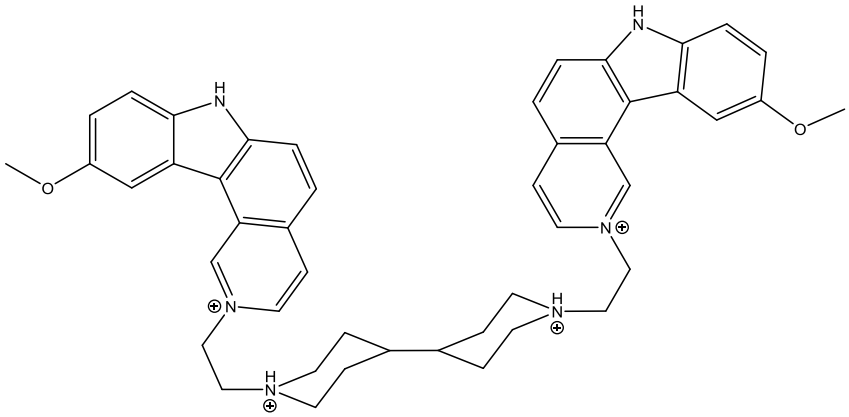

Figure 1.9. *The structure of Ditercalinium.*

With regards to DNA binding and targeting, much research has focussed on compounds that interact directly with the nitrogenous bases and recognize specific sequences. Despite this, other regions of the DNA molecule can be targeted to achieve stronger binding with more specificity. Researchers used a novel DNA ligand called TriplatinNC (a trinuclear platinum complex) (Figure 1.10) which did not bind to DNA grooves or intercalate with DNA but instead bound to phosphate oxygen atoms and associated with the sugar-phosphate backbone of DNA.[14] Here, 3 square [planar tetra-amine platinum (II)] coordination units are separated by a spacer of 8 carbons and interact with the phosphate oxygen atoms of DNA. This mode of binding was referred to as a phosphate clamp (Figure 1.11). TriplatinNC extended along the minor groove and the DNA bent towards the major groove by electrostatic forces involved.[14]

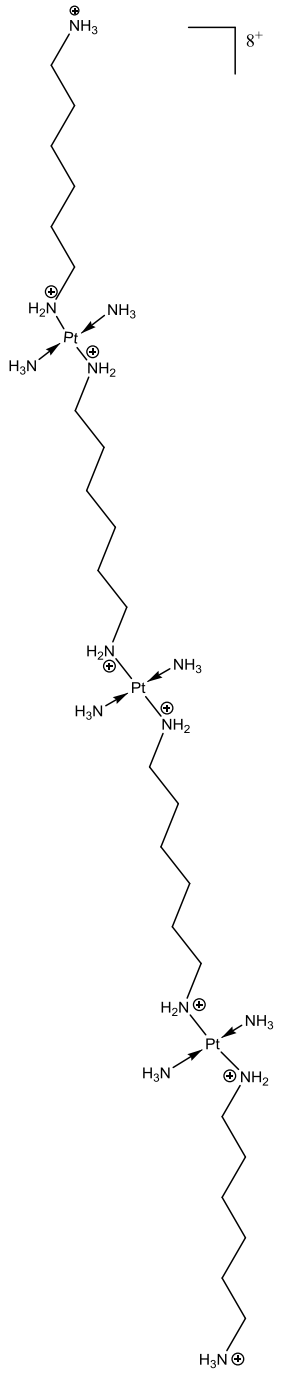

Figure 1.10. *The structure of TriplatinNC.*

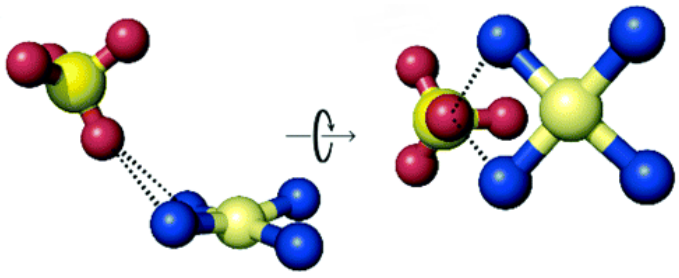

Figure 1.11. *A phosphate clamp representing a phosphate oxygen atom accepting 2 hydrogens from an amine group. Red: Oxygen. Blue: Nitrogen. Yellow: Phosphorous and White: Pt. Taken from ref 14.*

1.3 DNA Fluorescent Probes

Techniques including X-ray crystallography and nuclear magnetic resonance spectroscopy have provided information about the physical, chemical and structural properties of DNA. However, it is not possible to image in real-time using these methods and resolution is limited. Fluorescence provides a different way to study the structural and functional properties of DNA and allows real time measurements to be obtained. Spectroscopy allows cellular processes to be monitored at the DNA level using a fluorescent probe which is incorporated into a specific site of the molecule. As DNA is not naturally fluorescent, the fluorescent signal does not have to compete with any biological signal.[15] Many DNA fluorescent probes have been used in research to gain a better understanding of DNA binding and drug interactions.[15] Classic nucleic acid stains can be grouped by their interactions with DNA and include minor groove binders (Hoechst dyes and DAPI), intercalators (ethidium bromide and propidium iodide) as well as other stains such as acridine orange and hydroxystilbamidine.[16]

Studies on complexes between the fluorescent DNA probe, DAPI (Figure 1.12) and DNA have shown a range of interactions with differing strengths and specificities. The exact sequence of DNA with which DAPI interacts has a strong influence on the mode of DNA binding. Minor groove binding, major groove binding and intercalation have all been identified when different sequences of DNA have been used. The presence of 4 sequential AT/TA sequences are believed to be required for DAPI to bind in the minor groove of DNA. If the DNA sequence only consists of GC regions, DAPI is believed to intercalate between the base pairs.[17]

A recent study used the process of solvation (association of solvent molecules with solute ions) as a novel way of investigating binding of DAPI to 2 different DNA sequences. The sequence of oligomer 1 contained an AT rich region and oligomer 2 was made of only GC base pairs. Solvation relaxation times for DAPI bound to oligomer 1 were similar to the well-researched minor groove binder Hoechst 33258. Solvation did not occur with oligomer 2 within the time frame examined. This together with an extended lifetime of DAPI in complex and fluorescence quenching due to electron transfer from GC bases to DAPI correlates with the dye intercalating with DNA. This study provided evidence for two independent binding modes of DAPI with DNA by looking at the dynamics of the sequence-dependent complexes formed.[17]

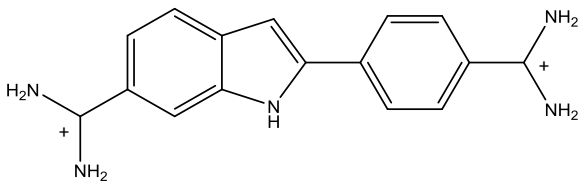

Figure 1.12. *The structure of DAPI.*

DNA detection methods often involve a fluorescent signal produced by the hybridization of a nucleic acid probe to a complementary sequence of single stranded DNA. TaqMan probes and molecular beacons are examples of these. Double stranded DNA sequences can also be detected using fluorescence methods and results can be more specific than those obtained from methods where all the DNA is denatured.[18] Recently duplex DNA was opened at a target site using a pair of peptide nucleic acid openers and thereby exposing one of the strands. As this DNA region was now single stranded, the sequence could be directly detected using a molecular beacon probe which hybridized to it leading to the production of a 'PD-loop' structure (Figure 1.13).[18]

High specificity is achieved as the PD loop structure requires independent recognition by the molecular beacon probe and two peptide nucleic acid openers. Once opened, a circular oligonucleotide probe was assembled onto the single stranded sequence which provided a template for rolling circle amplification (Figure 1.13). This resulted in the production of a long single stranded continuous DNA molecule containing multiple copies of the sequence complementary to the circular DNA. This approach was successfully used to identify marker sequences in plasmid DNA in the absence of false positives. Peptide nucleic acid openers can only act on homopurine sites and therefore only specific target sites can be detected using this method.[18]

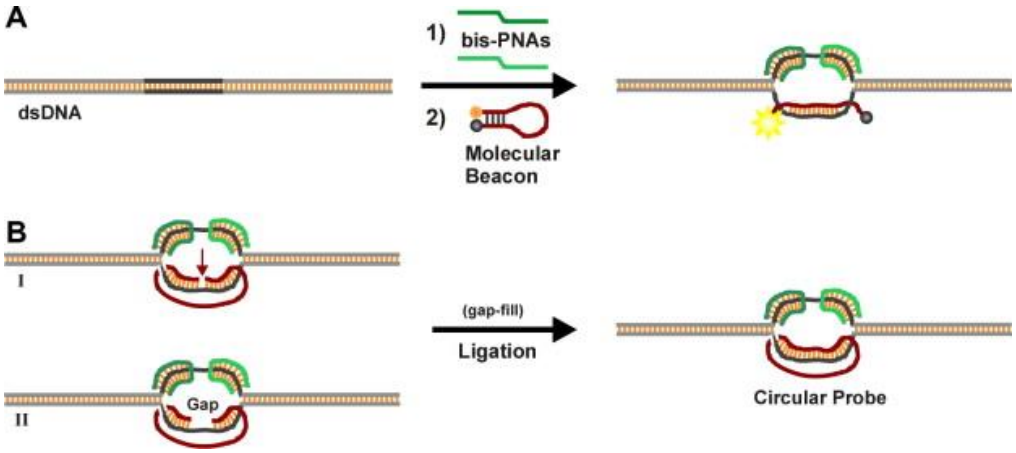

Figure 1.13. ***(A)*** *The structure of a PD loop formed at opening site of double-stranded DNA by a pair of peptide nucleic acid openers followed by hybridization with a molecular beacon probe.* ***(B)*** *Circular probe assembling at the opened target site. Taken from ref 18.*

Fluorescence and confocal laser scanning microscopy are routinely used to directly visualize nucleic acid staining and confocal offers several advantages when compared to conventional fluorescence microscopy including optical sectioning where focussed images from selected depths can be captured and 3D reconstructions can be acquired.[19] Two dyes readily used in immunofluorescence microscopy are rhodamine and fluorescein which emit red or green fluorescence respectively. As mentioned previously a range of dyes that recognise nucleic acids have been developed. One study compared the suitability of 5 such stains (TOTO-3, TO-PRO-3, YO-PRO-1, SYBR Green I and propidium iodide) for histochemical staining and visualization by confocal or fluorescence microscopy.[20]

As propidium iodide intercalates between bases, it stains RNA in addition to DNA and therefore cytoplasmic staining occurred in samples that received no RNAse treatment. Furthermore, tissues such as pancreatic samples with high levels of cytoplasmic RNA required further RNA digestion when propidium iodide was chosen as a nucleic acid stain. The SYBR Green I dye which binds preferentially to double stranded DNA strongly stained nuclei of cells examined and appeared as a bright green fluorescence. This was used successfully together with the red immunofluorescent stain, rhodamine and a clear contrast was achieved. SYBR Green I stained cells revealed very little staining of cytoplasmic RNA and therefore samples did not require RNAse treatment. Image capture with this dye had to be done quickly as the fluorescent signal was rapidly lost and this was noted as a disadvantage when using this dye for microscopy.[20] The membrane-impermeable carbocyanine dye, YO-PRO-1 also showed as a green fluorescence when bound to DNA. The signal faded less quickly than that seen for SYBR Green I stained cells but RNAse treatment was required as YO-PRO-1 had a higher affinity for RNA than SYBR Green I.[20]

Imaging the red and green nucleic acid stains (propidium iodide, SYBR Green I or YO-PRO-1) using fluorescence microscopy allowed only one fluorescent immunostain to be used in combination. Triple staining such as that achieved with two immunostains and a DNA stain was carried out using the two far-red fluorescent DNA dyes, TOTO-3 and TO-PRO-3. TOTO-3 staining of DNA was weaker than that observed for any other nucleic acid stain. Furthermore, RNA in the nucleus and cytoplasm were strongly stained when using this dye requiring RNA digestion of samples. Despite this, the fluorescent

signal produced by TOTO-3 was more stable than that produced by the other stains. Finally, TO-PRO-3 revealed strong, highly-specific DNA staining but the signal degraded rapidly and therefore images needed to be captured quickly.[20]

Research has also been carried out on fluorescent dyes that have the ability to distinguish between specific structural conformations of DNA. Double stranded DNA has been a popular target for many fluorescent probes with the majority of molecules intercalating between base pairs and therefore spanning the distance of a base pair. Quadruplexes are 4 stranded structures of DNA containing 4 grooves. Single stranded DNA can be distinguished from quadruplex structures using circular dichroism by measuring the difference between absorption of left and right-handed circularly polarized light.[21] Raman spectroscopy which relies on the scattering of light has also been used to look at quadruplex DNA specifically.[21]

A study recently investigated molecules spanning 4 bases as specific binders of quadruplex DNA.[21] Previously, it had been shown that nucleic acid aptamers containing sequences that could form quadruplexes, bound to porphyrins with high specificity.[22] Therefore, porphyrins binding specifically to quadruplexes were investigated in a mixture containing other DNA structures including single and double stranded DNA. The 2 specific porphyrins investigated were T4 and NMM (Figure 1.14).[21] It was previously shown that some porphyrins could bind to double stranded structures but do so in between bases on the same DNA strand as opposed to intercalating between base pairs of both strands of the helix.[23]

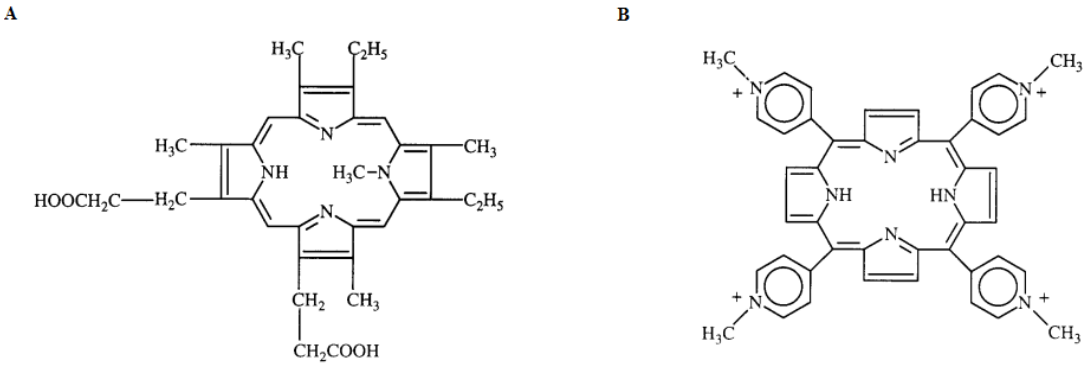

Figure 1.14. *The structure of porphyrins:* ***(A)*** *NMM and* ***(B)*** *T4. Taken from ref 21.*

2 kinds of quadruplex DNA (a 12mer basket form and a 15mer chair form) were used and the binding of the porphyrins to these structures was compared to that with duplex DNA (Figure 1.15). A substantial increase in fluorescence was observed for NMM in the presence of both types of quadruplexes and no fluorescence increase was seen with calf thymus duplex DNA. A slight increase in T4 fluorescence occurred in the presence of duplex DNA and no increase was observed in the presence of the 12mer DNA. However, a significant enhancement in T4 fluorescence was seen with the 15mer DNA. These results showed that all quadruplex structures caused a substantial increase in the fluorescence of NMM but duplex structures were not able to do this. Duplex DNA was able to increase fluorescence of T4 to a greater extent than basket form quadruplexes and chair type quadruplexes significantly enhanced T4 fluorescence. In their free states, neither T4, nor NMM showed high fluorescence.[21]

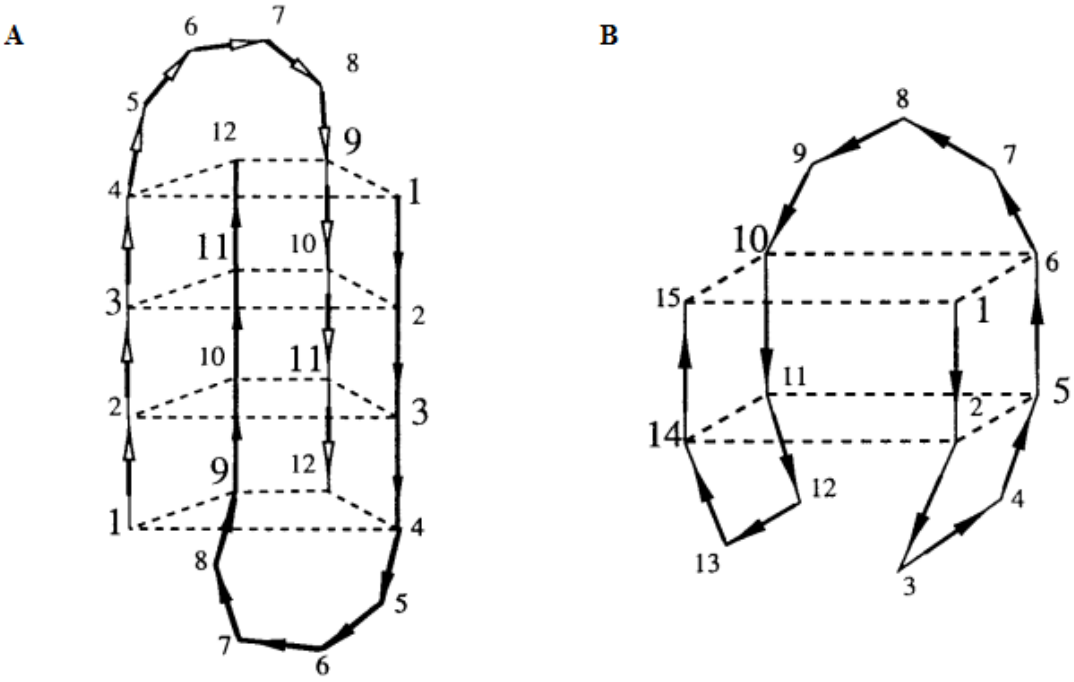

Figure 1.15. *Quadruplex types:* ***(A)*** *Basket type DNA formed by 12mer d(GGGGTTTTGGGG).* ***(B)*** *Chair type formed by 15mer d(GGTTGGTGTGGTTGG). Taken from ref 21.*

Results from this study showed that fluorescent porphyrin probes could be used to screen for quadruplex DNA in a mixture containing other structures. Despite not having absolute specificity, the dyes did show high specificity. By using both T4 and NMM, the presence and estimated percentage of quadruplex DNA in a mixture could be determined. These dyes can further be used to monitor how quickly quadruplexes may form as a result of specific influences. Furthermore, studying the displacement of dye from DNA can provide further insight into the dynamics of protein-quadruplex complexes. Other interesting observations were made during the course of this study including a drastic increase seen in the fluorescence of T4 in the presence of potassium.[21]

1.4 DNA as a Target for Anticancer Compounds

Nucleic acids are crucial to the processes of DNA replication and protein synthesis (transcription and translation) which occur in both healthy and cancerous cells. DNA has long been a target of anti-cancer drugs with some directly interacting with it and others inhibiting the enzymes responsible for its structure and processing. Topoisomerase inhibitors including doxorubicin and etoposides, alkylating agents such as nitrogen mustard, antimetabolites including the folic acid antagonist, methotrexate and covalent modifiers of DNA such as platinum compounds all cause non-specific damage and are used extensively as effective anticancer drugs. Furthermore, DNA is also the major target for γ-irradiation.[24]

DNA is believed to be the central unit responsible for driving tumour development and growth. There are a number of reasons as to why it is chosen as a primary target when developing novel chemotherapeutics. It is the material which is damaged in cancer cells through the process of genetic mutations as well as variations occurring in the length of its cycle when compared with healthy cells. In addition, due to increased DNA replication and errors in cell cycle control/ DNA repair processes, cancer cells are more likely to obtain extra DNA damage than normal cells making DNA an ideal target for cancer treatment.[24]

Despite being an ideal target for cancer drugs, there are several concerns when targeting DNA. In addition to severe side effects of treatment and development of secondary tumours, treatment does not provide a cure for the disease. The majority of treatment

available causes intense damage to DNA and so reducing this would decrease side effects as well as increasing the chances of achieving a curable situation. If drugs available were more specific in their interaction with DNA, the large number of mutations produced would be minimized. Therefore, much novel research is trying to develop strategies to alter the mechanism by which DNA is targeted by anticancer treatment.[24]

Quinacrine (Figure 1.16) was first discovered in the 1920s as an antimalarial drug. Later, its anti-inflammatory activity was noted and used in the treatment of autoimmune conditions including systemic lupus erythematosus. Recently quinacrine was tested for its anticancer activity by P53 activation. P53 is a tumour suppressor gene which stops the cell cycle to allow repair of damaged DNA or induces apoptotic pathways if the damage is beyond repair. Quinacrine was found to induce P53 activation and also activated P53-dependent genes downstream. Furthermore, it showed greater toxicity to tumour cells than healthy cells.[24]

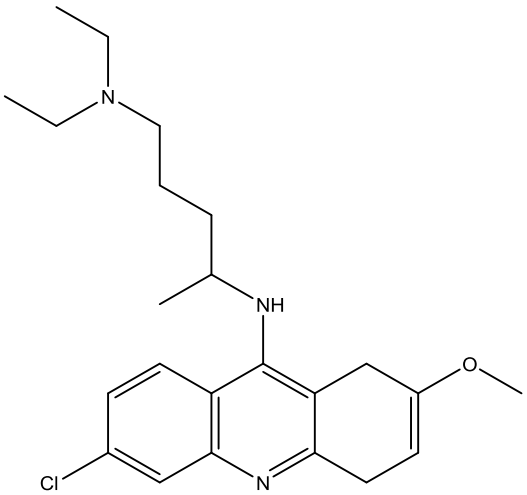

Figure 1.16. *The structure of Quinacrine.*

Previously, quinacrine had been classed as a DNA-damaging agent known to intercalate with DNA. However, this particular study found no evidence of quinacrine-induced DNA damage in mammalian cells. A number of assays were used to confirm this including the bacterial mutagenicity, ames test and the comet assay which showed no difference in number of strand breaks as a result of treatment when compared to the control. In addition, no H2AX histone phosphorylation occurred and no activation of the serine/threonine kinase, ATM occurred which would normally happen in response to DNA strand breaks. Furthermore, quinacrine offered protection from toxicity caused by the DNA-damaging agents, bleomycin and doxorubicin in eukaryotic cells. *In vivo* studies also supported these findings where quinacrine did not promote tumour growth in P53 deficient mice which normally show high levels of radiation induced tumour development. These findings highlight the fact that the cytotoxicity of a compound that binds to DNA is not always a result of genotoxic effects or DNA damage. The mechanism by which quinacrine has these anticancer activities was further investigated.[24]

Quinacrine has been found to interact with both nucleic acids and phospholipid bilayers. Methods including calorimetry, structural studies and FRET (fluorescence resonance energy transfer) have been used to study its intercalation with DNA. Quinacrine increases the length of DNA and keeps the helical structure stable thereby preventing temperature-induced strand separation. During DNA replication, frame shift mutations can occur in the pre-disposed intercalator-DNA complex. However, as quinacrine inhibits the DNA polymerase I enzyme and therefore replication, this mutagenicity does not occur in quinacrine-treated mammalian cells.[24]

In addition to the planar tricyclic structure which intercalates with DNA, quinacrine also has a tail structure which is believed to protrude into the minor groove further strengthening its binding to DNA. High specificity for AT-rich regions is seen when quinacrine interacts with DNA which is similar to the HMG (high mobility group) group of proteins that bend DNA. 2 enantiomers of quinacrine leads to 2 alternative positions for the 'tail' part of the molecule in the minor groove. The R-enantiomer which is directed along the minor groove fits better and shows stronger activation of P53 and inhibition of NF-KB (transcriptional activator) than the S-enantiomer which is positioned in the opposing direction to the groove. Furthermore, a higher affinity for DNA binding has been found with the R-enantiomer. Using the evidence obtained, researchers proposed a mechanism by which quinacrine effectively kills tumour cells.[24]

This mechanism involves initial intercalation of the drug with its 'tail' binding to AT-rich sequences in the minor groove. The binding results in reduced movement of the DNA molecule and interferes with HMG protein function. This leads to inhibition of transcription factors that require certain DNA conformations to bind and specific contact with the HMG proteins. These include HSF1 and NF-KB which are important factors in tumour cell growth and development. The FACT (facilitates chromatin transcription) protein complex also recognizes the quinacrine-DNA complex and causes P53 activation. Specificity of quinacrine for cancer cells may be due to the fact that many of the transcriptional pathways involved are not required by healthy tissues. Quinacrine offers a very promising mechanism for effective anticancer treatment.[24]

Another potent anticancer drug, ellipticine (Figure 1.17) was recently investigated in terms of its binding and interaction with DNA.[25] Earlier studies using X-ray crystallography showed ellipticine complexed with a self-complementary ribodinucleoside monophosphate.[25] The interaction appeared similar to that of cryptolepine showing intercalation parallel to the hydrogen bonds of base pairs with the aromatic rings stacking into the bases. However, in this study, oligonucleotides of very short lengths were used and therefore, the structure's true representation of the mode by which ellipticine binds DNA was debated.[25]

This study concluded that the intercalation caused DNA unwinding and lengthening to occur. With ellipticine bound in complex, the DNA conformation is in the B-form. Despite this, to accommodate the intercalation of ellipticine, the DNA helix twists slightly at the two sites by 21^{o}. The sugar phosphate backbone of DNA becomes distorted to open the bases at both sites by around 7 Å. This study suggested that derivatives of ellipticine with similar structures would bind in the same way to form complexes with DNA. However, further structural research into such interactions would be necessary to confirm this.[25]

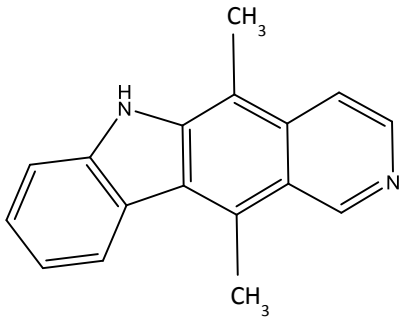

Figure 1.17. *The structure of Ellipticine.*

1.5 Cisplatin

The anticancer properties of cisplatin were identified by serendipity in the late 1960s when the microbiologist, Barnett Rosenberg was investigating the effects of electric fields on bacterial cell division.[26] Cisplatin was produced electrochemically by cell culture media components and the platinum electrodes where it was found to inhibit *E.coli* growth.[27] In 1969, the discovery was made that cisplatin had the ability to completely stop growth of solid sarcomas and this was published in *Nature*.[26] Following clinical studies, in 1978 the FDA granted approval for this drug to be used in clinic and currently it is the most commonly used anticancer agent in the world.[28] The structure of cisplatin contains a platinum ion surrounded by the four ligands, two chlorides and two amines.[29] This drug provides a good example of the drastic changes in biological activity that can occur when minor alterations are made in molecular structure. With the chlorides and the amines arranged consecutively (as shown in Figure 1.18), cisplatin functions as an anticancer agent. However, if the chlorides are arranged diagonally, separated by the amines, the compound has no biological activity.[29]

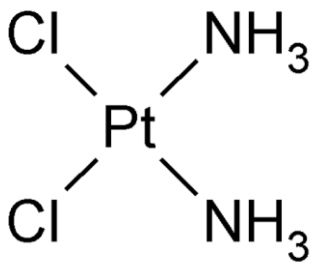

Figure 1.18. *The structure of Cisplatin.*

Cisplatin is believed to exert its anticancer effects and induce programmed cell death (apoptosis) through its interactions with DNA.[29,30] When administered, cisplatin enters the bloodstream and encounters a high plasma chloride concentration. This prevents the process of aquation whereby the chloride ligands become replaced by water molecules. Despite this, proteins such as glutathione and albumin, especially those containing thiol groups target cisplatin, binding to it, causing chloride displacement and inhibiting its action.[30] Cisplatin diffuses across the plasma membrane of cancer cells where the chloride concentration is low. Therefore, a chloride ligand becomes replaced by water and the resulting positively charged molecule is not able to exit the cell.[29]

The interaction between cisplatin and DNA has been extensively studied. The N7 atoms of the purines of DNA base pairs coordinate to cisplatin as they do not form hydrogen bonds with any other bases (Figure 1.19). A number of different adducts may be formed with 1,2-intrastrands being the most common. These adducts form when cisplatin's two chlorine ligands become replaced by nitrogen atoms of purines on adjacent bases from the same DNA strand. Two guanines are the most commonly involved in the formation of these adducts. Alternatively, adducts involving one guanine and one adenine are formed (Figure 1.20).[31] Base destacking is associated with the GG or GA binding and leads to significant distortion of the DNA and this distortion is recognized by DNA- binding proteins. Cell cycle arrest and DNA repair mechanisms are triggered by the damage caused to the DNA and if the repair is not successful, apoptosis is triggered leading to cell removal.[32]

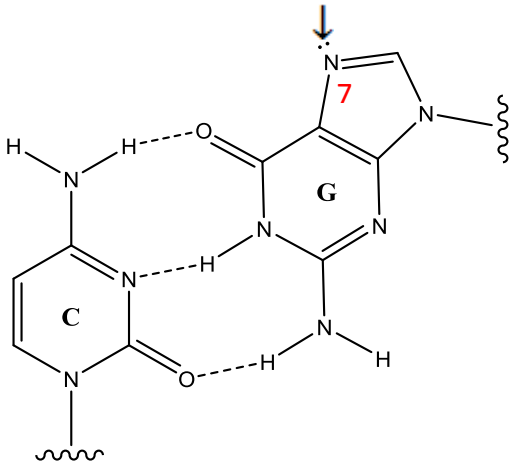

Figure 1.19. *N7 position of Guanine.*

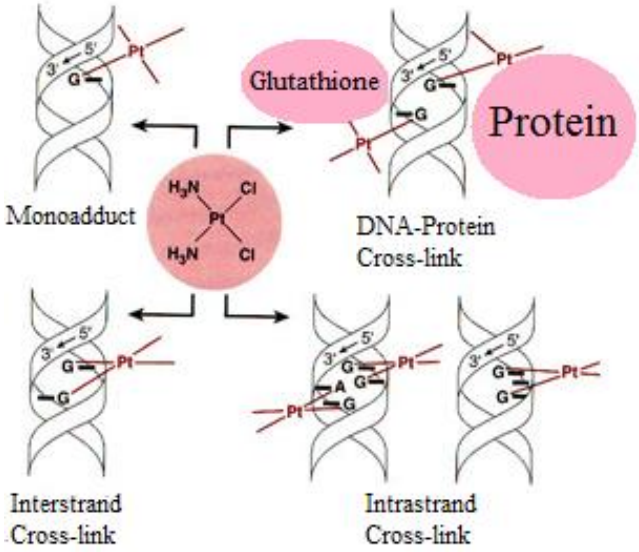

Figure 1.20. *Crosslinking of cisplatin to form adducts. Taken from ref 31.*

Cisplatin is successfully used to treat many solid tumours including, bladder, testicular, lung and head and neck cancers.[33, 34] It has been found to be particularly active against testicular cancer and a cure rate of almost 100 % is reached if tumours are detected early.[35] For non-small-cell lung carcinoma and melanoma, cisplatin is one of the most

effective drugs used. Furthermore, when used in combination with other drugs, it is very active against ovarian cancer.[26] Despite the therapeutic success of this platinum compound, many patients in clinic have shown intrinsic resistance to platinum-based therapies.[35] In addition, a significant proportion of cisplatin- sensitive tumours gradually develop a resistance to the drug which is especially common in ovarian cancers.[36] Despite the initial 70 % curable success rate when using cisplatin to treat ovarian cancer, this is reduced to 15–20% within five years as the tumour becomes resistant.[37]

Cisplatin-induced interstrand crosslinks (ICLs) block transcription and replication in cells by preventing the DNA strands from separating. Fanconi anaemia has provided a greater understanding into the processes by which these lesions are repaired as cells taken from patients with this genetic condition show high sensitivity to interstrand crosslinks.[38] Activation of the Fanconi anaemia pathway is crucial in the repair process and involves identification of a stalled replication fork, removal of the lesion, homologous recombination and nucleotide excision repair.[39]

Cisplatin resistance may occur through a variety of cellular events, including TLS (translational DNA synthesis). 4 TLS polymerases exist in humans (Polκ, Polȷ, Polη and Rev1) each with its own bypass for DNA damage and specific profile.[28] Polη and Pol ζ (a member of the B-family of polymerases) are specialized polymerases which are able to replicate through the 1,2 intrastrand crosslink formed by cisplatin-DNA adducts.[40] The process by which these two cause cisplatin resistance involves Polη inserting a cytosine base opposite the lesion site and Pol ζ then extending the structure fully bypassing the

lesion.[40] Human Polη is potentially a very useful target for cancer treatment as it can replicate from a cisplatin-DNA adduct. Researchers are working to find specific inhibitors for this polymerase and as the cleft at its active site is more open than that of the other polymerases, it may be possible to identify small molecule inhibitors of Polη.[28]

In addition to drug resistance, cisplatin's use is strictly limited due to its severe side effects. These include nephrotoxicity, peripheral neurotoxicity, cardiotoxicity and myelosupression.[41] Cisplatin-associated nephrotoxicity is believed to be caused by renal excretion of the drug. The terminal proximal tubule and distal nephron of the kidney accumulate a high concentration of cisplatin which induces necrotic or apoptotic cell death. Short exposures to the drug tend to cause necrosis with prolonged exposures leading to apoptosis.[27] Ototoxicity is especially common in pediatric patients receiving cisplatin which causes damage to the cochlea's outer hair cell reducing their function. The resulting production of reactive oxygen species and apoptosis activation in the inner ear is believed to be caused by induction of NOX3, a NADPH oxidase which resides in the cochlea. Increased production of the superoxide radical occurred when nox3 – transfected kidney cells were treated with cisplatin. This is believed to cause ototoxicity when converted into hydrogen peroxide and the hydroxyl radical by enzymes present in the cells.[27] When administered to patients, this drug has also been shown to cause a decrease in plasma antioxidant concentrations which can decrease the effectiveness of defence mechanisms against genotoxicity.[42] As cisplatin is not specific in its action, genetic damage can result in unaffected tissues leading to accumulation of mutations and secondary tumors several years after cessation of treatment.[43]

As with other drugs, cisplatin also has a family of related second and third generation compounds. Carboplatin which has been successfully used to treat ovarian cancer, is less toxic than cisplatin but still has high efficacy. Oxaliplatin is used for colorectal cancer in combination with other drugs and is effective for certain tumours that have developed resistance to cisplatin treatment (Figure 1.21).[26] The drawbacks associated with cisplatin have prompted research into modifying the strategy used to target DNA to develop novel metal drugs focussing on alternative metals and new modes of interaction.[44] As mentioned previously, developing drugs which bind to DNA but do not damage it, will prevent undesirable side effects such as those associated with cisplatin treatment.[24]

A

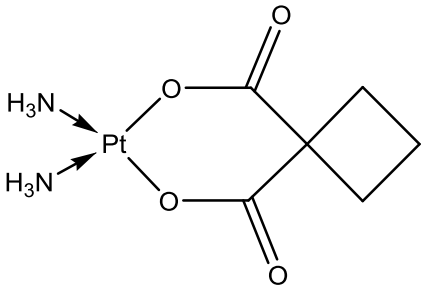

B

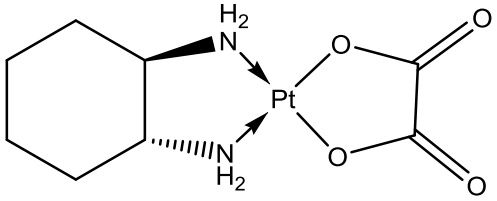

Figure 1.21. *The structures of Carboplatin* ***(A)*** *and Oxaliplatin* ***(B)****.*

1.6 Supramolecular Chemistry

Supramolecular chemistry is concerned with chemical systems consisting of assembled molecular subunits and explores larger structures containing weak and reversible noncovalent interactions between molecules.[45] Examples of such interactions include: hydrogen bonds, hydrophobic forces, van der Waals forces and metal coordination.[46] Supramolecular chemistry is important in the understanding of molecular recognition and self-assembly, host-guest chemistry and mechanically-interlocked molecular architectures.[47] As many biological interactions including those between the two strands of the DNA helix depend on these processes, research into noncovalent interactions is necessary to understand their structure and function.[46]

The field of supramolecular chemistry has created many chemically appealing self-assembled structures containing metals as the driving elements.[48] The self-assembly process under thermodynamic control is attractive when compared to traditional multi-step covalent organic synthesis and produces larger, ordered structures.[49] Much work has focussed on the recognition of DNA by cylindrical metallo-supramolecular agents (see section 1.8).[49] and has led to the creation of large synthetic structures which closely resemble the size and shape of protein DNA recognition motifs. Therefore, these agents are predicted to have novel DNA-binding properties and to display novel types of biological activity.[49,50]

1.7 Metal-based Drugs

Many transition metals have been used in the design of anticancer drugs due to various properties they exhibit including a range of redox and spectroscopic properties as well as changeable coordination geometries. In recent years, photodynamic therapy using metal-based photosensitizers able to photocleave DNA under conditions of visible light has led to the development of a number of platinum, dirhodium and ruthenium complexes. Recently, novel cobalt (II) complexes with terpyridine ligands made with phenyl, pyrenyl and anthracenyl moieties were synthesized and tested for their photochemotherapeutic properties (Figure 1.22).[51]

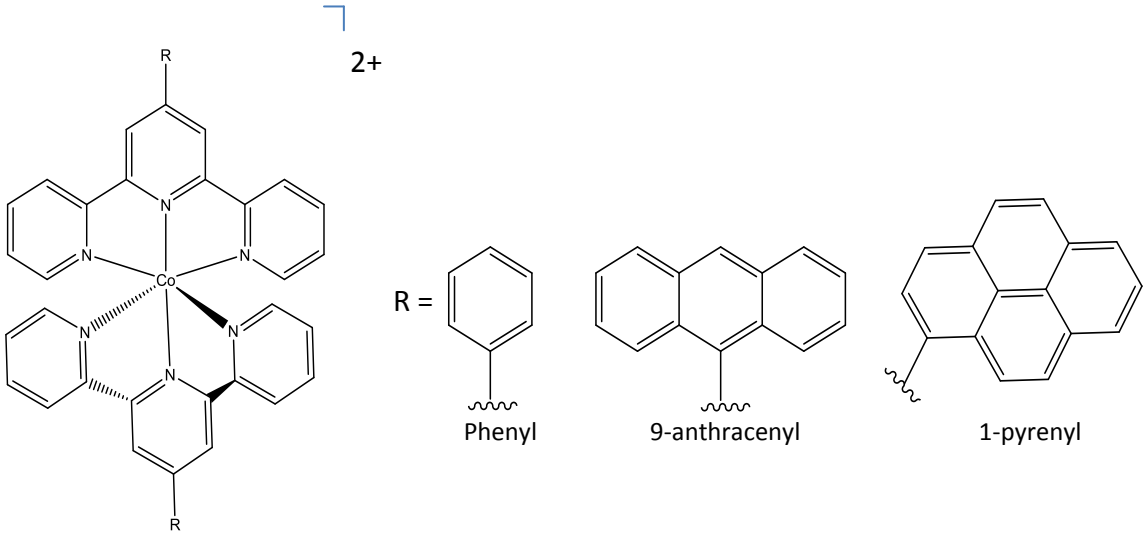

Figure 1.22. *The structures of cobalt (II) complexes.*

The complexes with pyrenyl and anthracenyl moieties bound strongly to calf thymus DNA and cleaved plasmid DNA when induced by visible light. Hydroxyl radicals were produced through a photo-redox pathway and in HeLa (cervical cancer) cells, a photodynamic therapeutic effect was seen. The photoactive pyrenyl and anthracenyl

moieties aided cellular imaging and live-cell microscopy identified the complexes crossing the plasma membrane and accumulating in the cytoplasm. The amount taken into cells was less for the complex with the phenyl moiety. Toxicity studies for the light-exposed pyrenyl cobalt (II) complex revealed a similar IC50 value to that of the popular cancer drug, cisplatin.[51]

Copper (II) complexes conjugated to ferrocene have also been synthesized and investigated in relation to their photocytotoxic activity under visible light conditions. Complexes lacking the ferrocene moiety showed reduced photocleavage of DNA and cytotoxicity against HeLa and MCF-7 (breast adenocarcinoma) cells when compared with ferrocene-appended complexes. A complex containing a napthyl fluorophore was successfully used for fluorescence microscopy to show uptake and nuclear localization of complexes in HeLa cells.[52]

As many cellular enzymes and transcription factors have binding sites for zinc, the Zn (II) ion can potentially have an effect on many areas of cell signaling. In addition, previous studies have shown that zinc reduces the levels of metal-induced hepatotoxicity.[53] Recently, macrobicyclic dinuclear zinc (II) complexes were investigated for their interaction with DNA and anticancer activity against HeLa and BeWo (placental cancer) cells.[54] DNA-binding studies including circular dichroism, fluorescence and absorption spectral studies showed the zinc complexes interacted with calf thymus DNA through intercalation. The mechanism by which plasmid DNA was cleaved was studied in the presence of a hydroxyl radical scavenger (DMSO), a superoxide quencher (SOD)

and a singlet oxygen quencher (L-histidine). As the cleavage activity of complexes was not affected, an oxygen- independent hydrolytic mechanism was identified.[54]

The strongest activity against cancer cells was displayed by complexes with macrobicyclic ligands containing phenanthroline (Figure 1.23). Results revealed that a complex's ability to bind and cleave DNA required a synergistic interaction of metal ion and ligand which is important when designing anticancer drugs. Therefore, stacking of phenanthroline-coordinated complexes resulted in strong DNA binding, cleavage, efficient transfer across the plasma membrane and high toxicity against cancer cells. Furthermore, activation of caspase 3/caspase 9 and increased membrane permeability occurred with these compounds which are phenotypically associated with apoptotic induction.[54] Further studies on uptake would be required to understand the precise mechanism by which these complexes cause cancer cell death.

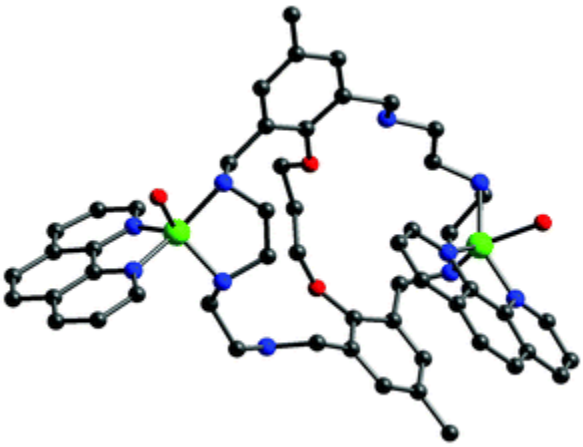

Figure 1.23. *The structure of* $[Zn_2L(phen)_2(H_2O)_2](ClO_4)_4$ *(macrobicyclic dizinc (II) complex) Oxygen: red, Nitrogen: blue, Carbon: grey, Zinc: green. Taken from ref 54.*

Another novel soluble Zinc (II) complex has recently been synthesized and its interaction with DNA has been studied. This complex was derived from the sulfa drug, sulfasalazine and the dipeptide, glycine-glycine.[55] As they contain a range of donor centers including N-terminal oxygen atoms and carbonyl oxygens, peptides are good binders of metal ions. These properties of peptides have been exploited and combined with metals to be used as therapeutics. The anticancer drug, bleomycin is an example of a metallopeptide that shows strong DNA specificity.[55] The structure of the complex was designed with several pharmacologically active properties including a metal-binding domain, the sulfasalazine's planar rings which could partially intercalate into DNA and good solubility allowing efficient plasma membrane uptake.[55] Binding studies for the zinc (II) complex *in vitro* revealed electrostatic interactions with DNA and preference for binding to AT-rich regions in the minor groove (Figure 1.24). A hydrolytic mechanism by which plasmid DNA was cleaved was suggested. The complex was able to recognize a specific sequence of DNA and therefore control gene expression via inhibition of overactive transcriptions factors.[55] Designing new anticancer agents with well-defined properties could help move past resistance that has been displayed by many tumours against platinum drugs.

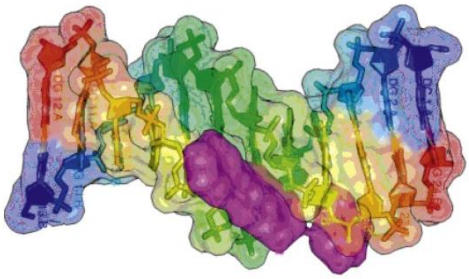

Figure 1.24. *Partial intercalation of zinc (II) complex with adjacent AT base pairs in DNA minor groove. Taken from ref 55.*

Ruthenium has received much attention as a metal of choice in the development of anticancer agents. This is due to its many advantageous properties including high cellular toxicity against cancer cells, low toxicity against healthy cells and many oxidation states. Currently, the two octahedral ruthenium complexes, KP1019 and NAMI-A have been successful in phase 1 of clinical trials (Figure 1.25).[56] The anticancer activity of these complexes has been studied with various methods being proposed including DNA binding, metastatic growth inhibition, ROS production and activation of apoptotic signaling pathways.[57,58] Biologically active imidazole derivatives are found in many naturally occurring products and have been used in ligand synthesis of metal complexes including that of NAMI-A.[56]

A **B**

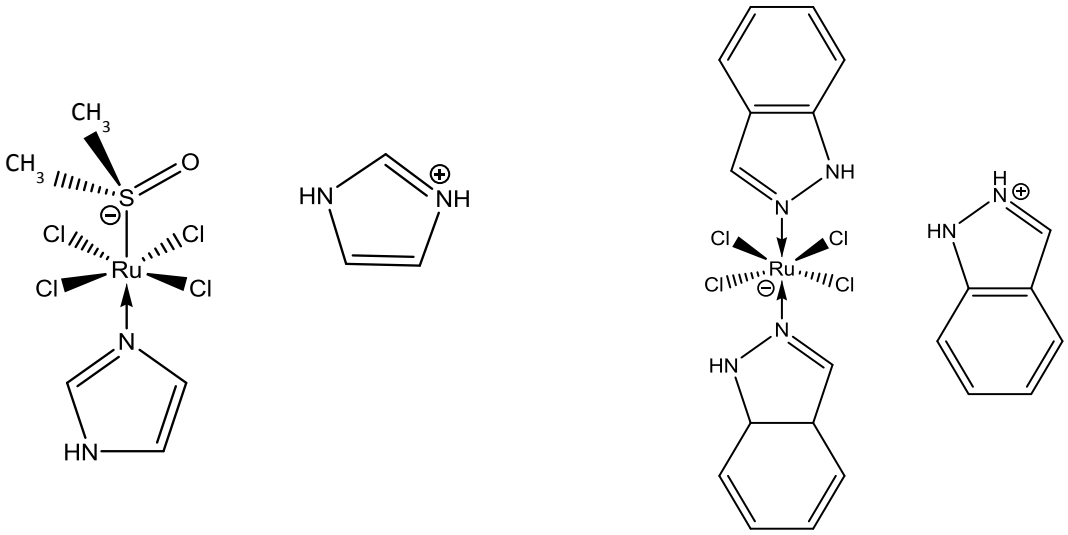

Figure 1.25. *The structure of ruthenium complexes:* ***(A)*** *NAMI-A* ***(B)*** *KP1019.*

In a recent study, 3 fluorescent ruthenium complexes (RuIP1, RuIP2, RuIP3) were synthesized with ligands made of imidazole derivatives and studied for their anticancer properties to try understand their mechanism of action at the molecular level (Figure 1.26).[57] Results showed all the complexes had strong anti-proliferative activity against HepG2 (hepatocellular carcinoma), A375 (melanoma) and SW480 (colorectal adenocarcinoma) cells. In addition, the complexes were not as toxic as cisplatin to healthy HK-2 (kidney) and HS68 (fibroblast) cells of humans. Cell cycle analysis confirmed apoptotic cell death as the method of cancer cell killing for the RuIP1 complex. This was further confirmed by the Tunel assay which identified nuclear condensation and DNA fragmentation. Furthermore, the study found this complex was able to induce internal mitochondrial-associated and external receptor-associated apoptotic pathways in tumour cells making it a promising candidate for further investigation as a chemotherapeutic.[57]

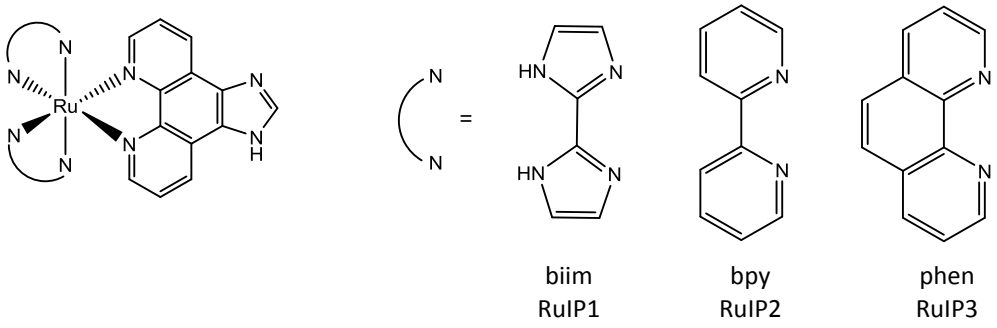

Figure 1.26. *The structure of 3 Ruthenium complexes: $[Ru(L)_2IP]^{2+}$ (IP: imidazole[4,5-f][1,10]phenanthroline) L: 2,2-biimidazole (biim); 2,2-bipyridine (bpy); 1,10-phenanthroline (phen).*

A different approach to understanding how cells respond to metal-based anticancer drugs has been the synthesis of fluorescent versions of these drugs. Fluorescein-labelled derivatives of cisplatin have been synthesized and visualized inside cancer cells using fluorescence microscopy allowing researchers to overcome some of the obstacles associated with imaging localization of drugs in cells.[59] Following on from this success, in a recent study, platinum (II) was co-ordinated to a fluorescent ligand (N,N-bis (anthracen-9-ylmethyl)propane-1,3-diamine) (bapda) and the complex's anticancer activity was investigated in relation to cisplatin (Figure 1.27).[60]

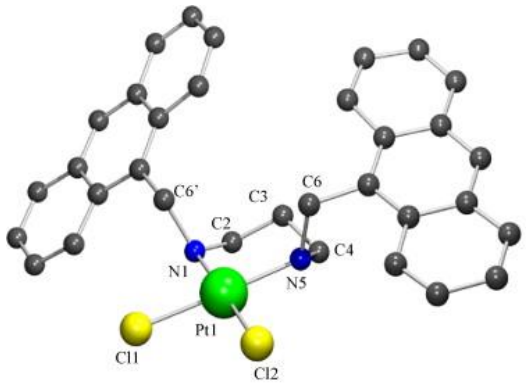

Figure 1.27. *The structure of cis-[Pt(bapda)Cl_2]. Taken from ref 60.*

The complex showed strong antiproliferative activity in A2780 (ovarian carcinoma) with resistance seen in A2780R (cisplatin-resistance) cells, similar to that seen with cisplatin. Glutathione molecules are believed to play an important part in the resistance mechanism with cisplatin. However, with cis-[Pt(bapda)Cl_2] no significant difference was observed in resistance to glutathione-depleted A2780R cells.[60] Cisplatin is believed to interact with glutathione via chloride displacement (see section 1.5) but bapda is co-ordinated to Pt (II) through a chelating mechanism, making cis-[Pt(bapda)Cl_2] stable against inhibition by

glutathione. Fluorescence quenching experiments where plasmid DNA and calf thymus DNA were added to solutions of cis-[Pt(bapda)Cl_2] were carried out to investigate the complex's ability to intercalate. Results revealed a drop in fluorescence when calf thymus DNA was used suggesting that anthracene rings were intercalating between base pairs.[60]

Cisplatin's success in clinic started the interest in metal-based chemotherapeutics with DNA as the target of choice. To date, many classes of metal have shown anticancer activity *in vitro*. These include gold (I,III), palladium (II), platinum (II,IV), ruthenium (II,III), rhenium (I), bismuth (III), copper (II), tin (IV) and gallium (III) derivatives.[61] Further improvements on drug design depends on specific targets, control of delivery and ideally a fluorescent version of each drug with the aim to improve cancer cell toxicity with minimal toxicity and better imaging in cells, tissues and organs.[61]

1.8 Metallo-supramolecular Cylinders

Cylindrical metallo-supramolecular agents able to recognize DNA have been designed and have the potential to be used as anticancer drugs.[48,62] Supramolecular chemistry has allowed these structures to be created that are analogous in size to the DNA recognition portion of protein zinc fingers (such as an α-helix) with the hope that alternative mechanisms of DNA binding to cisplatin will bring alternative activity in tumour cells.[63,64] Unlike the classic DNA-drug interactions mentioned above, they have been designed to be the right size (1 nm x 2 nm) and shape to fit perfectly into the major groove of DNA (spanning five base pairs) but too bulky to fit in the minor groove (Figure 1.28).[65,66]

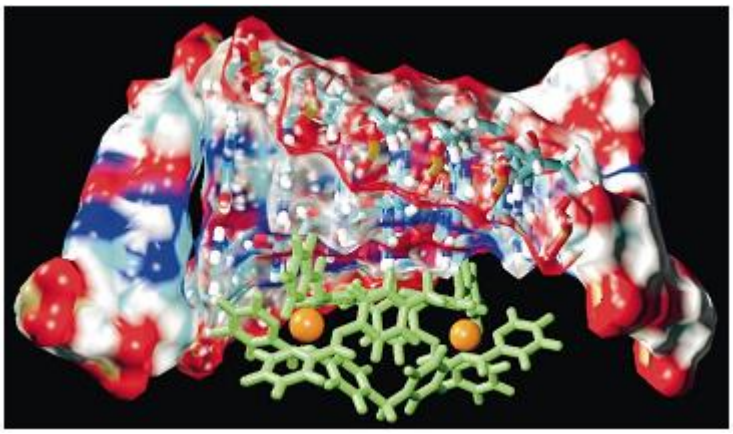

Figure 1.28. *NMR structure of a cylinder in the major groove of DNA. Taken from ref 49.*

The synthetic cylinders are made of two metal ions surrounded by three ligand strands and carry a tetra-cationic charge giving the formula $[M_2L_3]^{4+}$ with various metal ions used in their design (Figure 1.29).[49] The dimetallic nature of these compounds means they carry a high positive charge which has been predicted to strengthen their binding to the negatively charged DNA molecule. The binding properties of these cylinders have been further investigated using the commonly used technique, circular dichroism (CD). This technique is defined as the difference in absorption between right and left-handed circularly polarized light.[67] The CD is specifically affected by the chirality or asymmetry of an environment. Therefore, when a CD signal in the optical transitions of cylinder is observed for a racemic mixture of iron cylinder in the presence of DNA, it indicates that cylinder is binding to DNA. The CD spectra produced have shown the cylinder to be interacting with DNA in a single mode of binding which is consistent with binding in the major groove.[49] Strong binding of cylinder to DNA has been indicated through the use of spectroscopic studies with a binding constant in excess of 10^7 M^{-1}.[66]

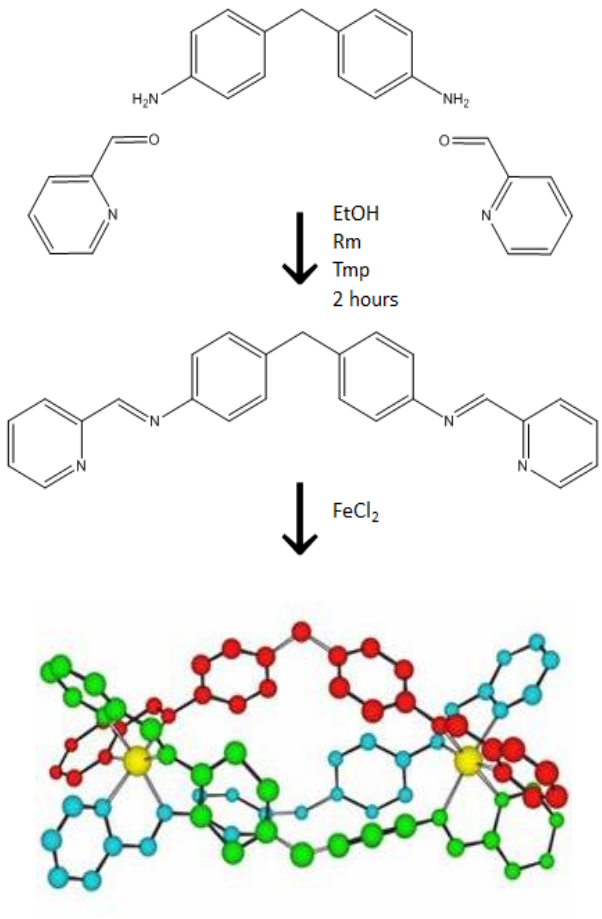

Figure 1.29. *A tetracationic triple-stranded supramolecular cylinder.*

Linear dichroism (LD) has also been used to analyse the orientation of the cylinder on the DNA.[49] LD is defined as the unequal absorption of light polarized parallel and perpendicular to an orientation axis.[68] A molecule bound to DNA in a particular orientation will also be oriented by the viscous drag and therefore a LD signal is produced. In comparison, a molecule that is unattached or randomly associated with DNA would produce no signal. When concentrations of cylinder ranging from 0 to 100 μM were examined with DNA, the LD signal produced confirmed the cylinder's binding to DNA was specific. Furthermore, the DNA signal produced by the bases was

significantly decreased in the presence of very low cylinder concentrations.[49] This could be attributed to an increased flexibility of the DNA molecule. Alternatively a shortening of DNA via bending, kinking, aggregation or compaction of the molecule may also be responsible.[68] However, as the CD spectra has confirmed the DNA structure is maintained and preserved upon cylinder binding, it suggests that DNA is not being shortened due to kinking.[49]

The binding of these cylinders to linear plasmid DNA has been imaged at the molecular level using atomic force microscopy. The majority of images obtained using this technique for metal compounds bound to DNA have been restricted to covalent binders such as cisplatin.[49] When in contact with low concentrations of cylinder, an increase in the number of bends and mean bend angle of DNA was observed in comparison to that seen with free DNA. More remarkable was the induction of intramolecular coiling, producing short coils of DNA that occurred with moderate concentrations of cylinder (Figure 1.30). The exact dimensions of the cylinder are crucial factors in the coiling process with an increase in size by 10 % causing a great reduction in the extent of coiling of DNA.[49]

When the cylinder was crystallized with a palindromic hexanucleotide, a second mode of binding was uncovered. The crystal structure showed the cylinder to be located at the center of a DNA 3-way junction (Figure 1.31).[69] This is feasible as palindromic sequence hydrogen-bonding (Watson-Crick) can be fulfilled via 3-way junctions, duplex structures or other junction structures including 4-way junctions. At the 3-way cylinder junction, the

DNA has a similar structure to DNA in junctions crystallized with proteins. In addition, the cylinder in the junction almost precisely overlaps with the crystal structure of free cylinder. This verifies that neither structure is significantly disturbed by the binding.[32]

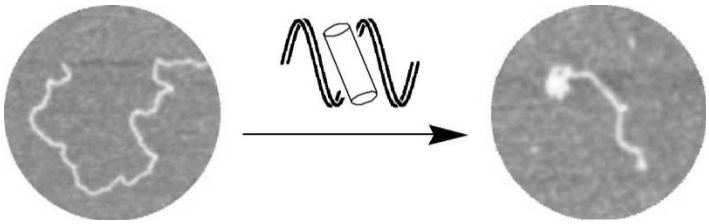

Figure 1.30. *AFM images showing the dramatic intra-molecular coiling induced by the cylinders. Taken from ref 68.*

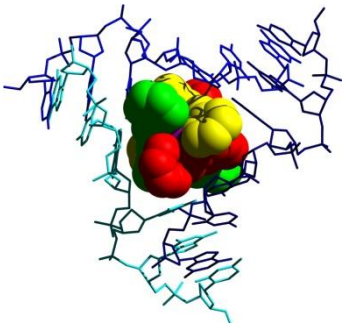

Figure 1.31. *Recognition of the centre of a 3-way DNA junction by a supramolecular cylinder. Taken from ref 70.*

The perfect fit of the cylinder binding to 3-way junctions is unlike any other known DNA-interacting molecule. Despite being less studied than 4-way (Holliday) junctions, 3-way junctions are of interest as the replication fork is a type of Y-shaped junction. Therefore, whenever the DNA helix is unwound to replicate or transcribe DNA, a Y-shaped, 3-way junction is formed.[71] In cancer cells, DNA replication and transcription occurs at a much faster rate when compared to normal cells. Therefore a compound that

can recognize this particular structure of DNA and interfere with the replication of DNA has the potential for clinical applications.[69]

3-way junctions are also believed to occur in triplet repeat expansions present in unstable genomic DNA associated with the development of diseases including Huntington's. These cylinders may therefore have potential therapeutic effects in these cases due to their ability to bind to 3-way junctions and stall the replication fork. Gel electrophoresis studies have shown that the cylinders can also recognize 3-way junctions with unpaired nucleotides.[72] The ruthenium (II) and iron (II) cylinders have been shown to be active against certain cancer cells with a similar potency to cisplatin. It is not known how normal cells compare to cancer cells when treated with these compounds as this has not been investigated.

Interactions of enantiomers of the iron cylinder have been examined to understand the mode in which this compound binds to DNA. The P-enantiomer is the positively twisted right-handed helicate and the M-enantiomer is the negatively twisted left-handed version (Figure 1.32). Earlier data showed that both caused the DNA to bend significantly. It has been found that they also cause considerable unwinding of the DNA helix with the M-enantiomer being much more effective at doing this. In addition, the M-enantiomer preferentially binds to normal sequences of alternating purines and pyrimidines.[73]

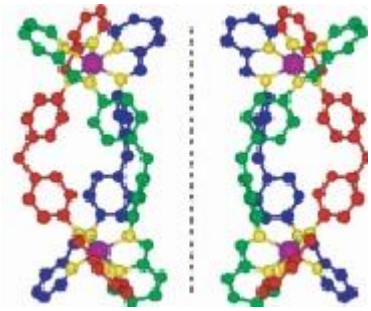

Figure 1.32. *The structures of the M-enantiomer (left) and P-enantiomer (right) of Iron cylinder. Iron atoms: purple, nitrogen: yellow, carbon atoms in three ligands: red, green and blue. Taken from ref 74.*

Maintenance of telomere length is one of the important features of tumour development which makes telomere quadruplexes an anticancer target. Recently, metal complexes were investigated for their ability to stabilize G-quadruplexes. The P-enantiomer of iron cylinder was proposed to prefer G-quadruplex over double stranded helical DNA although this is proposed to be related to the loops above the quadruplexes. Furthermore, telomeric G-quadruplexes were stabilized and transformed from antiparallel to hybrid structures if sodium was present in the environment.[74]

Recently, cell growth inhibition was used as an endpoint to assess the potency of the cylinder in comparison to cisplatin. The mitochondrial enzyme function was assessed and used to calculate IC50 values for both drugs against a range of tumour cell lines. Results showed cisplatin to be a more potent inhibitor of cell growth. However, the IC50 of cisplatin as assessed via the MTT assay was found to be 5 times greater than that of cylinder. Both drugs were found to be effective at stopping cell growth but the results indicated that they operated via different mechanisms of action. The researchers

highlighted that the IC50 values obtained for the cylinder were similar to those for carboplatin which is used as alternative to cisplatin in cancer patients as it is less toxic and causes less undesirable effects (see section 1.5).[63]

The iron cylinder's ability to induce mutations was assessed by the Ames test. The Ames test is a bacterial mutagenicity assay used specifically to identify chemicals that cause genetic damage leading to mutations.[75] Results showed no evidence of frameshift or base pair mutations occurring in bacteria as a result of cylinder treatment. The Comet assay was also employed to investigate the cylinder's genotoxic potential in mammalian cells. This is a single cell gel electrophoresis assay which allows single and double strand breaks to be detected. Concentrations of iron cylinder ranging between 0 and 25 μM were investigated over a 24 hour period. The results showed no evidence of DNA strand breaks in breast, ovarian and leukemic cell lines.[63] The results for the alkaline Comet assay provided evidence for the mechanism by which the cylinder was acting indicating that it was not directly inducing DNA strand breaks and therefore not directly genotoxic. The iron cylinder therefore has a significant advantage over cisplatin as it is able to stop cell growth and do so in the absence of genotoxicty and mutagenicity.[63]

Investigating the effect of iron cylinder on the cell cycle in the HL60, myeloid leukemia cell line, revealed a significant arrest in the G0/G1 phase together with a reduced number of cells entering the S phase upon cylinder treatment (10 μM for 24 hours). These results provide supporting evidence for the cylinder's ability to stop cells from entering the growth phase and reducing DNA synthesis. Programmed cell death, apoptosis occurred in

both adherent cell lines and HL60s when treated with 25 μM cylinder. This is consistent with the cylinder binding to the DNA and is further supported by evidence from flow-cytometry and cell-cycle based assays showing a decrease in propidium iodide staining in cells.[63] It is believed that the cell cycle arrest is due to non-covalent interactions with the DNA helix and through the use of two independent assays, researchers have been able to show that the mechanism by which the iron cylinder induces its effect is apoptosis as opposed to inflammatory necrotic cell death which disrupts surrounding viable tissues.[63]

The exact mechanism of iron cylinder's activity on the molecular level is yet to be investigated but so far research in several tumour cell lines has indicated that it works in a different way to cisplatin. As it is known that the cylinder interacts non-covalently with DNA, it has been hypothesized that its mechanism of action may involve it binding to and inhibiting replication forks which are a type of 3-way DNA junction. The potential ability of iron cylinder to stall the replication fork, inhibiting progression of the cell cycle and induce apoptosis in the absence of genotoxicity, puts it forward as a promising anticancer therapeutic.[76] However, due to its lack of fluorescence, the iron cylinder cannot easily be imaged using fluorescence microscopy in cells. Although the fluorescent ruthenium analogue shows strong anticancer activity,[63] it is difficult to synthesize and there is a need to create a much more fluorescent iron cylinder and develop indirect imaging methods. This will improve our understanding of the cellular fate and activity of iron cylinder.

1.9 Aims of the Thesis

The aims of this thesis were to develop novel methods to investigate the localization, distribution and mechanism of action for the novel potential chemotherapeutic, iron cylinder. A breast cancer cell line (MDAMB-231), an ovarian cancer cell line (SKOV3) and a leukemic cancer cell line (HL60) were investigated with regards to their sensitivity to the cylinder. Novel methods of imaging non-fluorescent cylinder were developed. The cylinder's genotoxic potential was investigated and compared to that of classic chemotherapeutics including cisplatin and etoposide in leukaemia cells. A goal of this thesis was to pioneer the first *in vivo* research relating to the iron cylinder by further exploring its effects in embryos of the model organism, *Danio rerio* (zebrafish). Specifically, the following areas were investigated:

- Visualize Hoechst quenching through fluorescence microscopy in cancer cells
- Quantify Hoechst quenching through fluorimetry / flow cytometry in cancer cells
- Investigate the effect of increasing cylinder concentrations on the extent of Hoechst quenching in cancer cells
- Compare sensitivity to cylinder across a range of cancer cell types
- Confirm if 20 minutes of cylinder treatment is sufficient time for cylinder to gain access to DNA
- Study the cylinder's interaction with other fluorescent probes
- Visualize quenching of nuclear GFP by iron cylinder in breast cancer cells using fluorescence microscopy
- Quantify GFP quenching through fluorimetry in breast cancer cells

- Identify a therapeutic window over which the cylinder can bring about its effects in zebrafish embryos

1.10 References

[1] Watson, J. D., Crick, F. H. (1953) A structure for deoxyribose nucleic acid. *Nature*. 171: 737-738.

[2] Pray, L. (2008) Discovery of DNA structure and function: Watson and Crick. *Nature Education 1*. 1:100.

[3] Packer, M. J., Hunter, C. A. (1998) Sequence-dependent DNA Structure: The Role of the Sugar-phosphate Backbone, *J. Mol. Biol*. 280 (3): 407-420.

[4] Rich, A., Zhang, S. (2003). Timeline: Z-DNA: the long road to biological function. *Nature Reviews Geneticis*. 4 (7): 566-572.

[5] Lam, E. Y., Beraldi, D., Tannahill, D., Balasubramanian, S. (2013) G-quadruplex structures are stable and detectable in human genomic DNA. *Nat Commun*. 4: 1796.

[6] Burge, S., Parkinson, G., Hazel, P., Todd, A., Neidle, S. (2006) Quadruplex DNA: sequence, topology and structure. *Nucleic Acids Res*. 34 (19): 5402-5415.

[7] Ma, D-L., Ma, V. P-Y., Leung, K-H., Zhong, H-J., He, H-Z., Chan, D. S-H., Leung, C-H. (2013) Structure-Based Approaches Targeting Oncogene Promoter G-Quadruplexes, Oncogene and Cancer - From Bench to Clinic, Dr. Yahwardiah Siregar ed. Chapter 6, section 2, page 133.

[8] Hamilton, P. L., Arya, D. P. (2012) Natural product DNA major groove binders. *Nat. Prod. Rep*. 29 (2): 134-143.

[9] Sasikala, W. D., Mukherjee, A (2012) Molecular Mechanism of Direct Proflavine−DNA Intercalation: Evidence for Drug-Induced Minimum Base-Stacking Penalty Pathway. *J. Phys. Chem. B*. 116 (40): 12208-12212.

[10] Boer, D. R., Canals, A., Coll, M (2009) DNA-binding drugs caught in action: the latest 3D pictures of drug-DNA complexes. *Dalton Trans*. 21 (3) 399-414.

[11] Seville, S., Phillips, R. M., Shnyder, S. D., Wright, C. W. (2007) Synthesis of cryptolepine analogues as potential bioreducible anticancer agents. *Bioorganic & Medicinal Chemistry*. 15 (19): 6353–6360.

[12] Olajide, O. A., Heiss, E. H., Schachner, D., Wright, C. W., Vollmar, A. M., Dirsch, V. M. (2007) Synthetic cryptolepine inhibits DNA binding of NF-kappaB. *Bioorg. Med. Chem*. 15 (1): 43-49.

[13] Chen, A. Y., Yu, C., Gatto, B., Liu, L. F. (1993) Pharmacology DNA minor groove-binding ligands: A different class of mammalian DNA topoisomerase I inhibitors. *Proc. Natl. Acad. Sci. USA*. 90 (17) 8131-8135.

[14] Komeda, S., Moulaei, T., Woods, K. K., Chikuma, M., Farrell, N. P., Williams, L. D. (2006) A third mode of DNA binding: Phosphate clamps by a polynuclear platinum complex. *J. Am. Chem. Soc*. 128 (50): 16092-16103.

[15] Daly, C. J., McGrath, J. C. (2003) Fluorescent ligands, antibodies, and proteins for the study of receptors. *Pharmacology and Therapeutics*, 100 (2): 101-118.

[16] Haughland, R. P. (2010) The Molecular Probes Handbook, Invitrogen Life Sciences. Nucleic Acid Detection and Analysis. 11th ed. Chapter 8. Nucleic Acid Stains. Section 8.1.

[17] Banerjee, D., Pal, S. K. (2008) Dynamics in the DNA Recognition by DAPI: Exploration of the Various Binding Modes, *J. Phys. Chem. B*. 112 (3): 1016-1021.

[18] Smolina, I. V., Kuhn, H., Lee, C., Frank-Kamenetskii, M-D. (2008) Fluorescence-based detection of short DNA sequences under non-denaturing conditions. *Bioorganic & Medicinal Chemistry*. 16 (1): 84-93.

[19] Pawley, J. B. (2006). Handbook of Biological Confocal Microscopy. 3rd ed.

[20] Suzuki, T., Fujikura, K., Higashiyama, T., Takata. K. (1997) DNA Staining for Fluorescence and Laser Confocal Microscopy. *J Histochem Cytochem*. 45 (1): 49-53.

[21] Li, Y., Sen, D. (1997) Toward an efficient DNAzyme. *Biochemistry*. 36 (18): 5589-99.

[22] Lipscomb, L. A., Zhou, F. X., Presnell, S. R., Woo, R. J., Peek, M. E., Plaskon, R. R., Williams, L. D. (1996) Structure of a DNA-Porphyrin Complex. *Biochemistry*. 35 (9): 2818-2823.

[23] Arthanari, H., Basu, S., Kawano, T. L., Bolton, P. H. (1998) Fluorescent dyes specific for quadruplex DNA. *Nucleic Acids Res.* 26 (16): 3724-3728.

[24] Gurova, K. (2009) New hopes from old drugs: revisiting DNA-binding small molecules as anticancer agents. *Future Oncol*. 5 (10): 1685-1704.

[25] Purciolas, M., Canals, A., Coll, M., Aymamí, J. (2005) The anticancer agent ellipticine unwinds DNA by intercalative binding in an orientation parallel to base pairs. *Acta Crystallogr D Biol Crystallogr*. 61 (7): 1009- 1012.

[26] Arnesano, F., Giovanni, N. (2009) Mechanistic insight into the cellular uptake and processing of cisplatin 30 years after its approval by FDA. *Coordination Chemistry Reviews*. 253 (15): 2070-2081.

[27] Rabik, C. A., Dolan, M. E. (2007) Molecular mechanisms of resistance and toxicity associated with platinating agents. *Cancer Treatment Reviews*. 33 (1): 9–23.

[28] Ummat, A., Rechkoblit, O., Jain, R., Choudhury, J. R., Johnson, R. E., Silverstein, T. D., Buku, A., Lone, S., Prakash, L., Prakash, S., Aggarwal, A. K. (2012) Structural basis for cisplatin DNA damage tolerance by human polymeraseη during cancer chemotherapy. *Nat Struct Mol Biol*. 19 (6): 628-632.

[29] Goodsell, D. S. (2006) The molecular perspective: cisplatin. *Oncologist*. 11 (3): 316-317.

[30] Alderden , R. A., Hall, M. D., Hambley. T. W. (2006) The discovery and development of cisplatin. *J. Chem. Educ.* 83 (5): 728-734.

[31] http://cmgm.stanford.edu/biochem201/Slides/DNARepair, Accessed on 03/06/14.

[32] Hannon, M. J. (2007) Metal-based anticancer drugs: From a past anchored in platinum chemistry to a post-genomic future of diverse chemistry and biology. *Pure Appl Chem.* 79 (12): 2243-61.

[33] Wang, D., Lippard, S. J. (2005) Cellular processing of platinum anticancer drugs. *Nature Reviews Drug Discovery*. 4 (4): 307-320.

[34] Galluzzi, L., Senovilla, L., Vitale, I., Michels, J., Martins, I., Kepp, O., Castedo, M., Kroemer, G. (2012) Molecular mechanisms of cisplatin resistance. *Oncogene*. 31 (15), 1869-1883.

[35] Cerasino, L., Hannon, M. J., Sletten, E. (2007) DNA Three-Way Junction with a Dinuclear Iron (II) Supramolecular Helicate at the Center: A NMR structural Study. *Inorg Chem*. 46 (16): 6245-6251.

[36] Koberle, B., Tomicic, M. T., Usanova, S., Kaina, B. (2010) Cisplatin resistance: preclinical findings and clinical implications. *Biochim Biophys Acta* 1806 (2): 172-182.

[37] Siddik, Z. H. (2003) Cisplatin: mode of cytotoxic action and molecular basis of resistance. *Oncogene*. 22 (47): 7265-7279.

[38] Deans, A. J., West, S. C. (2011) DNA interstrand crosslink repair and cancer. *Nat Rev Cancer*. 11 (7): 467–480.

[39] Huang, Y., Li, L. (2013) DNA crosslinking damage and cancer - a tale of friend and foe. *Transl Cancer Res*. 2 (3): 144–154.

[40] Reißner, T., Schneider, S., Schorr, S., Carell, T. (2010) Crystal Structure of a Cisplatin–(1,3-GTG) Cross-Link within DNA Polymerase eta. *Angew. Chem. Int. Ed Engl*. 49 (17): 3077-3080.

[41] El-Awady el, S. E., Moustafa, Y. M., Abo-Elmatty, D. M., Radwan, A. (2011) Cisplatin-induced cardiotoxicity: mechanisms and cardioprotective stratergies. *Eur J Pharmacol*. 650 (1): 335-341.

[42] Jung, Y., Lippard, S. J. (2007) Direct cellular responses to platinum-induced DNA damage. *Chem Rev.* 107 (5): 1387-1407.

[43] El-Sayyad, H. I., Ismail, M. F., Shalaby, F. M., Abou-El-Magd, R. F., Gaur, R. L., Fernando, A., Raj, M. H., Ouhtit, A. (2009) Histopathological effects of cisplatin, doxorubicin and 5-flurouracil (5-FU) on the liver of male albino rats. *Int J Biol Sci.* 5 (5): 466-73.

[44] Goto, S., Iida, T., Cho, S., Oka, M., Kohno, S., Kondo, T. (1999) Overexpression of glutathione S-transferase pi enhances the adduct formation of cisplatin with glutathione in human cancer cells. *Free Radic Res*. 31 (6): 549-558.

[45] Lehn, J. M. (1993) Supramolecular chemistry. *Science.* 260 (5115): 1762-1763.

[46] Jayaraj, N., Zhao, Y., Parthasarathy, A., Porel, M., Liu, R. S., Ramamurthy, V. (2009) Nature of Supramolecular Complexes Controlled by the Structure of the Guest Molecules: Formation of Octa Acid Based Capsuleplex and Cavitandplex. *Langmuir.* 25 (18): 10575-10586.

[47] Pitt, M. A., Johnson, D. W. (2007) Main group supramolecular chemistry. *Chem Soc Rev*. 36 (9): 1441-1453.

[48] Lavalette, A., Tuna., F, Clarkson, G., Alcock, N. W., Hannon, M. J. (2003) Aggregation of metallo-supramolecular architectures by metallo-assembled hydrogen bonding sites. *Chem Commun*. 21: 2666-2667.

[49] Hannon, M. J., Moreno, V., Prieto, M. J., Molderheim, E., Sletten, E., Meistermann, I., Isaac, C. J., Sanders, K. J., Rodger, A. (2001) Intramolecular DNA coiling mediated by a metallo supramolecular cylinder. *Angew Chem Intl Ed*. 40 (5): 879-884.

[50] Hambley, T. W. (2007) Developing new metal-based therapeutics: challenges and opportunities. *Dalton Trans*. 43: 4929-4937.

[51] Roy, S., Roy, S., Saha, S., Majumdar, R., Dighe, R. R., Jemmis, E. D., Chakravarty, A. R., (2011) Cobalt(II) complexes of terpyridine bases as photochemotherapeutic agents, showing cellular uptake and photocytotoxicity in visible light. *Dalton Trans*. 40 (6): 1233-1242.

[52] Goswami, T. K., Gadadhar, S., Karande, A. A., Chakravarty, A. R. (2013) Photocytotoxic ferrocene-appended (L-tyrosine) copper(II) complexes of phenanthroline bases. *Polyhedron*. 52: 1287-1298.

[53] Bhasin, P., Singla, N., Dhawan, D. K. (2014) Protective role of zinc during aluminium-induced hepatotoxicity. *Environmental Toxicology*. 29 (3): 320-327.

[54] Anbu, S., Ravishankaran, R., Karande, A. A., Kandaswamy, M. (2012) DNA targeting polyaza macrobicyclic dizinc(II) complexes promoting high in vitro caspase dependent anti-proliferative activity against human carcinoma cancer cells. *Dalton Trans*. 41 (41): 12970-12983.

[55] Tabassum, S., Al–Asbahy, W. M., Afzal, M., Shamsi, M., Arjmand, F. (2012) DNA binding and cleavage studies of new sulfasalazine-derived dipeptide Zn (II) complex: Validation for specific recognition with 5'-TMP. *Journal of Luminescence*. 132 (11): 3058-3065.

[56] Aitken, J. B., Antony, S., Weekley, C. M., Lai, B., Spiccia, L., Harris, H. H. (2012) Distinct cellular fates for KP1019 and NAMI-A determined by X-ray fluorescence imaging of single cells. *Metallomics*. 4 (10): 1051-1056.

[57] Liu, Y., Chen, T., Liu, J., Wong, Y-S. (2013) Identification of fluorescent ruthenium complexes containing imidazole derivatives as a new class of apoptosis inducers by living cell real-time imaging. *Med. Chem. Commun*. 4 (5): 865-869.

[58] Tan, C-P., Lu, Y-Y, Ji, L-N., Mao, Z-W. (2014) Metallomics insights into the programmed cell death induced by metal-based anticancer compounds, *Metallomics*, 6 (5): 978-995.

[59] Molenaar, C., Teuben, J-M., Heetebrij, R. J., Tanke, H. J., Reedijk, J. (2000) New insights in the cellular processing of platinum antitumor compounds, using fluorophore-labeled platinum complexes and digital fluorescence microscopy. *J. Biol. Inorg. Chem*. 5 (5): 655-665.

[60] Marqués-Gallego, P., den Dulk, H., Brouwer, J., Tanase, S., Mutikainen, I., Turpeinen, U., Reedijk, J. (2009) Cytotoxic activity and cellular processing in human ovarian carcinoma cell lines of a new platinum(II) compound containing a fluorescent substituted propylene diamine ligand. *Biochem Pharmacol*. 78 (4): 365-373.

[61] Marques, M. P. M. (2013) Platinum and Palladium Polyamine Complexes as Anticancer Agents: The Structural Factor. *Hindawi Journals*. 2013:1- 29.

[62] Hannon, M. J., Painting, C. L., Alcock, N. W. (1999) A metallo-supramolecular double-helix containing a major and a minor groove. Chem Commun. (20) 2023-2024.

[63] Hotze, A. C., Hodges, N. J., Hayden, R. E., Sanchez-Cano, C., Paines, C., Male, N., Tse, M. K., Bunce, C. M., Chipman, J. K., Hannon M. J. (2008) Supramolecular iron cylinder with unprecedented DNA binding is a potent cytostatic and apoptotic agent without exhibiting genotoxicity. *Chem Biol*. 15 (12): 1258-1267.

[64] Tuna, F., Lees, M. R., Clarkson, G. J., Hannon, M. J. (2004) Readily Prepared Metallo-Supramolecular Triple Helicates Designed to Exhibit Spin-Crossover Behaviour. *Chem. Eur. J*. 10 (22): 5737 –5750.

[65] Moldrheim, E., Hannon, M. J., Meistermann, I., Rodger, A., Sletten, E. (2002) Interaction between a DNA oligonucleotide and a dinuclear iron(II) supramolecular cylinder; an NMR and molecular dynamics study. *J. Biol. Inorg. Chem.* 7 (7-8): 770-780.

[66] Khalid, S., Hannon, M. J., Rodger, A., Rodger, P. M. (2006) Simulations of DNA Coiling arounda Synthetic Supramolecular Cylinder That Binds in the DNA Major Groove. *Chem. Eur. J*. 12 (13): 3493-3506.

[67] Greenfield, N. J. (2006) Using circular dichroism spectra to estimate protein secondary structure. *Nat Protoc*. 1 (6) 2876-2890.

[68] Meistermann, I., Moreno, V., Prieto, M. J., Moldrheim, E., Sletten, E., Khalid, S., Rodger, P. M., Peberdy, J. C., Isaac, C. J., Rodger, A., Hannon, M. J. (2002) Intramolecular DNA coiling mediated by metallo-supramolecular cylinders: differential binding of P and M helical enantiomers. *Proc. Natl. Acad. Sci*. 99 (8): 5069-5074.

[69] Hannon, M. J. (2007) Supramolecular DNA recognition. *Chem Soc Rev.* 36 (2): 280-295.

[70]Oleksy, A., Blanco, A. G., Boer, R., Usón, I., Aymamí, J., Rodger, A., Hannon, M. J., Coll, M. (2006) Molecular recognition of a three-way DNA junction by a metallosupramolecular helicate. *Angew. Chem., Intl. Ed.* 45 (8): 1227-1231.

[71] Thompson, K. H., Orvig, C. (2006) Metal complexes in medicinal chemistry: new vistas and challenges in drug design. *Dalton Trans.* 6: 761-764.

[72] Malina, J., Hannon, M. J., Brabec, V. (2007) Recognition of DNA three-way junctions by metallo-supramolecular cylinders; gel electrophoresis studies. *Chem. Eur. J.* 13 (14): 3871-3877.

[73] Malina, J., Hannon, M. J., Brabec, V. (2008) DNA binding of dinuclear iron(II) metallosupramolecular cylinders. DNA unwinding and sequence preference. *Nucleic acids research*. 36 (11) 3630-3638.

[74] Yu, H., Wang, X., Fu, M., Ren, J., Qu, X. (2008) Chiral metallo-supramolecular complexes selectively recognize human telomeric G-quadruplex DNA. *Nucleic Acids Research*, 36 (17): 5695-5703.

[75] Mortelmans, K., Zeiger, E. (2000) The Ames Salmonella/microsome mutagenicity assay. *Mutat Res*. 455 (1-2): 29-60.

[76] Pascu, G. I., Hotze, A. C., Sanchez-Cano, C., Kariuki, B. M., Hannon, M. J. (2007) Dinuclear ruthenium(II) triple-stranded helicates: luminescent supramolecular cylinders that bind and coil DNA and exhibit activity against cancer cell lines. *Angew Chem Int Ed*. 46 (23): 4374-4378.

CHAPTER 2

Methods and Experimental Details

2.1 Compound Synthesis

2.1.1 Synthesis of Ligand

All chemicals were purchased from Sigma Aldrich (UK) and used without further purification. Ligand, (*N*,*N'*-bis(pyridin-2-ylmethylene)-4,4‟‟-diaminodiphenylmethane), was synthesized by combining 4,4‟‟-methylenedianiline (1.56 g, 8.00 mmol) and pyridine-2-carboaldehyde (1.40 ml, 15 mmol) in 50 ml ethanol. The solution was left to stir overnight and the resulting yellow precipitate filtered and recrystallised from ethanol. Yield: 65 %

1H NMR (CD2Cl2): δ 8.72 (2H, d, *J = 3.9 Hz*, H6), δ 8.62 (2H, s, Him), δ 8.23 (2H, d, *J = 8.1 Hz*, H3), δ 7.85 (2H, t, *J = 7.5 Hz*, H4), δ 7.41 (2H, t, *J = 7.0 Hz*, H5), δ 7.30 (8H, m, Ha/b), δ 4.09 (2H, s, CH2).

ESI MS: *m/z* 399 $[(C_{25}H_{20}N_4) + Na]^+$.

2.1.2 Synthesis of Iron Cylinder [1]

The synthesized ligand (1.36 g, 0.003 mol) and Iron (II) chloride tetrahydrate (0.48 g, 0.002 mol) was added to 200 ml methanol in a round bottom flask. The solution was refluxed for 3 hours, rotary evaporated, re-dissolved and precipitated with diethyl ether. Yield: 85 %

1H NMR (MeOD): δ 9.21 (2H, s, Him), δ 8.75 (2H, d, *J = 7.0 Hz*, H3), δ 8.51 (2H, t, *J = 6.5 Hz*, H4), δ 7.90 (2H, t, *J = 6.1 Hz*, H5), δ 7.49 (2H, d, *J = 4.2 Hz*, H6), δ 7.08 (4H, s, Ha/b), δ 5.62 (4H, s, Ha/b), δ 4.08 (2H, s, CH2).

ESI MS: *m/z* 310 $[Fe_2(C_{25}H_{20}N_4)_3]^{4+}$.

Synthesis of iron cylinder was carried out every three months with the purity and stability being confirmed by CHN and NMR analysis prior to solutions being prepared. Sterile PBS was added to prepare a 5 mM stock solution of iron cylinder which was prepared fresh prior to use in assays.

2.2 Cell Culture

2.2.1 Cell Lines

SKOV3, human caucasian ovary adenocarcinoma (91091004), MDAMB-231, human caucasian breast adenocarcinoma (92020424) and HL60, human caucasian promyelocytic leukaemia (98070106) cell lines were obtained from ECACC (European Collection of Cell Cultures). Luciferase-expressing MDAMB-231 (AKR-231) and GFP-expressing MDAMB-231 (AKR-201) cell lines were obtained from Cell Biolabs, Inc. These stable cell lines were created by having luciferase or GFP introduced by either lentivirus transduction or plasmid transfection, followed by selection of stable clones.

MDAMB-231 and SKOV3 were chosen as previous work investigating the iron cylinder has used these two cell lines which represent commonly occurring cancers in women. It was important to compare the cylinder's effects between adherent and suspension suspension cells and so the HL60 leukemia cell line was chosen for this purpose.

2.2.2 Complete Media Preparation

GIBCO® RPMI (Roswell Park Memorial Institute) Media 1640 and GIBCO® DMEM (Dulbecco's Modified Eagle Medium) were supplemented with foetal bovine serum, FBS (10 % v/v), penicillin (100 U/ml), streptomycin (100 µg/ml) and L-glutamine (2 mM). Complete media was stored in the fridge.

2.2.3 Starting Cell Cultures

SKOV3 and HL60 cell lines were cultured using complete RPMI media and MDAMB-231 cell lines were cultured in complete DMEM. The cell lines were removed from liquid nitrogen storage and thawed in a 37 °C water bath. Complete media was also warmed in a 37 °C water bath. Each cell line (1×10^6 cells/ml) was added to 15 ml of fresh complete media in a 75 cm^3 tissue culture flask with a vented cap (T_{75}) (Costar). Cultures were incubated at 37 °C in a 5 % CO_2, 95 % air incubator (Sanyo, MCO-17A). Media was changed every 2 days and cells were passaged every 3 or 4 days.

2.2.4 Passage of Cells

Once cells were confluent, they were passaged. Complete media, trypsin- EDTA (GIBCO®) and 0.01 M phosphate buffered saline, (PBS) (Sigma-Aldrich) were warmed in a 37 °C water bath. For MDAMB-231 cell lines and SKOV3 cells, the old media was carefully removed from the flask and 10 ml of PBS was added. The flask was tilted to ensure the entire surface had been covered. This was then removed and 2 ml trypsin added to the flask. The flask was placed in an incubator for 3 minutes. Flasks were checked under the microscope to ensure the cells had detached (flasks were tapped to

encourage the cells to detach). Fresh media (8 ml) was added to inhibit the trypsin and the contents of the flask were transferred to a 15 ml falcon tube. The cell suspension was centrifuged (Rotofix 32, Hettich Zentrifugen, Germany) for 5 minutes at 1000 rpm at room temperature and the supernatant discarded. Cells were resuspended in 1 ml of fresh media. To ensure a 1 to 5 passage, 200 µl of cell suspension was added to 15 ml of fresh media in a new T_{75} flask. HL60 cells were split by removing 10 ml of cell suspension from the T_{75} flask and adding the same volume of complete RPMI.

2.2.5 Cryopreservation of Cells

Confluent SKOV3 and MDAMB-231 cells from a T_{75} were cryopreserved to ensure a stock of viable cells was maintained. The old media was removed and cells were trypsinized and centrifuged to produce a pellet as described in section 2.2.4. The pellet was resuspended in 3 ml freezing medium (FBS containing 10 % v/v DMSO) and 1 ml aliquots transferred into 3 cryovials (Nunc). The name, date and cell type was clearly labeled. They were stored overnight in a -80 °C freezer and then transferred to vapour phase liquid nitrogen for long term storage. HL60 cells were transferred to a 15 ml falcon tube and centrifuged for 5 minutes. The supernatant was discarded and the cells resuspended in freezing media as for the other cell types.

2.2.6 Maintenance of Cell Cultures (in T_{75} flasks)

Cell cultures were maintained in T_{75} flasks containing 15 ml fresh media. These flasks were placed in a humidified incubator at 37 °C and 5 % CO_2. The flasks were examined daily under the microscope for signs of contamination and general cell morphology.

Every 2 days, the old media was removed from the T_{75} flask. PBS (10 ml) was added to the flask and removed to eliminate any dead cells. Complete media (15 ml) was then added to the flask and the flask placed back in the incubator.

2.2.7 Cell Counting

A Neubauer haemocytometer was used to count cells. After the cells were trypsinized and centrifuged, the pellet was resuspended in 1 ml media (as described in section 2.2.4). 10 µl of this cell suspension was added to 90 µl of fresh media in an eppendorf, creating a 1:10 dilution. The diluted cells (20 µl) were then pipetted under the coverslip placed on top of the haemocytometer slide. The slide was viewed under a microscope and cells present in the central grid of the device were counted. Cells within two edges of the central square were also counted to take into account any cells on the borders. The number of cells/ml was calculated using equation 1.

Equation 1. Cell density (cells/ml) = Number of cells counted x dilution factor (10) x 10^4

2.3 MTT Reduction Assay

2.3.1 Evaluating Cytotoxic Effects of Hoechst and Iron Cylinder Treatment

Confluent SKOV3 and MDAMB-231 cells maintained in a T_{75} flask were trypsinized and centrifuged as described in section 2.2.4. The supernatant was discarded and the pellet was resuspended in 1 ml complete media. The cells were counted using a Neubauer Haemocytometer and seeded into 96 well plates at 1 x 10^4 cells/well. Plates were left in

the incubator at 37 °C and 5 % CO_2 for 24 hours to ensure they were confluent for treatment the following day.

Following incubation, the media was carefully removed and each well was washed with PBS (warmed to 37 °C). Cells were then treated with Hoechst (2.5 µg/ml) for 20 minutes and then with iron cylinder (0, 10, 25, 35, 50 or 100 µM, repeated in triplicate). Once treated, cells were incubated (5 % CO_2) for 20 minutes at 37 °C. Following incubation, each well was washed with 100 µl of PBS and 100 µl of complete media was added. The MTT (3-[4,5-dimethylthiazol-2-yl]-2,5-diphenyltetrazolium bromide) solution was prepared in PBS (5mg/ml). The plates were incubated for 3 hours (37 °C, 5 % CO_2) with 50 µl MTT solution being added to each well. Following incubation, the media was removed from each well and 100 µl of DMSO was added to solubilise the purple formazan product. DMSO (100 µl) was also added to three empty wells to serve as a blank. The plate was read using a plate reader at an absorbance setting of 540 nM (BIO-TEK, FL600, with KC^4 software). The percentages of viable mitochondria were calculated using the average absorbance of the three readings (DMSO blank adjusted, with the control set to 100 %). A similar procedure was carried out for HL60 cells in eppendorf tubes. After cylinder treatment, cells were centrifuged (1000 rpm, 4 minutes), washed with PBS and the pellet resuspended in media containing MTT. Following 3 hours of incubation, cells were centrifuged, the media was removed and replaced with 100 µl DMSO. Samples were transferred to a 96-well plate and read using the plate reader as described above.

2.3.2 Evaluating Cytotoxic Effects of ATP and Luciferin with Iron Cylinder Treatment

Confluent MDAMB-231 and luciferase-expressing MDAMB-231 cells maintained in a T_{75} flask were trypsinized and centrifuged as described in section 2.2.4. The cells were seeded into 96 well plates at 1 x 10^4 cells/well and incubated for 24 hours as described in section 2.3.1. Following incubation, the media was carefully removed and each well was washed with PBS (warmed to 37 °C). Cells were incubated (5 % CO_2) with iron cylinder (0, 10, 25, 35, 50 or 100 µM final concentration in final volume of 100 µl, repeated in triplicate) for 20 minutes. Following incubation, each well was washed with 100 µl of PBS and 100 µl of complete media was added. Cells were then treated with ATP and luciferin (final concentration of 1 mM for each in final volume of 100 µl). Following treatment, the plates were incubated with MTT using the procedure described in section 2.3.1 and mitochondrial viability was calculated in the same way.

2.4 Live Cell Fluorescence Imaging via Epifluorescence Microscopy

SKOV3, MDAMB-231 and HL60 cells were grown in 50 mm MatTek glass bottom petri dishes (seeded at 1.5 x 10^5 cells/well). After a 24 hour attachment period for SKOV3 and MDAMB-231, cells were preincubated with 2.5 µg/ml Hoechst 34580 in 3 ml culture medium for 20 minutes. Cells were then treated with iron cylinder for 20 minutes and imaged using a Nikon Eclipse Ti epifluorescence microscope (100x objective). Fluorescent and brightfield images were acquired before and after the treatment period. To prevent photobleaching, the laser was turned off following image capture. The samples were maintained at 37 °C by means of a heated stage.

2.5 Live Cell Fluorescence Imaging via Confocal Microscopy

GFP-expressing MDAMB-231 cells were grown in 50 mm MatTek glass bottom petri dishes (seeded at 1.5 x 10^5 cells/well). Cells were incubated for a 24 hour attachment period at 37 °C. Cells were viewed under the Leica DM IRE2 (63x objective) confocal system and nuclei were identified by focusing in the Z-plane. Cells were then treated with iron cylinder for 20 minutes, imaged and fluorescent/ brightfield images were acquired before and after the treatment period. To prevent photobleaching, the laser was turned off following image capture. The samples were maintained at 37 °C by means of a heated stage.

2.6 Quantifying Fluorescence Quenching via Fluorimetry and Flow Cytometry

Confluent SKOV3 and MDAMB-231 cells maintained in a T_{75} flask were trypsinized and centrifuged as described in section 2.2.4. The supernatant was discarded and the pellet was resuspended in 1 ml media. The cells were counted using a Neubauer Haemocytometer and seeded into 6 well plates at 1.5 x 10^5 cells/well. Plates were left in the incubator (37 °C, 5 % CO_2) for 24 hours to ensure they were confluent for treatment the following day. HL60 cells were used immediately after being seeded into wells (1.5 x 10^5 cells/well) as there was no need for attachment in this cell type.

MDAMB-231 and SKOV3 cells in the 6 well plates were trypsinized and centrifuged. HL60 cells were centrifuged and washed with PBS. Each pellet was resuspended in 1ml complete media containing 2.5 µg/ml Hoechst 34580 for 20 minutes at 37 °C. The iron cylinder was then added followed by a further 20 minute incubation at 37 °C. The

fluorescence of 200 µl of each sample was measured using a TECAN GENios Multifunction Microplate reader (λ_{exc} = 340 nm, λ_{em} = 460 nm). The remaining 800 µl of each sample was transferred to a FACS tube and 10,000 events counted using the BD FACS Aria Cell-Sorting System. Fluorescent cells (λ_{exc} = 340 nm, λ_{em} = 460 nm) were gated to eliminate the debris from the whole-cell population. Hoechst fluorescence was presented as a histogram with a distinct peak. The median value for each histogram was obtained and used in analysis. Three repeats were present at each concentration of iron cylinder used (0, 10, 25, 35, 50 and 100µM).

2.7 ToxiLight Assay

The ToxiLight assay is a bioluminescent, non-destructive cell lysis assay kit which measures the release of the enzyme, adenylate kinase from damaged cells into the surrounding media.

MDAMB-231 cells were seeded into 96-well plates at $1x10^4$ cells/well. Cells were treated with iron cylinder (0, 10, 25, 35, 50 or 100 µM in final volume of 100 µl) with 3 repeats present for each concentration tested. The plates were incubated for 20 minutes at 37 ^{0}C. Cell supernatant (20 µl) was transferred to a white-walled 96-well plate and 100 µl of adenylate kinase detection reagent was added to each sample. The plates were left to stand for 5 minutes for signal generation and the emitted light intensity was measured using a plate reader (TECAN GENios multifunction microplate reader). Positive control samples were present where cells were treated with a 100% lysis buffer and negative controls where no treatment or detection reagent was used.

The cylinder's ability to interfere with the ToxiLight kit was confirmed using whole cell lysate. A confluent T_{75} flask containing MDAMB231 cells was treated with lysis reagent (100 %) for 5 minutes at 37 ^{0}C. Aliquots of media (20 µl) were removed from the flask and transferred to a 96-well plate. Each well was then treated for 20 minutes with iron cylinder (0, 10, 50, 100 or 150µM) and 100 µl of adenylate kinase detection reagent was added to each well. Emitted light intensity was measured using the same procedure described above with each concentration of iron cylinder being tested in triplicate.

2.8. Investigating Inhibition of Luciferase by Iron Cylinder

The assay was carried out in a 96-well luminescence plate in the absence of cells. To bypass the first step of the ToxiLight assay, an excess of ATP was added to each well (1 mM). Concentrations of iron cylinder were then added (0, 10, 25, 35, 50 or 100 µM) keeping the final volume in each well at 20 µl. This was followed by 100 µl of adenylate kinase detection reagent in each well. Plates were incubated for 5 minutes before reading the luminescence. Each concentration was tested in triplicate. The synthesized ligand, it's components (4,4‟-methylenedianiline and pyridine-2-carboaldehyde) and iron (II) chloride tetrahydrate were also investigated for their role in luciferase inhibition. Each compound was made up in solution to the same concentration as present in the synthesized cylinder at each of the concentrations of cylinder tested. Each compound was examined using the method described above for iron cylinder. The chelating ligands: 2,2'-bipyridine and 1,10'-phenanthroline were also tested using the same method.

2.9 Quantifying Luminescence Production in MDAMB-231 Cells Stably Expressing Luciferase

MDAMB-231 and luciferase-expressing MDAMB-231 cells[2,3] were seeded into 96 well luminescence plates and incubated for 24 hours as described in section 2.3.2. ATP and luciferin were added to each well (1 mM for each in final volume of 100 µl) prior to recording luminescence. Emitted light intensity was measured using a plate reader (TECAN GENios multifunction microplate reader). Luminescence production was quantified over time using the same method where emission was recorded at 3 minute intervals over a 30 minute period.

2.10 Investigating Iron Cylinder's Inhibition of Luminescence in Luciferase-Expressing MDAMB-231 Cells

Confluent T_{75} flasks containing MDAMB-231 and luciferase- expressing MDAMB-231 cells were treated with lysis reagent (100 %) for 5 minutes at 37 ^{0}C. Aliquots of media (20 µl) were removed from each flask and transferred to a 96-well plate. Each well was then treated with iron cylinder (0, 10, 25, 35 50 and 100µM) for 20 minutes at 37 ^{0}C. ATP and luciferin were supplied (1 mM for each in final volume of 100 µl) prior to recording luminescence. A negative control was also present for each cell type where substrates were not provided before the luminescence recording. Each concentration of iron cylinder was tested in triplicate. The luminescence values shown in the results were calculated using the average of three readings. Emitted light intensity was measured using a plate reader (TECAN GENios multifunction microplate reader).

Trypsinized cells were also investigated where cells were seeded into 96 well plates as described in section 2.3.2. Following the 24 hour incubation, the media was carefully removed and each well was washed with PBS (warmed to 37 °C). Cells were then trypsinized where 30 µl trypsin was added to each well for 5 minutes at 37 °C. Trypsin was inhibited by adding 100 µl complete media to each well. Cells were then transferred to eppendorfs and centrifuged (1000 rpm, 4 minutes), washed with PBS and the pellet resuspended in 1 ml complete media treated with iron cylinder as described above. Following incubation, cells were centrifuged, washed with PBS and transferred to a 96-well luminescence plate. ATP and luciferin were supplied and the light emission quantified in the same way as described above. Adherent cells were also investigated using a similar procedure in 96 well plates. Following the 24 hour incubation period needed for cells to attach, cells were washed and treated with iron cylinder in the same way. Cells were then washed with PBS and treated with ATP and luciferin prior to recording luminescence as described above.

2.11 Investigating Quenching of Purified GFP by Iron Cylinder

Purified GFP in solution (250 µg/ml) was purchased from Applied Biological Materials Inc. The assay was carried out in a 96-well fluorescence plate in the absence of cells. GFP (0.5 µM in final volume of 100 µl) was added to distilled water. Each well was treated with concentrations of iron cylinder (0, 10, 25, 35, 50 and 100 µM in final volume of 100 µl) for 20 minutes at 37 ^{0}C for each incubation period. The fluorescence of purified GFP was measured using a fluorimeter (TECAN GENios multifunction microplate reader) (λ_{exc} = 485 nm, λ_{em} = 530 nm). Three repeats were collected at each

concentration of iron cylinder tested and the data was blank adjusted to remove background fluorescence of cylinder alone for each of the concentrations investigated.

2.12 Investigating GFP Quenching by Iron Cylinder in MDAMB-231 Cells Stably Expressing GFP

GFP-expressing MDAMB-231 cells[1, 2] were seeded into a 96 well fluorescence plate at 1 x 10^4 cells/well as described in section 2.2. The plate was left in the incubator at 37 °C and 5 % CO_2 for 24 hours to ensure cells were confluent for treatment the following day. Following incubation, the media was carefully removed and each well was washed with PBS (warmed to 37 °C). Cells were treated with iron cylinder and the fluorescence recorded as described in section 2.11. The data was blank adjusted using fluorescence values obtained from non-expressing MDAMB-231 cells treated with concentrations of cylinder in the same way.

2.13 Investigating Hoechst Quenching by Iron Cylinder in GFP-Expressing MDAMB-231 Cells

MDAMB-231 and GFP-expressing MDAMB-231 cells were seeded into 96 well fluorescence plates and incubated for 24 hours in the same way as described in section 2.12. Cells were washed with PBS prior to incubation with 2.5 µg/ml Hoechst 34580 for 20 minutes at 37 °C. Cells were then treated with concentrations of iron cylinder (0, 10, 25, 35, 50, 100 µM) for 20 minutes at 37 ^{0}C. Cells were washed with PBS prior to recording fluorescence. Each concentration of iron cylinder was tested in triplicate. The fluorescence was recorded in the same way as described in section 2.11. The data was

blank adjusted using fluorescence values obtained from cells treated with concentrations of cylinder alone.

2.14 Comparing the Intensity of Fluorescence Quenching between Hoechst and GFP in GFP-Expressing MDAMB-231 Cells

GFP-expressing MDAMB-231 cells were seeded into a 96 well fluorescence plate at 1 x 10^4 cells/well as described in section 2.2. The plate was left in the incubator at 37 °C and 5 % CO_2 for 24 hours to ensure cells were confluent for treatment the following day. Cells were washed with PBS prior to incubation with 2.5 µg/ml Hoechst 34580 for 20 minutes at 37 °C. Cells were then treated with 50 µM iron cylinder for 20 minutes at 37 ^{0}C. Cells were washed with PBS. Two experiments were set up. In the first, the cylinder treatment was washed away and the fluorescence recorded at 20 minute intervals over 3 hours (λ_{exc} = 340 nm, λ_{em} = 460 nm for Hoechst, λ_{exc} = 485 nm, λ_{em} = 530 nm for GFP) using a fluorimeter (TECAN GENios multifunction microplate reader). The data was adjusted using fluorescence values obtained from cells treated with cylinder alone. The average fluorescence of three readings was used for each time point investigated. In the second, the cylinder treatment was not washed away and left in contact with the cells for the duration of the experiment. The fluorescence was recorded similarly to the first experiment.

2.15 *In Vivo* Toxicity Studies

Zebrafish embryos at one-cell stage were injected using an injection needle pulled from borosilicate glass micro-capillary (with Fillament, OD 1.0 mm, ID 0.78 mm, Harvard

Apparatus) on P-97 Flaming/Brown Micropipette Puller (Sutter Instruments). The injection were performed by hand using a MINJ-1 microINJECTOR(tm) System (Tritech Research) under Nikon SMZ660 Zoom Stereo Microscope. Each embryo was injected with 1.5-2 nl injection solution supplemented with 0.1 % Phenol Red (Sigma) as injection marker.

Following injection the embryos were maintained at 28 °C in E3 media, supplemented with 50 microgram per ml gentamicin (Fisher) to prevent bacterial and fungal growth. E3 media consisted of 5.0 mM NaCl, 0.17mM KCl, 0.33mM Ca_2Cl, 0.33mM MgSO4, 2.3mM $NaHCO_3$ and had a pH of 7.4. Embryos were injected with 10 or 100 µM compound and survival was quantified by counting live embryos at 4 and 24 hours post fertilization (hpf). The percentages of viable embryos shown in the results were calculated using the average count of three experiments.

2.16 *In Vitro* Genotoxicity Studies

2.16.1 Alkaline Comet Assay

Confluent HL-60 cells maintained in a T_{75} flask were centrifuged as described in section 2.2. The supernatant was discarded and the pellet was resuspended in 1 ml media. The cells were counted using a Neubauer Haemocytometer and seeded into 6 well plates at 1.5 x 10^5 cells/well. Cells were treated with each compound for 8 hours at 37 °C. Following treatment, cells were transferred to eppendorfs and centrifuged at 1000 rpm for 4 minutes. Cells were then washed twice with PBS before being resuspended in 150µl of PBS. 15µl of the re-suspended cells was transferred to a sterile eppendorf containing 300

µl molten 2% low melting point agarose (LMPA). This cell suspension (150µl) was then transferred to a glass microscope slide pre-coated with 0.5 % normal melting point agarose (NMPA). A glass cover slip was then carefully placed on top of each slide. Slides were left to stand on a metal tray over ice and for approximately 20 minutes at 4 °C to allow the agarose to solidify.

Coverslips were then removed and the slides were incubated for 1h at 4° C in cold lysis buffer (2.5M NaCl, 0.1M Na_2-EDTA, 10mM Tris base, 1% sodium N-lauryl sarcosinate, 10% DMSO and 1% Triton X-100, pH 10).[4] Following lysis, slides were placed in a horizontal electrophoresis tank filled with cold electrophoresis buffer (300mM NaOH and 1mM Na_2-EDTA) for 20min without electrophoresis and were then electrophoresed for 20min (32V, 300mA). Slides were washed three times at five minute intervals using cold neutralization buffer (0.4 M Tris base, pH 7.5). Slides were then stained by adding 50µl SYBR gold (1 x solution) to each slide and carefully placing a cover slip over the top. Slides were stored in the dark at 4 °C overnight. Slides were examined with the 20 X lens using a Axiovert 10 inverted fluorescence microscope (Zeiss Ltd, Göttingen, Germany). Image analysis was carried out using the Comet 4.0 software program and 100 cells on each slide were randomly selected for analysis. The median percentage tail intensity was chosen to assess the extent of DNA damage. Median values obtained for 3 separate experiments were analyzed for each compound investigated.

2.16.2 Neutral Comet Assay

The same procedure was followed as described for the alkaline comet assay (section 2.16.1) using lysis buffer (146 mM NaCl, 30 mM Na_2-EDTA, 1 mM Tris-HCL, 1% sodium N-lauryl sarcosinate, pH 9) and electrophoresis buffer (0.4 M Tris Base, pH 8.3).[4]

2.17 Statistical Analysis of Data

Statistical analysis of all the data was carried out using SPSS statistics 20. The data was tested for normal distribution using the Shapiro-Wilk test. If the data was found not to be normally distributed, non-parametric statistics were used (Kruskal Wallis test, Mann-Whitney U test). Normally distributed data was tested for homogeneity of variances using Levene Statistic. If the data showed no homogeneity of variances, non-parametric statistics were used. For data showing homogeneity of variances, parametric statistics were used (One-way ANOVA with Post-hoc: Tukey test).

2.18 References

[1] Hotze, A. C., Hodges, N. J., Hayden, R. E., Sanchez-Cano, C., Paines, C., Male, N., Tse, M. K., Bunce, C. M., Chipman, J. K. Hannon, M. J. (2008) Supramolecular iron cylinder with unprecedented DNA binding is a potent cytostatic and apoptotic agent without exhibiting genotoxicity. *Chem. Biol*. 15 (12): 1258-1267.

[2] Rowan, B. G., Gimble, J. M., Sheng, M., Anbalagan, M., Jones, R. K., Frazier, T. P., Asher, M., Lacayo, E. A., Friedlander, P. L., Kutner, R., Chiu, E. S. (2014) Human Adipose Tissue-Derived Stromal/Stem Cells Promote Migration and Early Metastasis of Triple Negative Breast Cancer Xenografts. *PloS One.* 9 (2): 1-13.

[3] Zhang, K.,Chou, C. K., Xia, X., Hung, M. C., Qin, L. (2014) Block-Cell-Printing for live single-cell printing. *Proc. Natl. Acad. Sci. USA.* 111 (8) 2948-2953.

[4] Peycheva, E., Georgieva, M., Miloshev, G. (2009) Comparison between alkaline and neutral variants of yeast comet assay. *Biotechnol and Biotechnol.* 23 (1): 1090-1092.

CHAPTER 3

Hoechst Quenching as a Novel Method of Imaging the Non-Fluorescent Iron Cylinder

3.1 Introduction

The ability of the iron cylinder to stall the replication fork, inhibit cell cycle progression and induce apoptosis in the absence of genotoxicity suggests its potential use in anticancer treatment.[1] Research has been carried out to associate the cellular activity of the cylinder with its non-covalent methods of DNA-binding.[1] Due to its lack of fluorescence, the iron cylinder cannot be imaged directly by fluorescence microscopy. Although the ruthenium analogue is fluorescent, it is difficult to synthesize and does not have strong fluorescence.[2] To help improve our understanding of the cellular fate and activity of the iron cylinder, indirect methods of imaging the cylinder need to be developed.

Fluorescence occurs when an atom or molecule that has absorbed a photon of a particular wavelength, emits a photon of another wavelength. During the absorption/emission process, some energy is shifted to vibration and rotation leading to a reduction in energy (increase in wavelength) of the light emitted. The shift between the maximum of the excitation and emission curves is known as Stokes' shift. Fluorescent probes that have a very small Stokes' shift have limited use in fluorescence imaging as the sensitivity of detection is limited due to an inability to accurately separate the excitation and emission light.[3] Fluorophores can repeatedly undergo the fluorescence process which is very useful as a single fluorophore molecule can produce a signal many times. Therefore visualization of microscopic samples via fluorescence is an extremely sensitive method as very small concentrations of stain can be visualized.[4] One potential problem is that fluorophores are vulnerable to degradation due to their structural instability during the

excited lifetime. The structure of the fluorophore may change due to illumination at high intensity. This process is known as photobleaching and the fluorophore no longer fluoresces.[4] The use of fluorophores is necessary in fluorescence microscopy to observe structures of interest inside a specimen. For accurate measurements of fluorescence to be gained, the stain of choice should have stable fluorescence, be specific in its binding and be able to penetrate deep into tissue sections. Stains with distinct properties have been exploited for a diverse range of applications. There are three main classes of DNA stains. These are minor-groove binders (Hoechst and DAPI stains), intercalating dyes (propidium iodide and ethidium bromide) and other miscellaneous DNA stains (acridine orange).[4]

Hoechst 34580, 33342 and 33258 are supravital cell membrane-permeable bisbenzimide dyes which bind to the minor groove of double stranded DNA with a preference for AT-rich regions (4-5 base pairs in length) (Figure 3.1). Hoechst 33258 is less membrane permeable than 33342 although all three are relatively non-toxic and soluble in water. When bound to nucleic acids, Hoechst 34580 has a longer wavelength spectrum when compared to the other dyes. When excited by ultraviolet light (around 350 nm), they emit a cyan/blue fluorescence with an emission maximum around 461 nm. Hoechst stains are used for labeling in flow cytometry, fluorescence activated cell sorting and fluorescence microscopy. [4] Other fluorescent DNA stains include the blue nucleic acid stain, DAPI, which binds to the minor groove of DNA. DAPI (λ_{exc} = 358 nm, λ_{em} = 461 nm) binds double stranded DNA which causes a 20 fold increase in fluorescence intensity. This is believed to be caused by its protection from water when in minor groove of DNA.[4]

Unlike Hoechst, DAPI does not penetrate cell membranes and cannot be used to stain live cells. This makes the Hoechst the dyes of choice for live cell DNA staining.

A

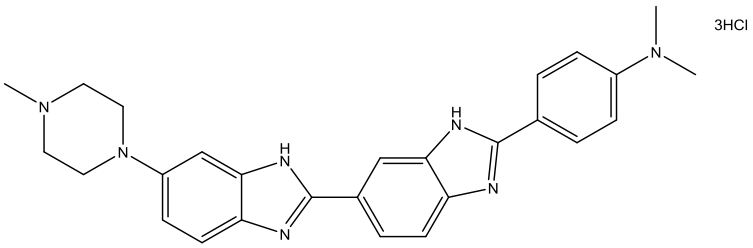

B

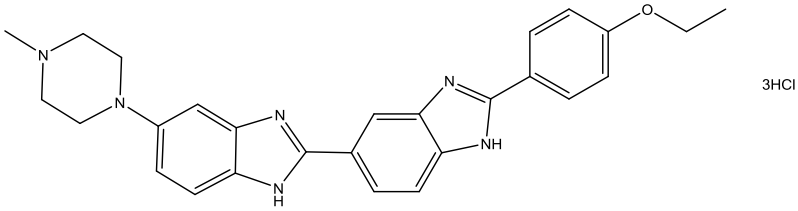

C

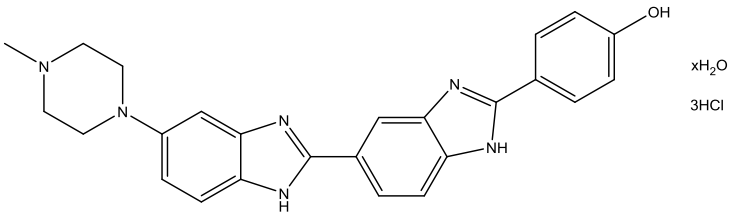

D

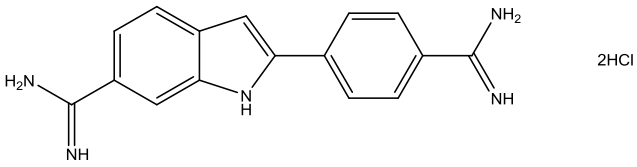

Figure 3.1. *Molecular structures of Hoechst dyes* ***(A)*** *34580* ***(B)*** *33342* ***(C)*** *33258 and* ***(D)*** *DAPI.*

To enable longer lengths of DNA to be recognized, the structure of the dyes can be expanded.[5] Two Hoechst 33258 moieties linked together were developed to recognize DNA with two A3T3 motifs. Due to the flexibility of the link, the molecule was able to bind to a separating DNA duplex with two A3T3 motifs. Despite this, it is also able to bind to a DNA 3-way junction where A3T3 motifs exist separately in two different arms.[6]

Recently, the covalent binding anticancer trinuclear platinum drug, BBR-3464 was investigated. The Pt-DNA interstrand adducts formed by this drug were found to be different from those formed by the classic chemotherapeutic, cisplatin. Cytotoxicity studies revealed the drug's uptake into ovarian cancer cell lines (SKOV3 and A2780) to be much greater than that of cisplatin. Kinetic analysis into the crosslinking occurring revealed changes in the AT pairs of the double helix which were consistent with pre-association occurring in the minor groove of DNA. Competition binding studies between minor groove ligands and BBR-3464 were carried out. The Hoechst 33258 dye was used which binds in the minor groove of DNA with high affinity for sequences rich in AT regions (Figure 3.2). The strength of binding was analysed and results showed that the interaction of Hoechst with DNA was improved in the presence of BBR-3464 as identified by increased Hoechst fluorescence intensity. Structural analysis of the interaction between Hoechst and DNA revealed that an induced fit and a choice of conformation were involved in the process. The level of induced fit was influenced by conformational changes in the sugar-phosphate DNA backbone and changes in base step factors.[7]

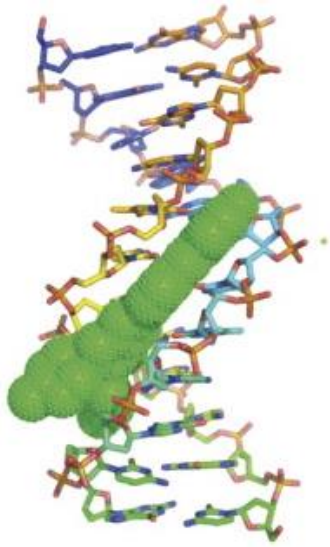

Figure 3.2. *Groove binding of Hoescht 33258 to the minor groove of DNA. Taken from ref 8.*

Fluorescence is commonly used in biochemistry to detect various compounds especially as an indicator in immunoassays. Fluorescence indicators provide many advantages including possible combination with dyes that have different excitations and emissions, highly sensitive measurements, availability of detection instruments and a range of markers that can be conjugated to reagents of interest.[9] The process by which a molecule's fluorescence intensity is reduced is referred to as fluorescence quenching. Fluorophore quenching can occur through a number of processes such as energy transfer, collision, formation of complexes and excitation reactions.[10] The occurrence of dynamic or collisional quenching involves collision leading to production of a transient complex between a fluorophore in the excited state and a quencher in the ground state. Upon deactivation, the complex in the excited state dissociates, which results in both the fluorophore and quencher returning to the ground state. Diffusion controls the process of

dynamic quenching as the quencher has to diffuse to the fluorophore during its lifetime in the excited state. Furthermore, when a non-fluorescent complex is produced between a quencher and fluorophore in the ground state, the method is known as static quenching.[10]

The commonly prescribed antibacterial drug, norfloxacin was recently investigated for fluorescence quenching by the metal ions, Mn^{2+} Cu^{2+}, Co^{2+} and Ni^{2+}. Results showed that when metal quenchers were added to a solution of norfloxacin, quenching took place even when very low concentrations were used. Quenching constants obtained were found to be much larger than would be expected with a diffusion- controlled mechanism of quenching. This was similar to values obtained for quenching constants of other closely related antibiotics. The results indicated that binding interactions were occurring between quencher and fluorophore as the constant value was beyond the limit of diffusion-controlled mechanisms.[10] The emitted fluorescence of the drug was reduced via formation of complex and collisional quenching. The large static and bimolecular quenching constants provided supporting evidence for strong orbital-orbital and ion-dipole interactions between metal quenchers and norfloxacin. From the metal cations investigated, the electron scavenger, Cu^{2+} was found to be most efficient at quenching the fluorescence.[10]

Recently studies were carried out to investigate the interactions of human serum albumin with the antipsychotic drug, chlorpromazine using fluorescent techniques. Researchers hoped to obtain information about the mechanism of quenching and fluorescence resonance energy transfer between chlorpromazine (Figure 3.3) and human serum

albumin. Spectral results showed a reduction in fluorescence intensity of the tryptophan in human serum albumin with increasing concentrations of the drug. As the emission wavelength of the tryptophan residue remained stable this suggested that the chlorpromazine/albumin interaction did not cause conformational changes in the protein's structure. This research provided methods to study drug-protein interactions through the use of fluorescence techniques. Results found chlorpromazine to interact with the protein through both static and dynamic quenching mechanisms. This work was of important biological significance as albumin is a transporter for numerous clinical drugs and its interactions have not been well studied.[11]

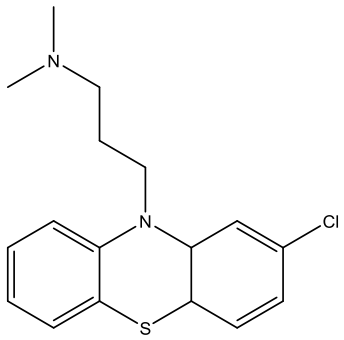

Figure 3.3. *The structure of Chloropromazine.*

Changes to the transmembrane mitochondrial potential are often examined through the use of fluorescent probes. In a recent study, the fluorescent mitochondrial dye, MitoTracker Red CMXRos (Figure 3.4) was used to investigate the effect of the anticancer drug, adaphostin (Figure 3.5) on mitochondria in live cells as well as isolated mitochondria.[12] The study aimed to confirm whether or not the drug interacted directly with the mitochondria. Through the use of an ion-selective electrode, adaphostin produced no effect on the transmembrane potential or on oxidative phosphorylation in

mitochondria. Despite this, the drug was found to interfere with membrane potential when fluorescent mitochondrial dyes were used.

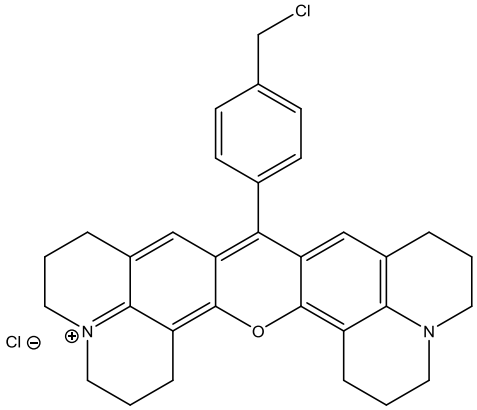

Figure 3.4. *The structure of Mitotracker red.*

Adaphostin was initially found to decrease fluorescence of MitoTracker Red in both isolated mitochondria and live cells. This fluorescence quenching was similar to that observed by compounds well-known for their disruption of the mitochondrial membrane potential. However, further investigations provided evidence against adaphostin's ability to directly affect the function of mitochondria. The drug did not cause cytochrome c leakage from the mitochondria. In addition, inhibitors of membrane potential did not prevent adaphostin –induced fluorescence quenching. Furthermore, using a non-fluorescent ion-selective probe did not produce any drug-induced reduction in membrane potential. This data provided evidence for adaphostin-induced fluorescence quenching of MitoTracker Red being due to a direct interaction. Moreover, the addition of adaphostin to solutions containing fluorescent mitochondrial dyes resulted in a decreased fluorescence.[12] This study highlights that caution should be taken when using fluorescent dyes to monitor changes in mitochondrial membrane potential.

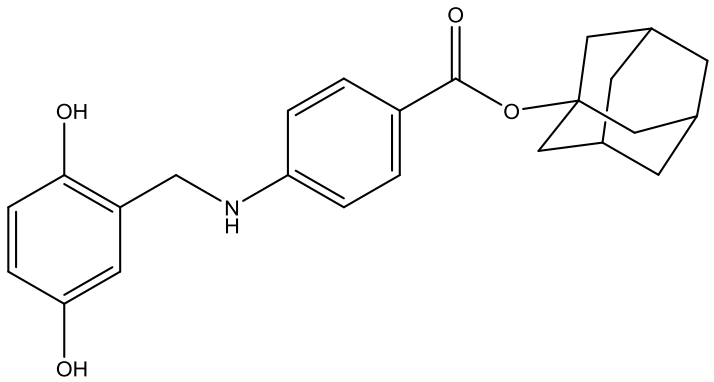

Figure 3.5. *The structure of Adaphostin.*

As the iron cylinder is not fluorescent, it is important to develop methods to image it indirectly. One potential method would be to investigate its ability to quench the fluorescence of the Hoechst molecule or displace it. It is known that the cylinder can quench Hoechst on DNA *in vitro*. It is assumed that occurs by Hoechst displacement from the minor groove when cylinder binds in close proximity in the major groove. In this chapter, iron cylinder's ability to quench nuclear fluorescence from cells stained with Hoechst 34580 was investigated. In three different cancer cell types: SKOV3, MDAMB-231 and HL60, epifluorescence microscopy was used to directly image changes in nuclear Hoechst fluorescence following treatment with iron cylinder. Flow cytometry was carried out to quantify changes occurring in the fluorescence of a large population of cells when treated with different concentrations of compound.

3.2 Results and Discussion

Their ability to act on DNA in a different way to cisplatin makes these metal cylinders a novel exciting group of agents. The iron cylinder not only binds to the DNA major groove but also fits into Y-shaped junctions including the fork junction important in

DNA replication. Its lack of fluorescence makes the iron cylinder difficult to image using fluorescence microscopy in cells. A focus for this thesis therefore, is to develop indirect ways of imaging this cylinder to identify its location in cells and help us to better understand its mechanism of action.

It is known that iron cylinder has the ability to competitively displace ethidium and propidium from DNA in vitro.[13] However, it can also displace other binders of DNA including Hoechst dyes.[14] An initial study had described how HL60 myeloid leukemia cells were incubated with the Hoechst dye for 20 minutes prior to being treated with increasing concentrations of iron cylinder for 20 minutes. The cells were then collected, washed twice, resuspended in PBS and the fluorescence signal recorded. The results identified a concentration-dependent decrease in the Hoechst fluorescence signal with increasing concentrations of iron cylinder.[14] This was consistent with the cylinder entering the cell nucleus, binding to the major groove of DNA and either displacing or quenching the Hoechst dye from the minor groove resulting in a decrease of nuclear fluorescence. This was the starting point for the work described in this chapter; which seeks to extend the work to investigate in more detail the cylinder's ability to quench nuclear Hoechst 34580 fluorescence in adherent cell lines (SKOV3, human caucasian ovary adenocarcinoma, MDAMB-231, human caucasian breast adenocarcinoma) as well as non-adherent cell lines (HL60, human caucasian promyelocytic leukaemia).

3.2.1 Cytotoxicity

To identify suitable non-toxic concentrations of cylinder and Hoechst for the experiments, cell viability was first assessed via an MTT assay. The MTT assay is a sensitive method of measuring the reductive function of mitochondria in cells and provides a measure of an endpoint related to cell viability. Metabolically active cells reduce the yellow tetrazolium MTT (3-(4, 5-dimethylthiazolyl-2)-2, 5-diphenyltetrazolium bromide) by the action of dehydrogenase enzymes generating the purple product, formazan. This is then solubilised and quantified by spectrophotometric means.

Mitochondrial MTT reduction was measured at five different concentrations of iron cylinder to determine non-toxic concentrations for treating SKOV3, MDAMB-231 and HL60 cells. The assay was carried out following treatment with Hoechst and then iron cylinder (20 minutes at 37 ^{0}C for each incubation period). The percentages of viable cells shown in the results were calculated using the average absorbance of three readings (DMSO blank adjusted) (Figure 3.6). The results show no significant reduction in the number of viable cells when treated with these concentrations of iron cylinder for these periods. Over 94% of SKOV3 and 98 % of MDAMB-231 and HL60 cells remained viable even when treated with the top concentration of 100 µM cylinder. Therefore, the MTT assay identified that concentrations at or below 100 µM would not significantly disrupt mitochondrial function which was used as an indicator of cell viability. Further evidence of viability was provided by assessing cell morphology at each of the concentrations tested. This involved visualizing the cells under the microscope to ensure

the membranes were intact and the cells were not showing any signs of stress. As a result, throughout this thesis, concentrations of 0, 10, 25, 35, 50 and 100 µM were selected for use in the assays.

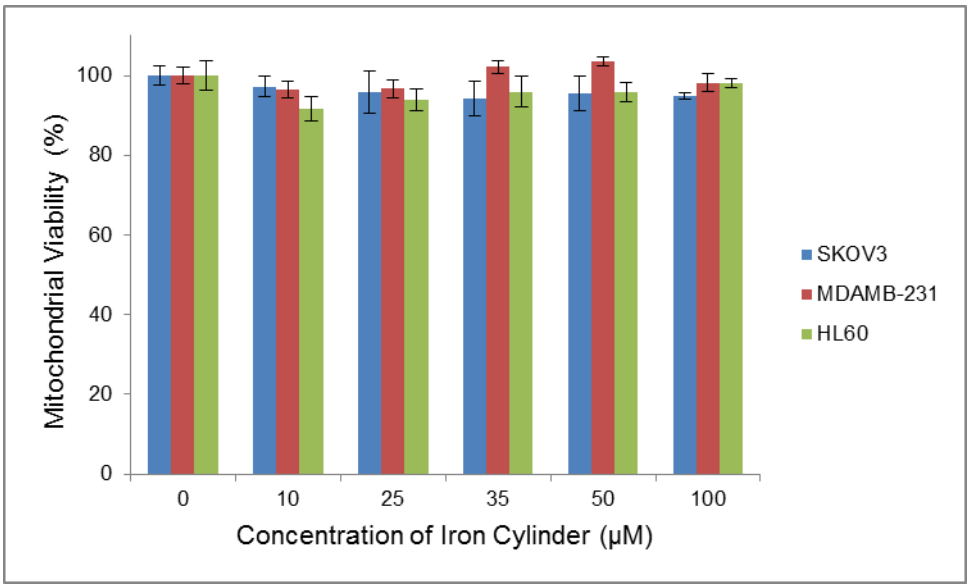

Figure 3.6. *Evaluation of cytotoxic effects of Hoechst and Iron cylinder treatment in SKOV3, MDAMB-231 and HL60 cells using the MTT assay. Cells were treated with Hoechst (0.5 µg/ml) followed by treatment with iron cylinder for 20 minutes at 37 ^{0}C prior to measuring MTT reduction. Values are the mean of three separate experiments ± S.E.M. No significant difference from control ($p>0.05$ in SKOV3, MDAMB-231 and HL60 cells, One-way ANOVA).*

3.2.2 Investigating Fluorescence Quenching via Live Cell Fluorescence Imaging

Live SKOV3, MDAMB-231 and HL60 cells grown in MatTek dishes were imaged by epifluorescence microscopy. Cells were pre-incubated with Hoechst for 20 minutes followed by treatment with 50 µM iron cylinder for 20 minutes. Brightfield and

fluorescent images were acquired at the start and end of the 20 minute cylinder treatment period with the laser turned off in between to prevent photobleaching. The fluorescence of the nucleus was monitored visually for changes. (Figures 3.7, 3.8 and 3.9).

A **Time: 0 minutes** **Time: 20 minutes**

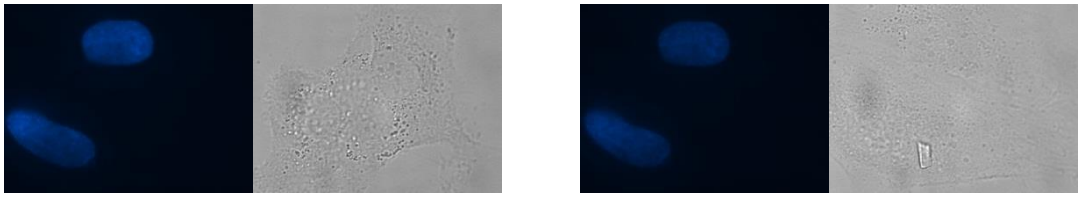

B **Time: 0 minutes** **Time: 20 minutes**

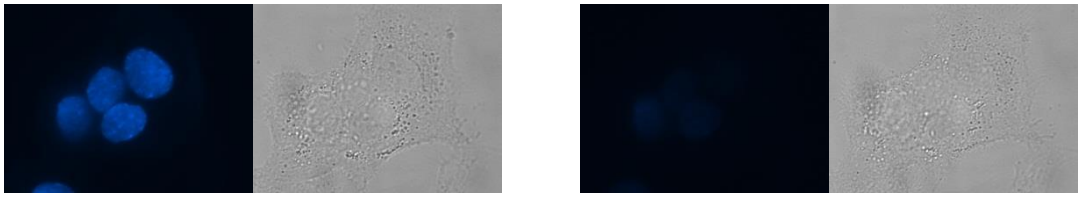

Figure 3.7. *Epifluorescence imaging showing fluorescent and brightfield images of SKOV3 cells treated with Hoechst for 20 minutes followed by treatment with 50 µM iron cylinder* ***(A)*** *Fluorescent and brightfield images of untreated control SKOV3 cells imaged at the start and end of the 20 minute period* ***(B)*** *Fluorescent and brightfield images of SKOV3 cells imaged immediately after cylinder treatment and 20 minutes after cylinder treatment.*

A **Time: 0 minutes** **Time: 20 minutes**

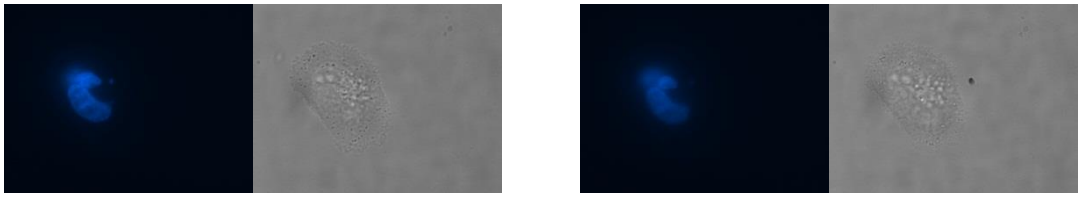

B **Time: 0 minutes** **Time: 20 minutes**

Figure 3.8. *Epifluorescence imaging showing fluorescent and brightfield images of MDAMB-231 cells treated with Hoechst for 20 minutes followed by treatment with 50 µM iron cylinder* ***(A)*** *Fluorescent and brightfield images of untreated control MDAMB-231 cells imaged at the start and end of the 20 minute period* ***(B)*** *Fluorescent and brightfield images of MDAMB-231 cells imaged immediately after cylinder treatment and 20 minutes after cylinder treatment.*

A **Time: 0 minutes** **Time: 20 minutes**

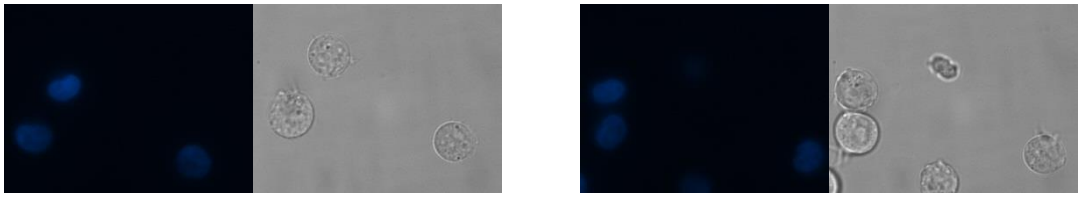

B **Time: 0 minutes** **Time: 20 minutes**

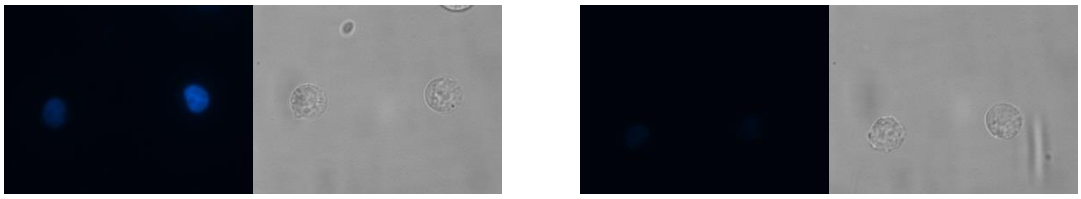

Figure 3.9. *Epifluorescence imaging showing fluorescent and brightfield images of HL60 cells treated with Hoechst for 20 minutes followed by treatment with 50 µM iron cylinder* ***(A)*** *Fluorescent and brightfield images of untreated control HL60 cells imaged at the start and end of the 20 minute period* ***(B)*** *Fluorescent and brightfield images of HL60 cells imaged immediately after cylinder treatment and 20 minutes after cylinder treatment.*

Previous work had explored effects on a bulk cell population using fluorimetry on a suspension of HL60 cells in a cuvette. Now in this work, fluorescence microscopy was used to image changes occurring in the intensity of nuclear Hoechst fluorescence of live

cells following treatment with iron cylinder. This allows the effect on individual cells to be visualised directly.

For each of the three cell types investigated, the results show a visual decrease in the fluorescence intensity of the nucleus at the end of each treatment period when compared to the untreated control cells (Figures 3.7, 3.8 and 3.9). This is consistent with the cylinder entering the nucleus and displacing Hoechst from the minor groove due its close proximity in the major groove. The results demonstrate that a non-fluorescent compound binding to the DNA can be indirectly imaged by its ability to quench another fluorescent molecule nearby. These results reflect changes taking place at a cellular level and any conclusions made can only be representative of the small number of selected cells in view. To quantify Hoechst quenching and investigate its occurrence in the entire sample population, flow cytometry and fluorimetry studies were undertaken.

3.2.3 Quantifying Hoechst Fluorescence via Fluorimetry and Flow Cytometry

Hoechst fluorescence for all three cell types at each cylinder concentration tested was measured. Adherent SKOV3 and MDAMB-231 cells were trypsinized and centrifuged and non-adherent HL60 cells were centrifuged. Cells were counted and pre-incubated with Hoechst 34580 for 20 minutes at 37 ^{0}C. This was followed by a further 20 minute incubation at 37 ^{0}C with concentrations of iron cylinder. 20 % of each sample was removed for analysis by fluorimetry (BIO-TEK, FL600, with KC^{4} software) which was used to record the fluorescence of the entire population present in each sample (λ_{exc} = 340 nm, λ_{em} = 460 nm).

The remaining 80 % of each sample was analysed by flow cytometry. This involved suspending cells in a fluid stream and passing them through a light beam in single-file. A BD FACSAria Cell-Sorting System was used to count 10,000 events using the Hoechst blue channel (λ_{exc} = 340 nm, λ_{em} = 460 nm). For each sample passing through the flow cytometer, a two-dimensional dot-plot was produced showing the distribution of 10,000 cells counted from each sample. The intact cell population was identified visually and a manual gate was applied to eliminate the debris from the intact-cell population (Figure 3.10A). A single-dimension histogram was plotted representing the median fluorescence intensity for the gated population of each sample (Figure 3.10B). Figure 3.7 represents a visual example of the data collected prior to analysis. Three repeats were undertaken at each concentration of iron cylinder used (0, 10, 25, 35, 50 and 100µM).

A

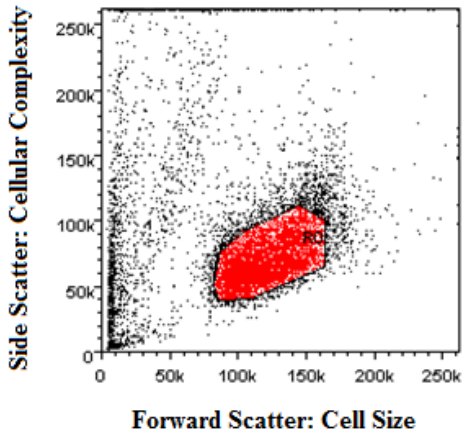

B

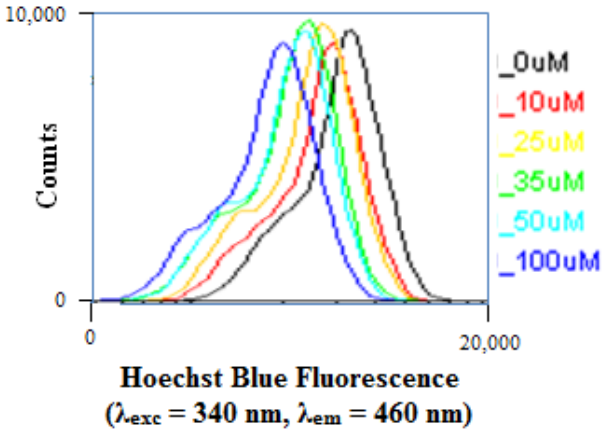

Figure 3.10. *Representative plots for a single experiment obtained by flow cytometry for HL60 cells treated with Hoechst followed by iron cylinder.* ***(A)*** *Representative gating of cells treated with 25 µM iron cylinder. Black represents debris; Red represents viable cells.* ***(B)*** *Histograms produced by cells treated with different concentrations of iron cylinder which were used to obtain median values. For each cell type investigated, 3 similar experiments were undertaken and the average median value was used in the analysis.*

Fluorimetry results for the entire SKOV3 cell population show a concentration-dependent decrease in fluorescence intensity with 100 µM causing a reduction to 23 % of the control ($p < 0.001$, One-way ANOVA followed by Tukey test). Results for the gated population in flow cytometry also show a concentration-dependent decrease in fluorescence but to a lesser extent than that seen by fluorimetry (fluorescence down to 65 % when treated with 100 µM cylinder) (Figure 3.11). These results were found to be very highly significantly different from the control ($p < 0.001$, One-way ANOVA followed by Tukey test).

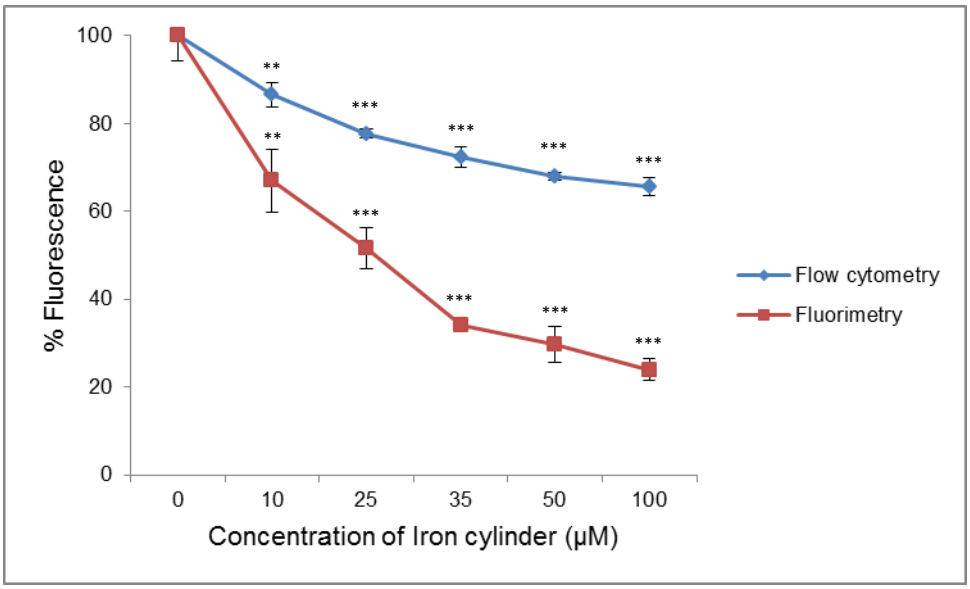

Figure 3.11. *Evaluation of Hoechst fluorescence in SKOV3 cells by fluorimetry and flow cytometry. Cells were collected, treated for 20 minutes with Hoechst followed by 20 minutes with cylinder at 37 ^{0}C prior to measuring fluorescence of the entire sample via fluorimetry and gated population via flow cytometry. Values are the mean of three separate experiments ± S.E.M. Significant difference from control, with p<0.05: *, <0.01: **, <0.001: ***. (One-way ANOVA followed by Tukey test).*

Fluorimetry results for the entire MDAMB-231 cell population show a concentration-dependent decrease in fluorescence intensity with 100 µM causing a reduction to 16 % of the control. Flow cytometry data representing the gated population also showed a decrease in fluorescence with increasing cylinder concentration but again to a lesser extent than that seen by fluorimetry (fluorescence down to 47 % when treated with 100 µM cylinder) (Figure 3.12). These results showed that there was a very highly significant difference between the control and all the concentrations tested ($p < 0.001$, One-way ANOVA followed by Tukey test).

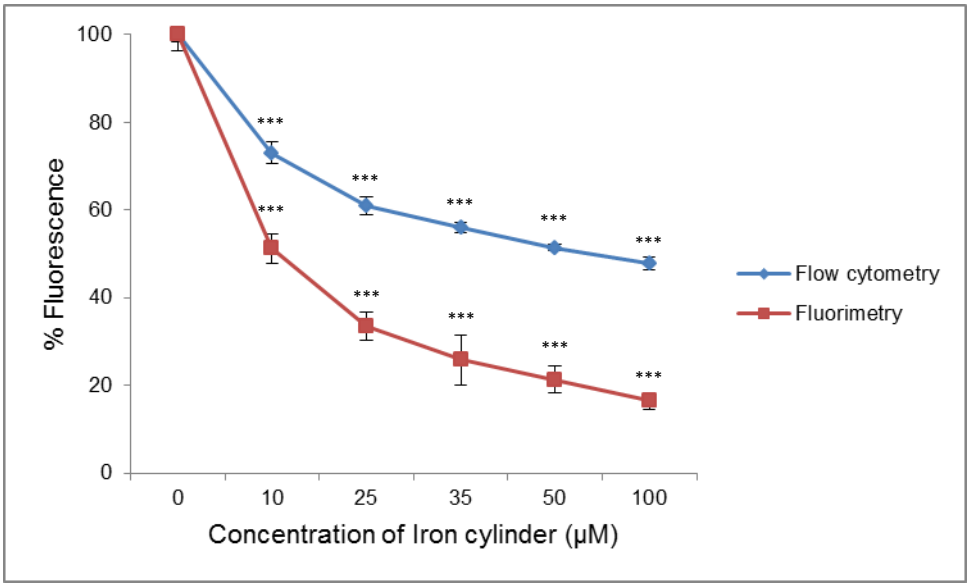

Figure 3.12. *Evaluation of Hoechst fluorescence in MDAMB-231 cells by fluorimetry and flow cytometry. Cells were collected, treated for 20 minutes with Hoechst followed by 20 minutes with cylinder at 37 ^{0}C prior to measuring fluorescence of the entire sample via fluorimetry and gated population via flow cytometry. Values are the mean of three separate experiments ± S.E.M. Significant difference from control, with p<0.05: *, <0.01: **, <0.001: ***. (One-way ANOVA followed by Tukey test).*

Fluorimetry results for the entire HL60 cell population show a concentration-dependent decrease in fluorescence intensity with 100 µM causing a reduction to less than 5 % of the control. Flow cytometry data representing the gated population also showed a decrease in fluorescence with increasing cylinder concentration but to a lesser extent than that seen by fluorimetry (fluorescence down to 58 % when treated with 100 µM cylinder) (Figure 3.13). These results showed very highly statistically significant differences ($p < 0.001$, One-way ANOVA followed by Tukey test).

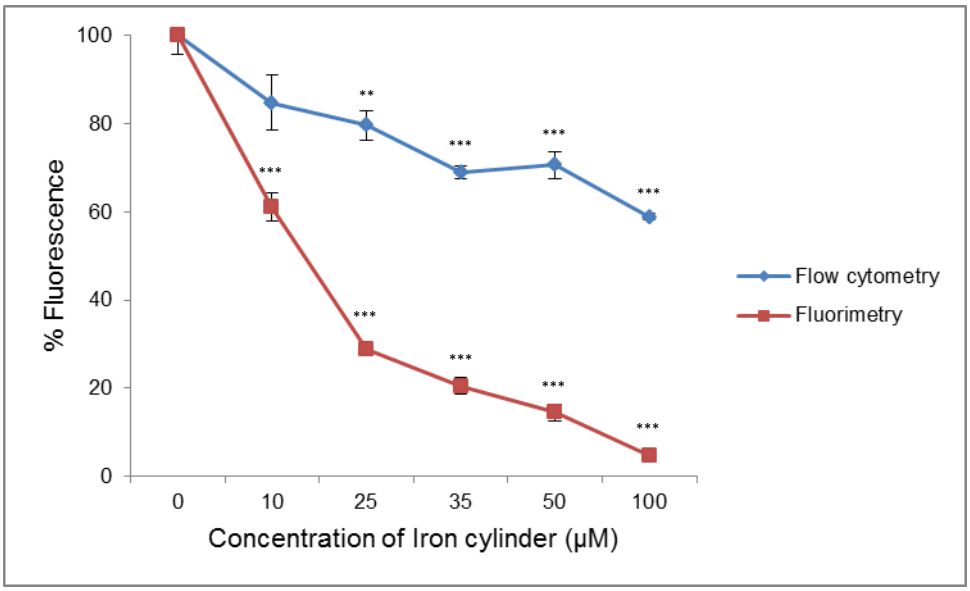

Figure 3.13. *Evaluation of Hoechst fluorescence in HL60 cells by fluorimetry and flow cytometry. Cells were treated for 20 minutes with Hoechst followed by 20 minutes with cylinder at 37 ^{0}C prior to measuring fluorescence of the entire sample via fluorimetry and gated population via flow cytometry. Values are the mean of three separate experiments ± S.E.M. Significant difference from control, with $p<0.05$: *, <0.01: **, <0.001: *** (One-way ANOVA followed by Tukey test).*

SKOV3, MDAMB-231 and HL60 cells were collected, incubated with Hoechst and then treated with cylinder. Fluorimetry and flow cytometry were used to measure the fluorescence of samples following treatment with different cylinder concentrations. Fluorimetry allows a measurement of the fluorescence of the entire population in each sample. Flow cytometry allows a more detailed analysis of the fluorescence of just live cells present in each sample (selected by gating out the debris). Fluorimetry and flow cytometry data obtained for each cell type are shown in Figures 3.11, 3.12 and 3.13.

Fluorimetry results obtained for all three cell types revealed a decrease in Hoechst fluorescence caused by increasing concentrations of cylinder. This provided support for the epifluorescence data showing that the quenching was not restricted to a few individual cells but was occurring for the entire population. Treatment with 100 μM cylinder reduced fluorescence by 77 % in SKOV3, 84 % in MDAMB-231 and 95 % in HL60 cells. The results showed very highly statistically significant differences from the control ($p < 0.001$). The difference in fluorescence quenching seen between the cancer cell types may be due to HL60 cells having increased sensitivity to the cylinder leading to a faster rate of uptake. The results are supported by previous research showing that mitochondrial function is most greatly affected by iron cylinder treatment in this cell type when compared with other cell types.[10] Furthermore, the data is consistent with previous investigations that found Hoechst 33258 fluorescence decreased with increasing concentrations of cylinder in HL60 cells.[10]

Flow cytometry data also revealed a concentration-dependent decrease in fluorescence intensity caused by increasing cylinder concentrations. Treatment with 100 μM cylinder reduced the fluorescence down to 65 % in SKOV3, 47 % in MDAMB-231 and 58 % in HL60 cells (Figures 3.11, 3.12 and 3.13). The concentrations tested showed very highly statistically significant differences from the controls ($p < 0.001$). Despite not seeing a similar extent of fluorescence reduction by fluorimetry and flow cytometry, the concentration-dependent decrease caused by the cylinder is consistent with both methods. Whereas the fluorimeter gathers fluorescence data from the entire sample including dead cells, aggregates and artefacts, the flow cytometer produces data for a selected (live) cell population in each sample. This may explain the differences seen between the two methods used. Future work to confirm this can use fluorescence activated cell sorting to physically separate the gated population and then measure the fluorescence via fluorimetry in those sorted populations. Again, SKOV3 cells were found to show the most resistance to the effect of the cylinder. Data obtained from the flow cytometer complements the fluorimetry and epifluorescence results. We have been able to show that it is possible to image a non-fluorescent compound such as the iron cylinder indirectly by exploiting its close proximity binding to another fluorescent molecule.

3.3 Conclusions and Future Work

The data revealed that iron cylinder quenched nuclear Hoechst fluorescence possibly via displacement from the minor groove in a concentration-dependent manner for all the tumour cell types studied. Epifluorescence microscopy allowed the changes occurring in the fluorescence over the 20 minute treatment period to be visualized. Quenching

occurring at a population level through use of fluorimetry and specifically in the live cells in each population by using flow cytometry was then confirmed. The three methods used produced results that complement each other. Of the cell types investigated, SKOV3 cells appeared to be the most resistant to the effect of the cylinder possibly due to over expression of multi-drug transporters leading to efflux of cylinder from the cells. This data provides novel possibilities supporting the imaging of non-fluorescent compounds indirectly through the use of fluorescent stains. To further support the results, circular dichroism (CD) has been used to show iron cylinder displacement of fluorescent probes from DNA.[14] A fluorescent version of the iron cylinder will function as a much better imaging tool and work towards this will take place in the future.

It is noteworthy that there is a superfamily of proteins known as ATP-Binding Cassette proteins and the over expression of ABC transporters such as MRP1 and P-glycoprotein has been identified in many cancer cells. They are believed to be responsible for the export of chemotherapeutics across the plasma membrane and therefore a reduced effect of anticancer treatment. The increased resistance displayed by SKOV3 cells to iron cylinder may be due to the over expression of certain multidrug resistance proteins.[15] Future work may involve using inhibitors to confirm over expression of certain drug transporters in the plasma membranes of SKOV3 cells or real-time polymerase chain reaction (PCR) to look at expression levels. The Hoechst quenching raises the question of whether other intrinsic fluorescent markers in cells might also be quenched to aid in visualizing entry of the cylinder and this is explored in the next chapters.

3.4 References

[1] Ducani, C., Leczkowska, A., Hodges, N. J., Hannon, M. J. (2010) Noncovalent DNA-binding metallo-supramolecular cylinders prevent DNA transactions in vitro. *Angewandte Chemie (International ed. in English)*. 49 (47): 8942-5.

[2] Pascu, G. I., Hotze, A. C., Sanchez-Cano, C., Kariuki, B. M., Hannon, M. J. (2007) Dinuclear ruthenium(II) triple-stranded helicates: luminescent supramolecular cylinders that bind and coil DNA and exhibit activity against cancer cell lines. *Angew Chem Int Ed*. 46 (23): 4374-4378.

[3] Vivian, J. T., Callis, P. R. (2001) Mechanisms of tryptophan fluorescence shifts in proteins. *Biophysical Journal*. 80 (5): 2093-2109.

[4] Haughland, R. P. (2010) The Molecular Probes Handbook, Invitrogen Life Sciences. Nucleic Acid Detection and Analysis. 11th ed. Chapter 8. Nucleic Acid Stains. Section 8.1.

[5] Hannon, M. J. (2007) Supramolecular DNA recognition. *Chem Soc Rev.* 36 (2): 280-295.

[6] Tanada, M., Tsujita, S., Sasaki, S. (2006) Design of new bidentate ligands constructed of two Hoechst 33258 units for discrimination of the length of two A3T3 binding motifs. *The Journal of organic chemistry*. 71 (1): 125-34.

[7] Harris, A., Qu, Y., Farrell, N. (2005) Unique cooperative binding interaction observed between a minor groove binding Pt antitumor agent and Hoechst dye 33258. *Inorganic chemistry*. 44 (5): 1196-8.

[8] Palchaudhuri, R., Hergenrother, P. J. (2007) DNA as a target for anticancer compounds: methods to determine the mode of binding and the mechanism of action. *Current Opinion in* Biotechnology. 18: 497–503.

[9] Sellrie, F., Graser, E., Lenz, C., Hillebrand, Timo., Schenk, J. A. (2013) Specific DNA detection using antibody mediated fluorescence quenching. *Biosensors and Bioelectronics*. 42: 512-515.

[10] Park, H., Seo, J., Shin, S. C., Lee, H. S., Bark. K. (2007) Fluorescence Quenching of Norfloxacin by Divalent Transition Metal Cations. *Bull. Korean. Chem. Soc*. 28 (9): 1573-1578.

[11] Bai, H., Liu, X., Yang, F., Yang, X. (2009) Interactions of Human Serum Albumin with Phenothiazine Drugs: Insights from Fluorescence Spectroscopic Studies. *Journal of the Chinese Chemical Society*. 56: 696-702.

[12] Le, S. B., Holmuhamedov, E. L., Narayanan, V. L., Sausville, E. A., Kaufmann, S. H. (2006) Adaphostin and other anticancer drugs quench the fluorescence of mitochondrial potential probes. *Cell death and differentiation*. 13 (1): 151-159.

[13]Peberdy, J. C., Malina, J., Khalid, S., Hannon, M. J., Rodger, A. (2007) Influence of surface shape on DNA binding of bimetallo helicates. *Journal of Inorganic Biochemistry*. 101 (11): 1937-1945.

[14] Hotze, A. C., Hodges, N. J., Hayden, R. E., Sanchez-Cano, C., Paines, C., Male, N., Tse, M. K., Bunce, C. M., Chipman, J. K. Hannon M. J. (2008) Supramolecular iron cylinder with unprecedented DNA binding is a potent cytostatic and apoptotic agent without exhibiting genotoxicity. *Chem Biol*. 15 (12): 1258-1267.

[15] Ferreira, M. U., Gyémánt, N., Madureira, A. M., Tanaka, M; Koós, K., Didziapetris, R., Molnár, J. (2005) The effects of jatrophane derivatives on the reversion of MDR1- and MRP-mediated multidrug resistance in the MDA-MB-231 (HTB-26) cell line. *Anticancer research*. 25 (6): 4173-8.

CHAPTER 4

Investigating Luciferase Quenching as a Novel Method of Imaging the Non-Fluorescent Iron Cylinder

4.1 Introduction

The work in this chapter builds on serendipitous observations made while employing the ToxiLight assay which was being used as an alternative to the MTT assay used to assess cell viability in Chapter 3. Although, The MTT assay is one of the most popular assays used to assess cell viability or detect cytotoxicity and it is generally accepted that the quantity of MTT formazan produced is directly related to cell viability,[1] this is complicated because it can also be considered an indicator of cell number and its applicability as a viability endpoint has been debated.[2] Recently, a number of researchers have also questioned the two commonly held assumptions of the MTT assay. The first is that the reduction of the MTT dye takes place in the mitochondria and the second is that this particular assay is a sufficient assessor of mitochondrial function and therefore a suitable evaluator of this organelle's activity.[2]

It is important to assess the cytotoxicity of a compound using a range of different assays designed to measure this and confirm viability using different endpoints. The ToxiLight assay is a highly sensitive non-destructive cytotoxicity assay which quantifies the leakage of adenylate kinase from cells whose membranes have been damaged. The reaction involved in this assay proceeds in two steps. In the first step, ADP is supplied in excess as the substrate and converted to ATP by the enzyme adenylate kinase (if present). In the second step, the bioluminescent reaction occurs where the enzyme luciferase uses the substrates ATP and luciferin to catalyze the production of light. The light given off is quantified using a luminometer and is directly related to the level of ATP and thus the amount of adenylate kinase present in the sample being analyzed.

Bioluminescent assays are extensively used in medical research with applications in many areas including cell viability testing and *in vivo/ in vitro* imaging. Fireflies (*Photinus pyralis*) are the best-studied bioluminescent organisms and the firefly luciferase enzyme is a popular tool used in imaging assays. The substrate for the enzyme is luciferin and for the reaction to occur, oxygen, ATP and a metallic cation are required (Figure 4.1).[3] D-luciferyl-adenylate is the enzyme bound intermediate produced in the reaction which undergoes oxidation, decarboxylation and is converted to a singlet excited state of oxyluciferin. As the oxyluciferin decays from its excited state to the ground state, emission of a photon at 562 nm occurs which follows a model of flash kinetics with the emission intensity rapidly decaying within just a few seconds.[4]

The structure of the luciferase protein has been well studied and is comprised of two folded domains close together (Figure 4.2). The small C-terminal domain is joined by a linker peptide to the larger N-terminal domain. The surface of both domains is believed to form the active site implying that they get closer together as the reaction proceeds holding the substrate between them which would require a change in the enzyme's conformation.[3]

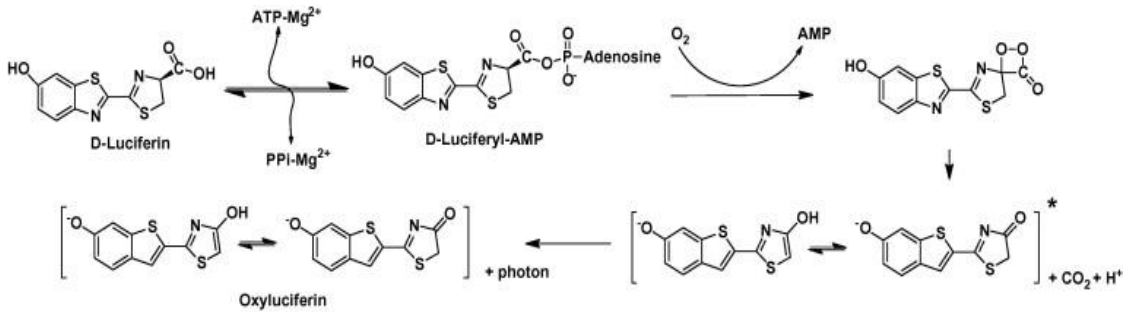

Figure 4.1. *The structure of luciferin and the chemical reaction carried out by firefly luciferase to produce a peak light emission wavelength. Taken from ref 4.*

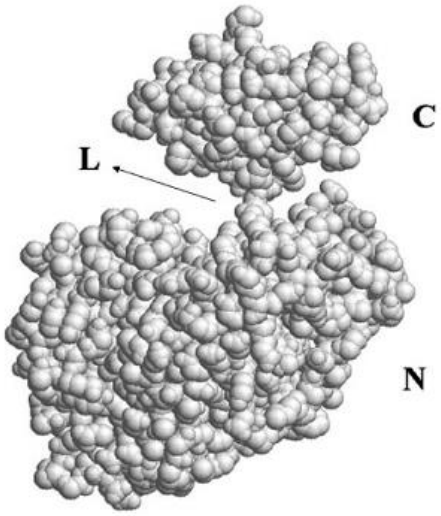

Figure 4.2. *Space-filling model of firefly luciferase showing the small C-terminal domain linked by the flexible linker peptide (L) to the large N-terminal domain. Taken from ref 3.*

Many systems based on luciferase have been developed because the enzyme can be introduced into cells genetically. *In vivo* imaging has recently been developed as a method to non-invasively monitor events occurring at a molecular level in model organisms and cells *in vitro*.[3] The labeling of proteins with luciferases which are then imaged following addition of substrate can be used to localize processes occurring in cells and organisms. A compound that interferes with this bioluminescent reaction catalyzed by luciferase or quenches the product could ultimately lead to development of a method to indirectly confirm the localization of the compound *in vivo* and this is further investigated with regards to iron cylinder in Chapter 4.

4.2 Results and Discussion

4.2.1 Cytotoxicity Assessed by ToxiLight Assay

The Lonza ToxiLight assay was used as an alternative approach to complement the MTT assay and assess the damage caused to cells by a cylinder. Due to financial constraints, one cell line was selected (MDAMB-231) for use in the ToxiLight Assay. Leakage of adenylate kinase from cells into the surrounding media was measured in MDAMB-231 cells at five different concentrations of iron cylinder. The ToxiLight assay was carried out following a 20 minute treatment period with iron cylinder at 37 ^{0}C. The percentages of luminescence shown in the results were calculated using the average luminescence of three readings. Using this assay, integrity of the plasma membrane would be identified through no change in luminescence output with increasing concentrations of cylinder. Alternatively, an increase in luminescence with increasing cylinder concentration would indicate damage occurring to the plasma membrane as a result of treatment. However, the results we obtained for this assay were unexpected and revealed a clear concentration-dependent decrease in luminescence caused by iron cylinder (Figure 4.3).

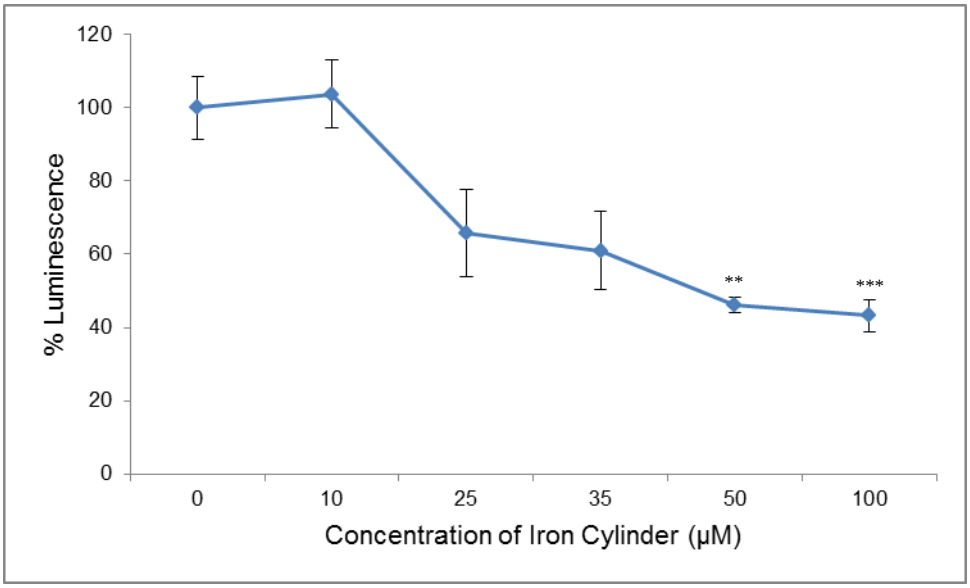

Figure 4.3. *ToxiLight assay carried out for MDAMB-231 cells following treatment with iron cylinder. Cells were treated with iron cylinder for 20 minutes at 37 ^{0}C prior to measuring luminescence. Values are the mean of three separate experiments ± S.E.M. Significant difference from control, with p<0.05: *, <0.01: **, <0.001: ***. (One-way ANOVA followed by Tukey test).*

Luminescence was reduced to 43 % when cells were treated with 100 µM cylinder and statistically this result was very highly significantly different from the control ($p < 0.001$, One-way ANOVA followed by Tukey test). These results suggested that the cylinder was inhibiting the ToxiLight assay. A working hypothesis was that it may be acting by inhibiting the actions of one of the enzymes present in the detection reagent. Further investigations were needed to determine the mechanism by which the drug was exhibiting its effect on this assay.

4.2.2 Investigations into Cylinder Interference with ToxiLight Assay Kit

Cell lysate obtained from MDAMB-231 cells containing adenylate kinase was used to confirm the interference of iron cylinder with the ToxiLight assay kit. Cells were treated with lysis buffer to damage their membranes and release large amounts of adenylate kinase into the surrounding media. This was then incubated with iron cylinder (0-150 µM) prior to carrying out the ToxiLight assay. The percentages of luminescence shown in the results were calculated using the average luminescence of three readings (Figure 4.4). Any changes observed in the luminescence would be occurring as a result of the direct effect of the cylinder's activity.

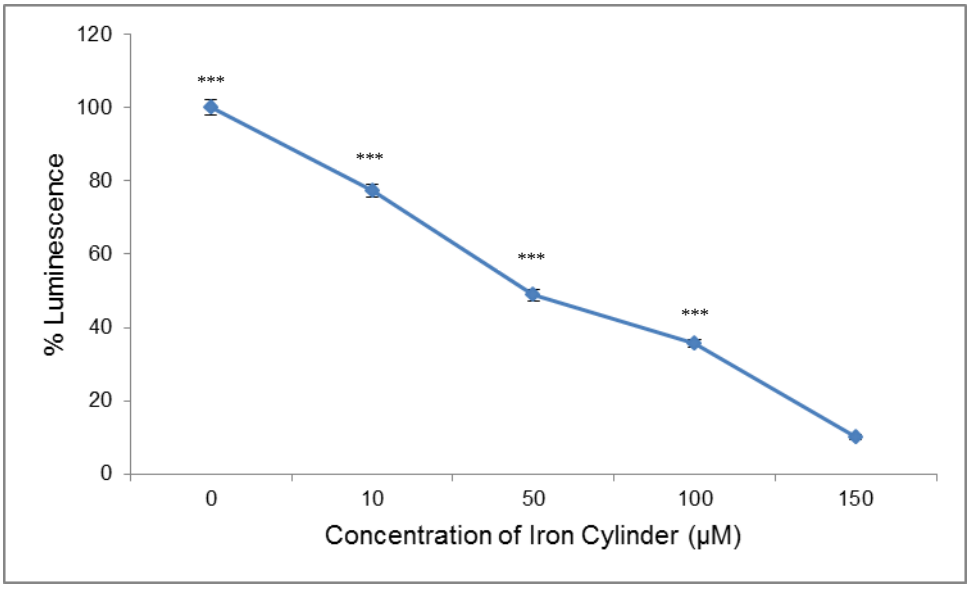

Figure 4.4. *Evaluation of interference by iron cylinder on ToxiLight assay using MDAMB-231 cell lysate. Cell lysate was treated with iron cylinder prior to carrying out the ToxiLight assay and measuring luminescence. Values are the mean of three separate experiments ± S.E.M. Significant difference from control, with p<0.05: *, <0.01: **, <0.001: ***. (One-way ANOVA followed by Tukey test).*

The results show a concentration-dependent decrease in luminescence with increasing concentrations of iron cylinder. The highest concentration of cylinder reduced luminescence by 90 % compared to the control (Figure 4.4). A very highly significant difference was identified between the control and all the concentrations of cylinder tested ($p < 0.001$, One-way ANOVA followed by Tukey test). These results confirm that the cylinder was responsible for the decrease in luminescence observed for the ToxiLight assay. The next step was to further investigate the mechanism by which the cylinder was reducing the luminescence.

The cylinder's ability to inhibit the enzyme luciferase as its possible mechanism of action was then investigated. The ToxiLight assay uses the two enzymes, adenylate kinase and luciferase in two separate steps. In the first step, ADP is phosphorylated to ATP (substrate for luciferase) by adenylate kinase. This step was bypassed by supplying an excess of ATP (1 mM in final volume of 100 µl) in a cell free system prior to testing the five concentrations of iron cylinder. Cylinder was then added and the assay carried out as before. The ToxiLight assay was carried out following cylinder treatment. The percentages of luminescence shown in the results were calculated using the average luminescence of three readings (Figure 4.5).

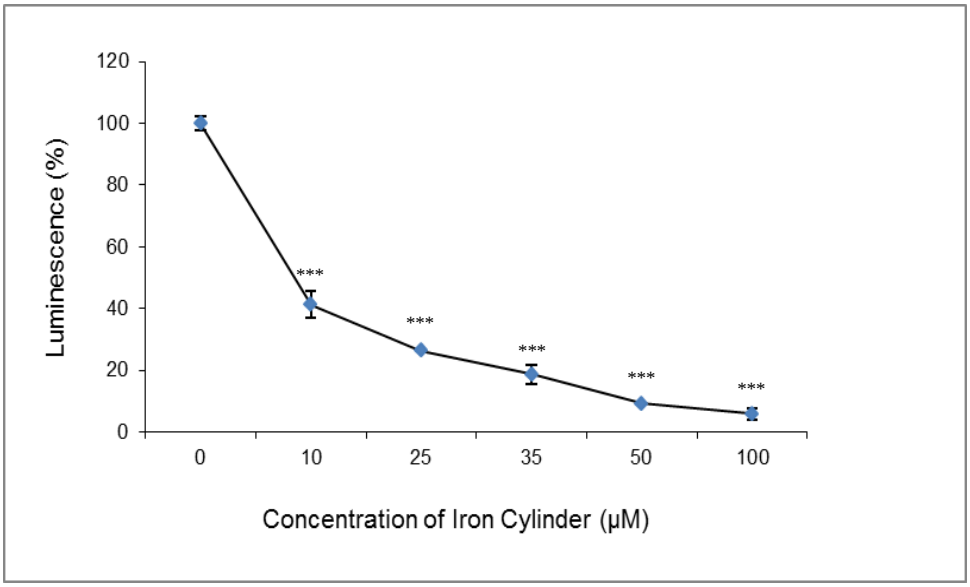

Figure 4.5. *Evaluation of luciferase inhibition by iron cylinder in a cell-free system. ATP was supplied in excess prior to cylinder addition. The ToxiLight assay was carried out and luminescence measurements obtained. Values are the mean of three separate experiments ± S.E.M. Significant difference from control, with p<0.05: *, <0.01: **, <0.001: ***. (One-way ANOVA followed by Tukey test).*

The results show a concentration-dependent decrease with the luminescence reduced to less than 6 % with 100 µM iron cylinder (Figure 4.5). A very highly significant difference was found to exist between the concentrations tested ($p < 0.001$, One-way ANOVA followed by Tukey test). This provided evidence for the inhibition of luciferase being a possible mechanism by which iron cylinder was interfering with the ToxiLight assay. Supplying the excess of ATP allowed adenylate kinase to be eliminated as the enzyme responsible for the effect caused by the drug on the ToxiLight assay.

To ensure that the inhibition seen in luminescence was a result of intact cylinder, the role of individual components required to synthesize the cylinder was investigated. The synthesized ligand, its components (4,4"-methylenedianiline and pyridine-2-carboxaldehyde) and iron(II) chloride tetrahydrate were tested in the same way. ATP was supplied in excess prior to addition of compound. The ToxiLight assay was carried out and the luminescence measured for each concentration tested. The percentages of luminescence shown in the results were calculated using the average luminescence of three readings (Figure 4.6).

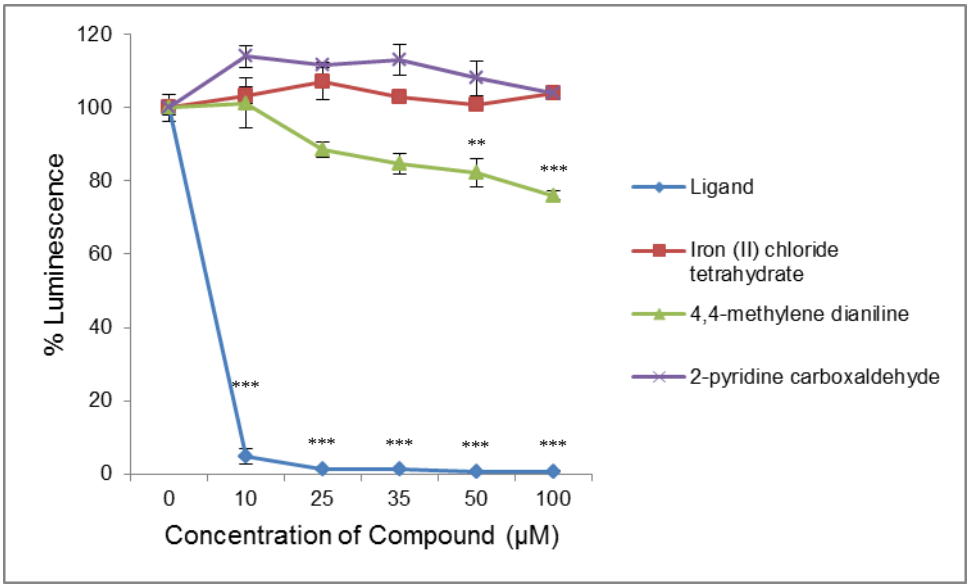

Figure 4.6. *Investigating the role of the ligand and cylinder components in luciferase inhibition. ATP was supplied in excess prior to compound addition. The ToxiLight assay was carried out and luminescence measurements obtained. Values are the mean of three separate experiments ± S.E.M. Significant difference from control, with p<0.05: *, <0.01: **, <0.001: ***. (One-way ANOVA followed by Tukey test).*

The results show that iron(II) chloride tetrahydrate and pyridine-2-carboxaldehyde did not reduce the luminescence significantly which was over 100 % when 100 µM of each compound was tested (Figure 4.6). There was no significant difference between any of the concentrations tested of these two compounds ($p > 0.05$, One-way ANOVA). The results suggest that these components are not dissociating from the cylinder in solution and provide support for the stability of the cylinder. The luminescence was reduced by 24 % of the control in a concentration-dependent manner by 100 µM 4,4‟-methylenedianiline. However, as this reduction in luminescence was not to the same extent as that seen for the intact cylinder, 4,4‟-methylenedianiline alone is unlikely to be responsible for the inhibition. The greatest reduction in luminescence was observed with increasing concentrations of ligand (luminescence reduced to less than 1 % of the control when treated with 50 and 100 µM ligand). A very highly significant difference was found to exist between the concentrations tested ($p < 0.001$, One-way ANOVA followed by a Tukey test). There may be many explanations for this reduction in luminescence caused by the ligand alone. One possible theory is that the ligand could be dissociating in solution and then chelating other metal species present in the ToxiLight detection reagent such as Mg^{2+}. To further investigate this metal chelators were used.

The chelating ligands: 2,2’-bipyridine and 1,10’-phenanthroline that readily form complexes with metal ions were also examined for their effect on the ToxiLight assay. ATP was supplied in excess prior to addition of compound. Increasing concentrations of both were used to test their ability to chelate free metal ions present in the assay. The ToxiLight assay was carried out and the luminescence measured for each concentration

tested. The percentages of luminescence shown in the results were calculated using the average luminescence of three readings (Figure 4.7).

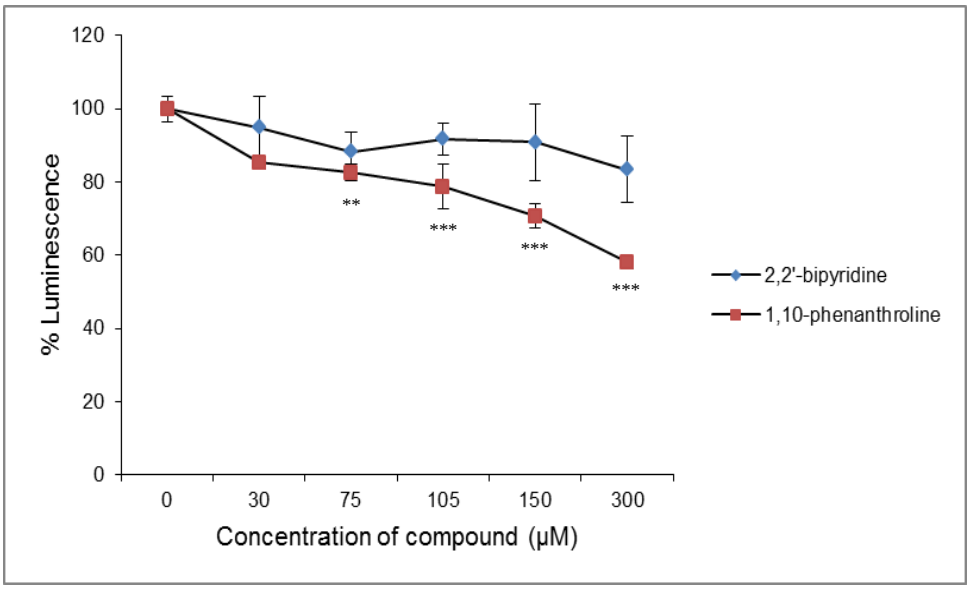

Figure 4.7. *Investigating the role of chelating ligands in luciferase inhibition. ATP was supplied in excess prior to compound addition. The ToxiLight assay was carried out and luminescence measurements obtained. Values are the mean of three separate experiments ± S.E.M. Significant difference from control, with p<0.05: *, <0.01: **, <0.001: ***. (One-way ANOVA followed by Tukey test).*

The results show that luminescence was reduced by 17 % of the control by 100 µM of 2,2'-bipyridine. None of the concentrations tested were found to be significantly different from each other ($p > 0.05$, One-way ANOVA). Luminescence was reduced to a greater extent by 1,10'-phenanthroline (42 % with 100 µM compound). A very highly statistically significant difference was found between the control and top dose of this compound ($p < 0.001$, One-way ANOVA followed by Tukey test) However, the

luminescence was not reduced to the same extent by the chelating ligands as that seen for the iron cylinder's ligand (Figure 4.7).

This suggests that the decreased luminescence seen to be caused by the iron cylinder's ligand was unlikely to be due to dissociation from the metal complex and more likely to be the effect of the complete cylinder. This is in agreement with stability data of the cylinder in aqueous solution. Much research has investigated the interaction between iron cylinder and DNA with molecular dynamic calculations and NMR spectroscopy supporting its ability to bind strongly to DNA and induce conformational changes (see section 1.8). This provides further evidence for the cylinder remaining intact and any responses observed being due to the actions of the complete compound.

4.2.3 Monitoring Luminescence Production Over Time in MDAMB-231 Cells Stably Expressing Luciferase

First the emission of luminescence from luciferase- expressing MDAMB-231 cells was quantified following addition of the substrates, ATP and luciferin (1 mM for each in final volume of 100 µl). As expected, the non-expressing MDAMB-231 cell line emitted very little light (76 luminescence units) when exposed to the substrates. This cell line provided the negative control for the experiment. A very high luminescence output of 16406 luminescence units was produced in the luciferase-expressing cancer cell line upon substrate addition (Figure 4.8). This experiment allowed us to determine the concentrations of luciferin (1 mM) and ATP (1 mM) required for the luciferase-expressing MDAMB-231 cells to catalyze the bioluminescent reaction and produce light.

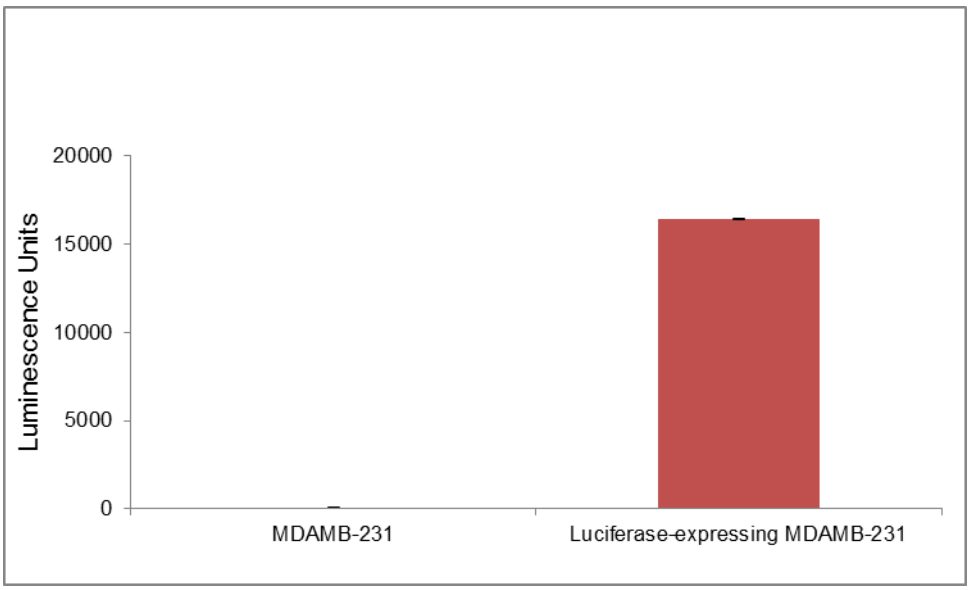

Figure 4.8. *Confirming luminescence production in luciferase-expressing MDAMB-231 cell line. ATP and luciferin were supplied prior to obtaining luminescence measurements. Values are the mean of three separate experiments ± S.E.M.*

The period of time over which the strength of the luminescent signal was maintained was then investigated. To achieve this, cells were incubated with substrates (using concentrations defined previously) and the luminescence was measured at intervals over 30 minutes. The luminescence values shown for each time point were calculated using the average luminescence of three recordings (Figure 4.9). The results show that 4 minutes after exposure to substrate, the signal is reduced by 84 % when compared to that measured at 2 minutes in luciferase-expressing MDAMB-231 cells. Following the sudden decline after 4 minutes, the luminescence continues to increase very slowly with time. Despite this, it does not increase to the emission observed at 2 minutes (at 28 minutes, the signal is still only 24 % of the signal acquired at 2 minutes). This confirmed that the luciferase enzyme had flash kinetics with maximum sensitivity due to the high signal

intensity produced despite the rapid decay of the light emitted. As expected, the non-expressing MDAMB-231 cells produced no luminescence output when exposed to substrate which was consistent over the time course.

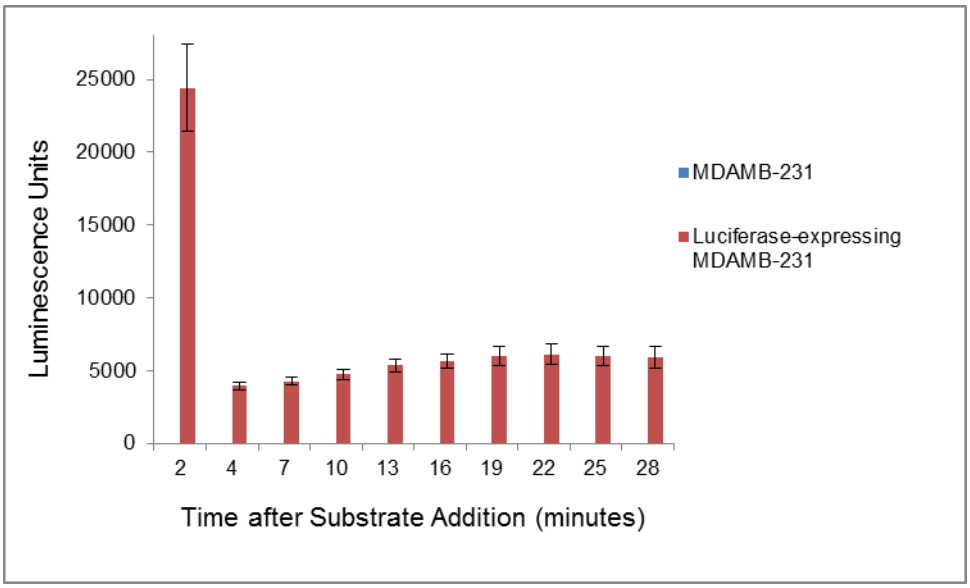

Figure 4.9. *Investigating strength of luminescent signal in luciferase-expressing MDAMB-231 cells over time. ATP and luciferin were supplied prior to obtaining luminescent measurements. Values are the mean of three separate experiments ± S.E.M.*

An MTT assay was used to assess mitochondrial viability in luciferase-expressing and non-expressing MDAMB-231 cells that had been treated with concentrations of iron cylinder for 20 minutes followed by exposure to ATP and luciferin. The percentages of viable mitochondria shown in the results were calculated using the average absorbance of three readings (DMSO blank adjusted). The results show that over 95 % of cells remained viable in both cell types when treated with the top dose of iron cylinder (100 µM). No statistical significance was observed between any of the concentrations

investigated ($p > 0.05$, Kruskal-Wallis test) (Figure 4.10). These results determined that treatment with cylinder together with exposure to substrates (at the concentrations pre-determined) did not cause any significant effect on the reductive function of mitochondria and therefore on cell viability. Any effects on luminescence inhibition seen in these cells following treatment could therefore not be associated with cytotoxicity as a result of drug or substrates. Therefore, concentrations of 0, 10, 25, 35, 50 and 100 µM were used in all future assays where cells were treated for 20 minutes with drug and then substrate.

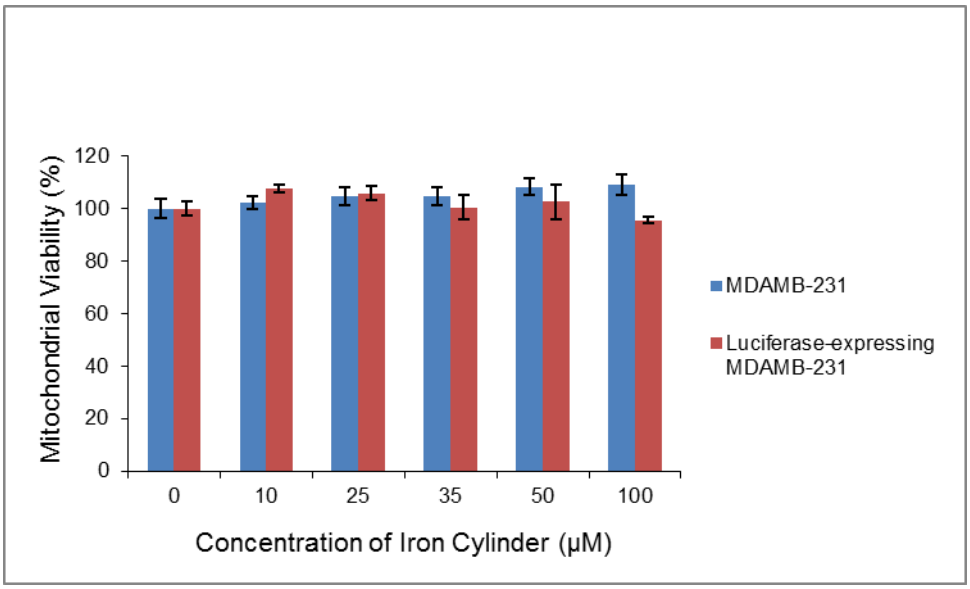

Figure 4.10. *Evaluation of cytotoxic effects of substrates and iron cylinder treatment in luciferase-expressing MDAMB-231 cells using the MTT assay. Cells were treated with iron cylinder for 20 minutes at 37 ^{0}C prior to ATP and luciferin addition and measuring MTT reduction. Values are the mean of three separate experiments ± S.E.M. No significant difference from control ($p>0.05$ in MDAMB-231, luciferase-expressing MDAMB-231 cells, Kruskal-Wallis test).*

4.2.4 Investigating Iron Cylinder's Inhibition of Luminescence in Luciferase-Expressing MDAMB-231 Cells

The cylinder's effect on luminescence production in luciferase-expressing MDAMB-231 cell lysate was tested. Cells membranes were lysed and then treated with increasing concentrations of iron cylinder (0, 10, 25, 35, 50, 100 μM) for 20 minutes at 37 ^{0}C. ATP and luciferin were supplied and the luminescence recorded. Cells were lysed to ensure that the cylinder had direct access to the contents of the cell and therefore its effect on luminescence could be measured without any access barriers. Non-expressing MDAMB-231 cells were present as a control. A negative control was also present for each cell type where substrates were not provided before the luminescence recording. The luminescence values shown in the results were calculated using the average of three readings (Figure 4.11).

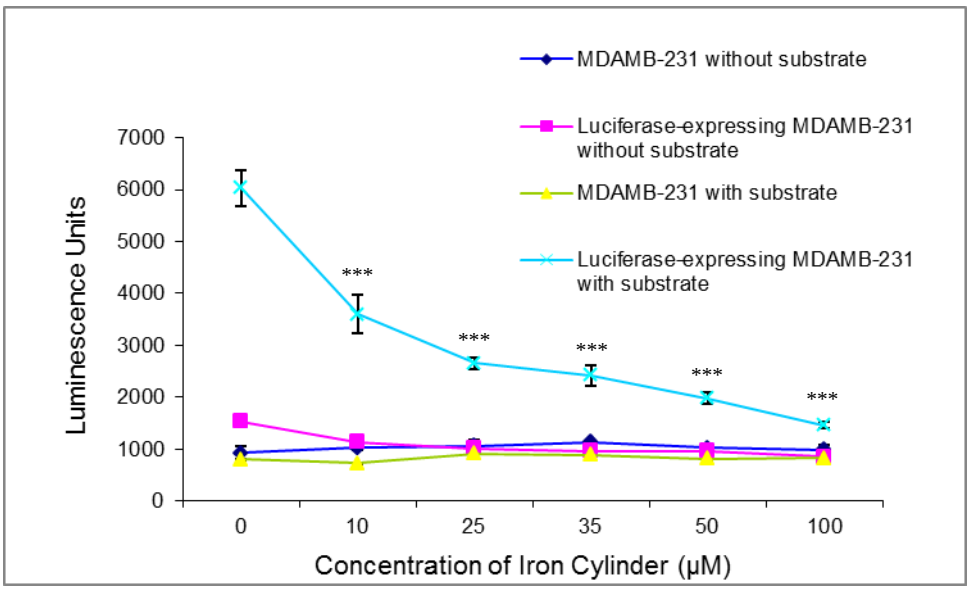

Figure 4.11. *Evaluation of luciferase inhibition by iron cylinder in lysed luciferase-expressing MDAMB-231 cells. Lysed cells were treated with iron cylinder for 20 minutes at 37 ^{0}C prior to ATP and luciferin addition and luminescence recorded. Values are the mean of three separate experiments ± S.E.M. Significant difference from control, with p<0.05: *, <0.01: **, <0.001: ***. (One-way ANOVA followed by Tukey test).*

The results showed that the cylinder caused a concentration-dependent decrease in luminescence which only occurred in the lysed luciferase-expressing MDAMB-231 cells that were supplied with substrate (luminescence reduced by 76 % of the control when treated with 100 µM drug) (Figure 4.11). Each concentration of cylinder tested was found to be very highly statistically significantly different from the control ($p < 0.001$, One-way ANOVA followed by Tukey test). These results provide support for the hypothesis that this cylinder inhibits the bioluminescent reaction possibly via inhibition of the luciferase enzyme.

Next, the cylinder's ability to inhibit this reaction in luciferase-expressing MDAMB-231 cells with intact membranes was tested. Cells were trypsinized before being treated with increasing concentrations of iron cylinder (0, 10, 25, 35, 50, 100 µM) for 20 minutes at 37 ^{0}C. ATP and luciferin were supplied and the luminescence recorded. Non-expressing MDAMB-231 cells were present as a control. A negative control was also present for each cell type where substrates were not provided before luminescence recording. The luminescence values shown in the results were calculated using the average of three readings (Figure 4.12).

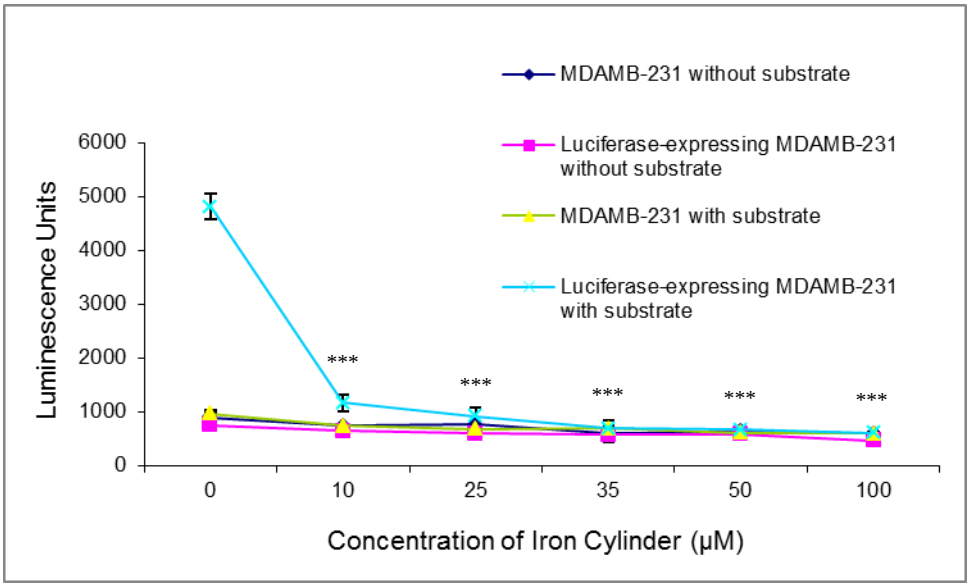

Figure 4.12. *Evaluation of luciferase inhibition by iron cylinder in trypsinized luciferase-expressing MDAMB-231 cells. Trypsinized cells were treated with iron cylinder for 20 minutes at 37 ^{0}C prior to ATP and luciferin addition and luminescence recorded. Values are the mean of three separate experiments ± S.E.M. Significant difference from control, with p<0.05: *, <0.01: **, <0.001: ***. (One-way ANOVA followed by Tukey test).*

The results revealed a concentration-dependent decrease in luminescence caused by increasing concentrations of iron cylinder which only occurred in luciferase-expressing MDAMB-231 cells following treatment with substrates. Luminescence was reduced by 88 % of the control when treated with the top concentration of 100 μM of cylinder. For each of the concentrations tested, a very high statistical significance was found in terms of difference from the control ($p < 0.001$, One-way ANOVA followed by Tukey test) (Figure 4.12).

The results indicate that iron cylinder is able to cross the cell membrane and inhibit the bioluminescent reaction in cells which have detached from a surface but still have their membranes intact. These results support data obtained for lysed cells and provide further support for the cylinder's inhibition of luminescence in a concentration-dependent manner via luciferase inhibition taking place in the cell.

Finally we investigated this inhibition in adherent cells. Cultured cells attached to a surface were treated increasing concentrations of iron cylinder (0, 10, 25, 35, 50, 100 μM) for 20 minutes at 37 ^{0}C. ATP and luciferin were supplied and the luminescence recorded. MDAMB-231 cells were present as a control. A negative control was also present for each cell type where substrates were not provided before recording luminescence. The luminescence values shown in the results were calculated using the average of three readings with concentrations of drug (Figure 4.13).

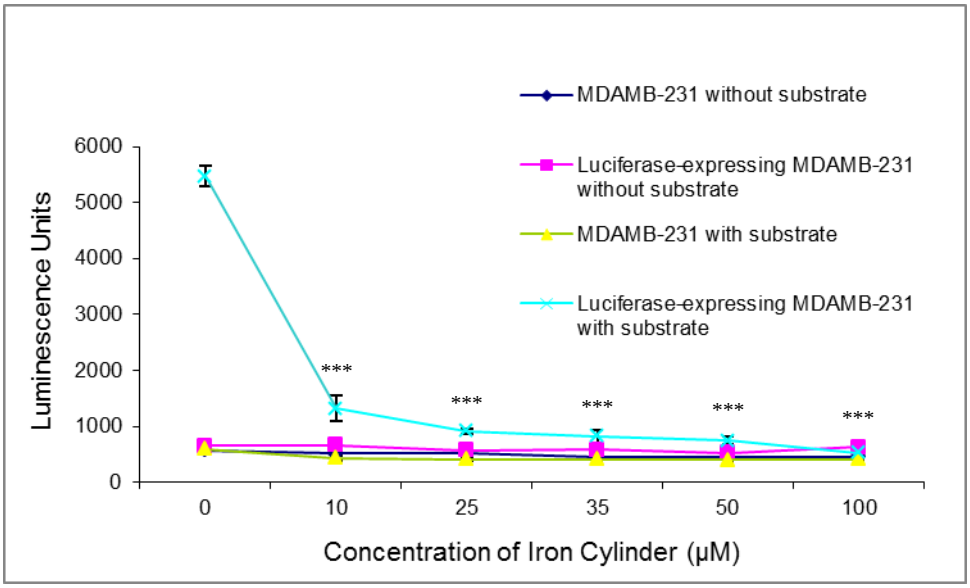

Figure 4.13. *Evaluation of luciferase inhibition by iron cylinder in adherent luciferase-expressing MDAMB-231 cells. Adherent cells were treated with iron cylinder for 20 minutes at 37 ^{0}C prior to ATP and luciferin addition and luminescence recorded. Values are the mean of three separate experiments ± S.E.M. Significant difference from control, with p<0.05: *, <0.01: **, <0.001: ***. (One-way ANOVA followed by Tukey test).*

The results support those obtained for lysed and trypsinized cells with a concentration-dependent decrease in luminescence caused by iron cylinder which only occurred in luciferase-expressing MDAMB-231 cells following exposure to substrates. Luminescence was reduced by 90 % of the control when treated with the top concentration of 100 µM of cylinder. For each of the concentrations tested, a very high statistical significance was found in terms of difference from the control ($p < 0.001$, One-way ANOVA followed by Tukey test) (Figure 4.13). The results indicate that iron cylinder is able to efficiently cross the cell membrane of cancer cells growing in culture and inhibit the bioluminescent reaction occurring in these cells.

Recent research carried out on a novel chemotherapeutic naphthoquinone drug, TU100 (Figure 4.14) has revealed that this too inhibits the bioluminescent enzyme, luciferase. This drug also irreversibly inhibits topoisomerase enzymes which are responsible for regulating the winding and unwinding of DNA. Its effects seen on the luciferase enzyme were found to proceed through different mechanisms which were reversible. The effect of naphthoquinone was investigated on a range of concentrations for the luciferase substrates, ATP and luciferin. The results revealed that the drug binds competitively with regards to luciferin and uncompetitively with regards to ATP. The results imply that the drug specifically binds the luciferase-ATP complex, preventing it from interacting with the luciferin and therefore inhibiting the bioluminescent reaction from occurring.[5] Light emission from luciferase-expressing kidney epithelial cells was reduced to 60 % when treated with 10 µM TU100. In comparison, treatment of luciferase-expressing breast cancer cells with 10 µM iron cylinder caused a much greater reduction to 10 % of the control.

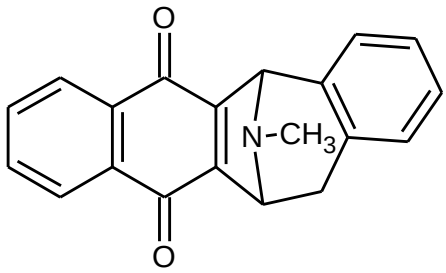

Figure 4.14. *The structure of the novel naphthoquinone drug, TU100.*

The iron cylinder might act via this mechanism also which makes it an important novel agent for the investigation and regulation of bioluminescent enzymes. Another possibility is that the iron cylinder directly interferes with the enzyme luciferase by irreversibly

binding to the active sites in the C/N-terminal or the peptide linker region, thereby preventing the enzyme from changing conformation and allowing substrates to bind at the active site which would prevent the reaction from proceeding (Figure 4.2).

4.2.5 Investigating Quenching of Luminescence by Iron Cylinder in Adherent Luciferase- Expressing MDAMB-231 Cells with Time

The iron cylinder's inhibition of the bioluminescent reaction over time was investigated with decay of the luminescent signal produced by luciferase expressing MDAMB-231 cells in the presence of substrate. Cells were treated with increasing concentrations of iron cylinder (0, 10, 25, 35, 50, 100 µM) for 20 minutes at 37 ^{0}C. ATP and luciferin were supplied and the luminescence recorded at 3 minute intervals over a 30 minute period. The results show a reduction in the luminescent signal of untreated cells by 90 % after 4 minutes of exposure to substrates when compared to the signal at 2 minutes after exposure (Figure 4.15).

These results support previous data showing a reduction in luminescence to 84 % at 4 minutes when compared to the signal produced at 2 minutes (Figure 4.9). The luminescence produced at 2 minutes after substrate exposure showed that 100 µM iron cylinder reduced the signal by 99 % of the control. The signal measured at 28 minutes showed the same concentration of cylinder reduced the luminescence by 96 % of the control (Figure 4.15). These results indicate that despite the flash kinetic nature of the luciferase with the signal decaying rapidly, the proportion by which the cylinder inhibits

this bioluminescent reaction is similar at 2 minutes and 28 minutes (100 µM drug reduced signal to 1 % of control at 2 minutes and 4 % at 28 minutes).

Therefore, despite the large difference in luminescence output at 2 minutes (24406 luminescence units) compared to 4 minutes (3937 luminescence units), the cylinder's ability to inhibit the bioluminescent reaction is proportionally consistent at each time point (Figure 4.15). This implies that data obtained at a later time point is equally valid as that obtained at an earlier one as long as the time point chosen is kept consistent across experiments.

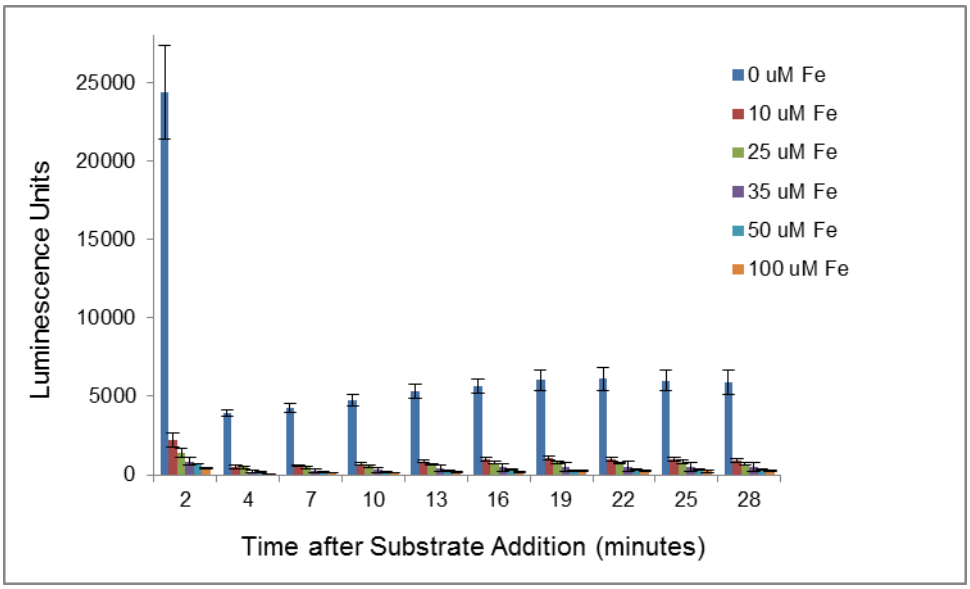

Figure 4.15. *Investigating intensity of luciferase inhibition by iron cylinder in adherent luciferase-expressing MDAMB-231 cells over time. Cells were treated with iron cylinder prior to addition of substrates and luminescence measured at 3 minute intervals over a 30 minute period. Values are the mean of three separate experiments ± S.E.M.*

Investigations into the cylinder's ability to inhibit a bioluminescent reaction provided another indirect mechanism by which this cylinder could be imaged. Its ability to block the mechanism by which a luminescent enzyme functions has the potential to be exploited for a number of studies. The quenching of light could be used to study biological processes occurring in real time as well as identifying the localization of this cylinder in cells and model organisms. Recently, bioluminescent imaging has been used to quantify and assess the efficacy of drugs in cancer research.[6] The light emitted when the excited oxy-luciferin relaxes back to its ground state can pass through mammalian tissues and can be used to investigate luciferase-expressing cancer cells non-invasively. However, many challenges remain in the development of animal models which can be used to sensitively study tumor development. Problems on the molecular level include development of effective methods to image using reporter systems that show cell processes occurring over time. When luciferase is used as a reporter, luciferin has to be supplied externally which is often not a practical approach *in vivo* for larger models such as rodents.

In addition, as the luciferin is rapidly used up, the bioluminescence signal can become increasingly unstable. Photons are both scattered and absorbed in the complex medium that makes up mammalian tissue. This is caused by changes which occur in the refractive index at organelles and membranes within the cell. These can limit the ability of studies to look at deep tissues due to scattering and a diminished signal.[6] Furthermore, other factors including the iron cylinder's ligand may interfere with the luciferase so this may

not be an ideal reaction. Therefore, research moved to investigate green fluorescent protein (GFP) in chapter 5.

4.3 Conclusions and Future Work

Through the use of luciferase-expressing breast cancer cells it has been shown that the cylinder directly affects luciferase-dependent light production in cells and does so in a concentration-dependent manner. The cylinder may be having its effect by physically interacting with the ATP-luciferase complex and preventing it from having access to the luciferin substrate. As a result, the production of oxyluciferin and light would be inhibited and the bioluminescent reaction blocked.

Kinetic analysis of iron cylinder's inhibition would provide further insight into which step of the biolumisnescent reaction is being affected, as well as giving information about the mechanism of inhibition. These experiments would involve determining Km values for luciferin and ATP (the substrate concentration at which half the enzyme's active sites are occupied by substrate), holding one substrate at its Km whilst titrating the other in. Analysis of the orientation of the straight line series generated from reciprocal plots would allow confirmation of competitive/uncompetitive binding of cylinder with respect to ATP and luciferin.[5]

The application where luciferase acts as a reporter gene has been well-established. This produces a signal that can be quantified under certain conditions, providing information about cell processes including receptor activity, gene expression patterns and protein-

protein interactions. An expression vector such as a plasmid carrying the luc gene is introduced into an organism and once inside a cell, the working luciferase protein is produced via translation of the luc gene. The ATP and luciferin substrates are supplied which leads to production of light and can be detected via a luminometer. This method has been employed in drug-screening and to identify certain sequences or parts of the genome. Bioimaging has been established since then which allows the emission of light to be followed in an animal (Figure 4.16) by placing the animal under a photon-detecting CCD (charge-coupled device).[3]

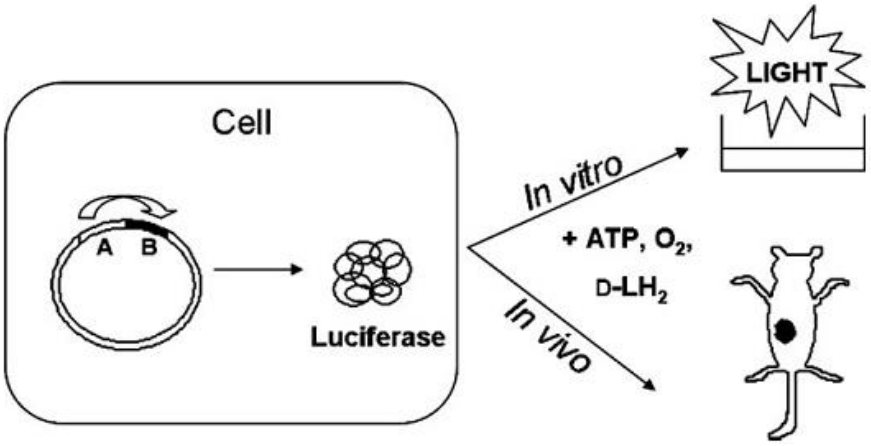

Figure 4.16. *Reporter gene technology related to luciferase. A regulatory sequence (A) is present on the expression vector which is introduced into the cell. (A) controls expression of the luc gene (B) leading to luciferase protein production. Light emission can be quantified in cells or in an organism when ATP and luciferin substrates are administered prior to acquiring data. Taken from ref 3.*

The inhibition of luciferase by iron cylinder is a very significant finding and could provide further insight into the distribution of this compound *in vivo.* For example, a transgenic mouse expressing luciferase cells or implanted with luciferase-expressing cancer cells could be used as a model to study distribution of cylinder *in vivo* and uptake into cancer cells. Following administration of substrates required for the luminescent reaction to occur, iron cylinder treatment would take place possibly through intravenous injection. Light emitted from the cancer cells would then be monitored over time which would provide information about the activity and location of the iron cylinder in the mouse. Tumour development could be quantified by using the inhibition of luciferase by cylinder and this could be compared in relation to untreated animals.

Drug inhibition of bioluminescent reactions has recently been investigated. Animals are usually anaesthetized prior to imaging using compounds such as lidocaine and halothane, both of which are known to directly inhibit the enzyme luciferase by binding and altering its catalytic speed.[7] A recent study compared the inhibitory effect of different types of anesthetics commonly used to sedate mice and rats. *In vitro* findings showed that all the volatile anesthetics tested caused a clear inhibitory effect on the activity of the luciferase enzyme with Avertin having the strongest inhibition. *In vivo* effects were largely due to changes in blood movement and to a lesser extent due to direct drug-enzyme interactions. The researchers concluded that it was best to use unanaesthetized animals for bioluminescent imaging but if necessary, phenobarbital was the best suited anaesthetic to use.[7]

In this Chapter, another novel method has been identified to indirectly image the non-fluorescent drug by using its inhibition of the luminescent enzyme, luciferase. However, it may be subject to effects from other molecular species including the iron cylinder's ligand and this needs to be considered when analyzing its effects.

4.4 References

[1] Fotakis, G., Timbrell, J. A. (2006) In vitro cytotoxicity assays: Comparison of LDH, neutral red, MTT and protein assay in hepatoma cell lines following exposure to cadmium chloride. *Toxicology Letters*. 160 (2): 171-177.

[2] Stockert, J. C., Blázquez-Castro, A., Cañete, M., Horobin, R. W., Villanueva, A. (2012) MTT assay for cell viability: Intracellular localization of the formazan product is in lipid droplets. *Acta Histochemica*. 114 (8): 785-796.

[3] Marques, S. M., Esteves, D. S., Joaquim, C. G. (2009) Firefly bioluminescence: a mechanistic approach of luciferase catalyzed reactions. *IUBMB Life*. 61 (1): 6-17.

[4] Liu, Y., Fang, J., Cai. H., Xiao. F., Ding, K., Hu, Y. (2012) Identification and synthesis of substituted pyrrolo[2,3-d]pyrimidines as novel firefly luciferase inhibitors. *Bioorganic & Medicinal Chemistry*. 20 (18): 5473-82.

[5] Bedford, R., Lepage, D., Hoffmann, R., Kennedy, S., Gutschenritter, T., Bull, L., Sujijantarat, N., Dicesare, J. C., Sheaff, R. J. (2012) Luciferase inhibition by a novel naphthoquinine. *Journal of Photochemistry and Photobiology. B, Biology*. 107: 55-64.

[6] Christoph, S., Schlegel, J., Alvarez-Calderon, F., Kim, Y-Mi., Brandao, L. N., Deryckere, D., Graham. D. K. (2013) Bioluminescence imaging of leukemia cell lines in vitro and in mouse xenografts: effects of monoclonal and polyclonal cell populations on intensity and kinetics of photon emission. *Journal of Hematology & Oncology*. 6: 10.

[7] Keyaerts, M., Remory, I., Caveliers, V., Breckpot, K.., Bos, T. J., Poelaert, J., Bossuyt, A., Lahoutte, T. (2012) Inhibition of firefly luciferase by general anaesthetics: Effects on in vitro and in vivo bioluminescence imaging. *PLoS ONE*. 7 (1): 1-10.

CHAPTER 5

Investigating GFP Quenching as a Novel Method of Imaging the Non-Fluorescent Iron Cylinder

5.1 Introduction

The work in this chapter builds on the results from bioluminescent observations in Chapter 4 which demonstrates proof of principal that the iron cylinder can be imaged with no fluorescent protein probes. Due to various considerations including factors that may influence the enzyme luciferase, research moved to investigate the green fluorescent protein (GFP) in this chapter.

Being able to image a molecule having its effect at a cellular level is very important in order to identify and study cellular proteins including those involved in cancer development. Bioluminescence imaging can be used to visualize cancer cells *in vivo* by expressing the luciferase gene in cancer cells enabling light emission from cells to be studied. However, there are several limitations to this approach. The luciferase enzyme, once inside mammalian cells needs to be supplied externally with the substrate luciferin. This is required each time imaging is being carried out which is not a practical method for whole organism studies. Using this method produces poor resolution of image and diminished signal. Therefore, long integration times are required to detect enough signal to construct an image from the animal. In addition, it is not known whether the luciferase genes have a stable expression in tumors over time as the luminescence emitted depends on the metabolic activity of the cells which have been transfected with luciferase.[1,2] Fluorescent imaging offers a number of advantages when compared to bioluminescent imaging.

An intense, highly specific signal with good resolution and physiological conditions is essential to image tumor development externally. Green fluorescent protein (GFP) was chosen as it meets these requirements and has good potential as a cell marker.[1] GFP was cloned from *Aequorea* jellyfish and discovered alongside the well-known chemi-luminescent protein, aequorin.[3] GFP absorbs blue light, re-emitting it as green fluorescence.[4] It is spontaneously fluorescent requiring no other proteins, co-factors or substrates.[1] In addition to *Aequorea*, GFP has also been found in a range of other symbiotic and non-symbiotic cnidarians. Here, it is not in conjunction with a bioluminescent system and its function is unknown.[4] During spontaneous cyclization and oxidation of the amino acid chain during protein folding, the GFP chromophore is formed. The chromophore has to be kept well protected deep within the barrel-shaped protein to produce the fluorescence (Figure 5.1). The cellular pH and other factors of the microscopic environment affect the intensity of GFP fluorescence and have been taken advantage of with the availability of pH and redox sensitive GFPs which can be used as probes.[4]

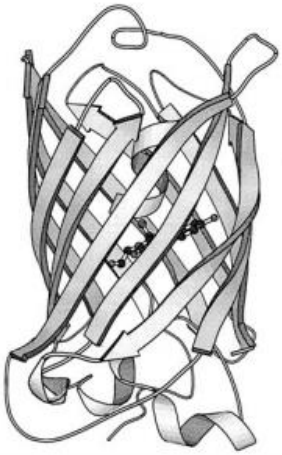

Figure 5.1. *3D structure of GFP, showing 11 β-strands that form a hollow cylinder through which is threaded an α-helix containing the chromophore. Taken from ref 3.*

GFP has been used to visualize numerous active processes taking place in cells including interactions of proteins and chromosome dynamics. Its use as a reporter gene was one of its first successful applications where the GFP gene is controlled by a promoter of interest and the fluorescence emitted can be used to indicate the level of gene expression in cells and tissues.[5] Furthermore, fusion of a cloned gene of interest with GFP has led to the development of chimeric proteins which are then expressed in cells and tissues. The design of the hisone-GFP fusion protein allowed small fragments of extra-chromosomal DNA known as double minute chromosomes to be visualized. Double-minute chromosomes have a vital role in the genetics of cancer cells as they are commonly linked with the overexpression of oncogene proteins.[6]

GFP has been stably expressed in certain cancer cell lines *in vitro* and these cells have successfully been transplanted into animals including rodents where they have been imaged in specific organs. Metastatic disease models using GFP have been defined for a range of cancers including breast, ovarian and prostate tumors.[1] Transfection of GFP into cancer cells provides a useful tool to image tumor growth and development *in vivo*.[1] In this chapter, the effect of the cylinder on GFP fluorescence is investigated and a method to directly visualize the location and mechanism of the cylinder *in vitro* is developed.

5.2 Results and Discussion

5.2.1 Investigating Quenching of Purified GFP by Iron Cylinder

The fluorescence of purified GFP was measured in the presence of different concentrations of iron cylinder (0, 10, 25, 35, 50 and 100 μM in final volume of 100 μl).

GFP (0.5 µM in final volume of 100 µl) was diluted in distilled water prior to treatment with cylinder (20 minutes at 37 ^{0}C for each concentration tested). A fluorimeter was used to record the fluorescence of each sample (λ_{exc} = 485 nm, λ_{em} = 530 nm). Three repeats were collected at each concentration of iron cylinder tested and the data was blank adjusted to remove background fluorescence of cylinder alone for each of the concentrations investigated (Figure 5.2).

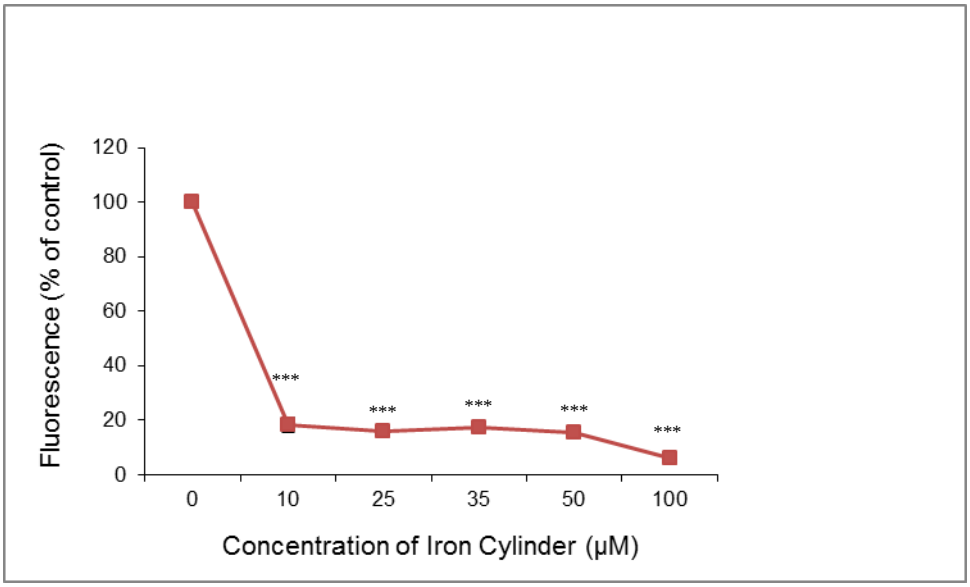

Figure 5.2. *Evaluation of fluorescence quenching of purified GFP by iron cylinder. GFP was treated for 20 minutes with iron cylinder at 37 ^{0}C prior to measuring fluorescence via fluorimetry. Values are the mean of three separate experiments ± S.E.M. Significant difference from control, with p<0.05: *, <0.01: **, <0.001: ***. (One-way ANOVA followed by Tukey test).*

Using this purified GFP *in vitro* allows direct investigation of the interaction of the cylinder with GFP, in the absence of endogenous mammalian proteins. Fluorimetry results show that exposure to 10 µM cylinder reduced fluorescence of GFP by 82 % of the control and this further decreased to 94 % when the protein was exposed to the top concentration of 100 µM cylinder. The results were found to be very highly significantly different from the control ($p < 0.001$, One-way ANOVA followed by Tukey test). These results indicate that the cylinder interacts with the GFP in solution and quenches its fluorescence. As the GFP chromophore is well protected in the protein's structure and this is required for it to fluoresce, these results suggest that the cylinder is able to access the core of this protein and inhibit its function, resulting in the decreased fluorescence observed.

5.2.2 Investigating GFP Quenching by Iron Cylinder in MDAMB-231 Cells Stably Expressing GFP

Next it was investigated whether the cylinder would be able to access GFP when it was present in a cellular environment. The fluorescence of adherent GFP-expressing MDAMB-231 cells was measured at different concentrations of iron cylinder (0, 10, 25, 35, 50 and 100 µM). Cells were treated with cylinder for 20 minutes at 37 ^{0}C for each concentration tested. A fluorimeter was used to record the fluorescence of each sample (λ_{exc} = 485 nm, λ_{em} = 530 nm) and three repeats were present at each concentration of iron cylinder tested. The data was blank adjusted using fluorescence values obtained from non-expressing MDAMB-231 cells treated with concentrations of cylinder (Figure 5.3).

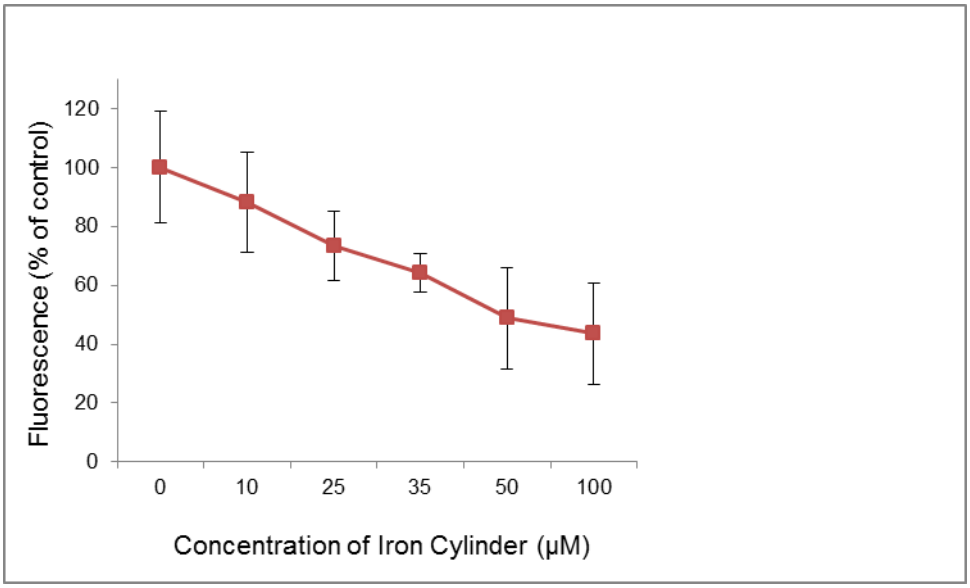

Figure 5.3. *Evaluation of fluorescence quenching in GFP-expressing MDAMB-231 cells by iron cylinder. Cells were treated for 20 minutes with iron cylinder at 37 ^{0}C prior to measuring fluorescence via fluorimetry. Values are the mean of three separate experiments ± S.E.M. No significant difference from control (p>0.05, One-way ANOVA).*

Results show a concentration-dependent decrease in GFP fluorescence intensity with increasing concentrations of iron cylinder. 100 µM cylinder caused a reduction by 56 % of the control. Despite no statistical significance ($p > 0.05$, One-way ANOVA), the biological trend seen is consistent with that shown in Figure 5.2. Further repeats are needed to achieve statistical significance. This data supports that obtained for purified protein indicating that the cylinder has the ability to cross the cell membrane and gain access to GFP inside living cancer cells and inhibit its action. The higher the concentration of cylinder used, the greater the strength of fluorescence quenching observed.

The precise mechanism by which the drug is able to quench GFP fluorescence in cancer cells remains unknown. However, it is tempting to speculate that the cylinder is directly interacting with the chromophore to have its effect. The well-known denaturant, guanidine disrupts the hydrogen bonding in protein molecules resulting in incorrect protein folding. As GFP fluorescence decreases by denaturing, guanidine is considered to be a quencher of GFP fluorescence having its effects by bringing about structural changes in the protein. The iron cylinder may be acting in the same way with regards to GFP.[7]

5.2.3 Investigating Hoechst Quenching by Iron Cylinder in GFP-Expressing MDAMB-231 Cells

To ensure that the GFP-expressing cell line was similar in every way to the non-expressing line other than in its expression of the GFP protein, the Hoechst quenching experiments (previously done using the MDAMB-231 cell line in Chapter 3) were carried out using the GFP-expressing version of these cells. The fluorescence for GFP-expressing MDAMB-231 and non-expressing cells was measured at each cylinder concentration tested (0, 10, 25, 35, 50 and 100 µM). Cells were treated with Hoechst and then cylinder (20 minutes at 37 ^{0}C for each incubation period). A fluorimeter was used to record the fluorescence of each sample (λ_{exc} = 340 nm, λ_{em} = 460 nm) and three repeats were collected for each concentration of iron cylinder used (Figure 5.4).

Results obtained for both cell lines revealed a decrease in Hoechst fluorescence caused by increasing concentrations of cylinder. Treatment of GFP-expresing MDAMB-231 with 100 µM cylinder reduced fluorescence intensity by 44 % of then control and 55 % in the non-expressing MDAMB-231 cells. This result was found to be statistically significant in terms of difference from the control ($p < 0.001$, One-way ANOVA followed by Tukey test) (Figure 5.4).

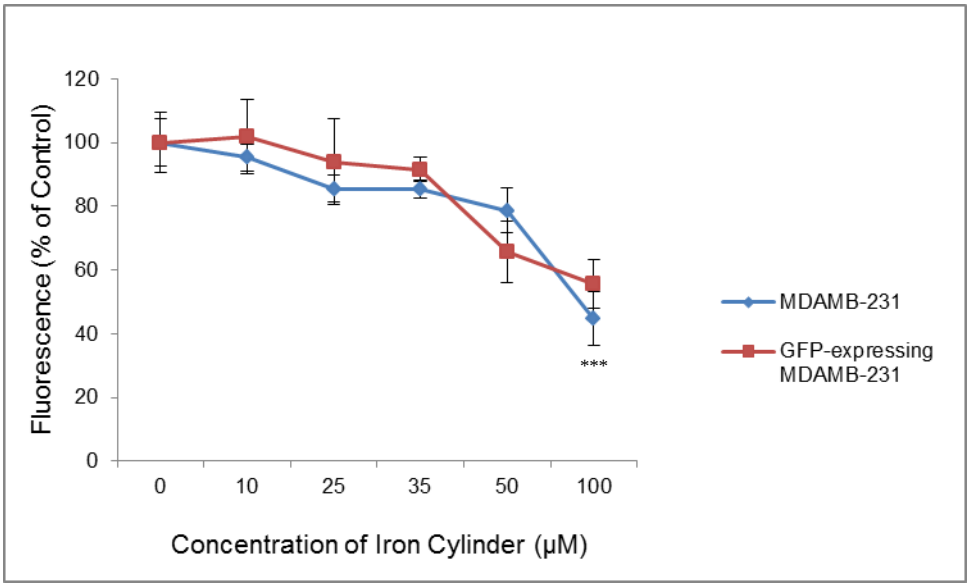

Figure 5.4. *Evaluation of Hoechst fluorescence in GFP-expressing MDAMB-231 and non-expressing MDAMB-231 cells. Cells were treated for 20 minutes with Hoechst followed by 20 minutes with cylinder at 37 ^{0}C prior to measuring fluorescence via fluorimetry. Values are the mean of three separate experiments ± S.E.M. Significant difference from control, with p<0.05: *, <0.01: **, <0.001: ***. (One-way ANOVA followed by Tukey test).*

The results confirm that the cylinder is able to access the nuclear DNA in both cell lines and cause displacement or quenching of the Hoechst dye in both cases. When investigating Hoechst quenching, the general trend is similar across both cell types and no statistical difference was found between the two cell types ($p > 0.05$, Two-way ANOVA). These results provided further confidence with regards to results obtained for GFP quenching in this cell line. Furthermore, despite the slight variation in extent of quenching, the trend seen here is similar to that seen in Figure 3.9 with increasing concentrations of cylinder causing greater Hoechst quenching.

The intensity of Hoechst and GFP quenching over time was then compared using GFP-expressing MDAMB-231 cells treated with 50 μM cylinder. This concentration of cylinder was chosen as it was previously shown to quench both Hoechst and GFP significantly in these cells (Figures 5.3 and 5.4). Two experiments were carried out. In the first, cells were treated with Hoechst and then cylinder (20 minutes at 37 ^{0}C). The cylinder containing media was washed away and the fluorescence recorded at 20 minute intervals over 3 hours (λ_{exc} = 340 nm, λ_{em} = 460 nm for Hoechst, λ_{exc} = 485 nm, λ_{em} = 530 nm for GFP) (Figure 5.5A). In the second, cells were treated with Hoechst (20 minutes at 37 ^{0}C) and then cylinder for 3 hours at 37 ^{0}C but remained in contact with the cylinder over the 3 hour period as the cylinder containing media was not washed away (Figure 5.5B). The fluorescence was recorded at 20 minute intervals over the 3 hour period (λ_{exc} = 340 nm, λ_{em} = 460 nm for Hoechst, λ_{exc} = 485 nm, λ_{em} = 530 nm for GFP). The fluorescence values shown for each time point were calculated using the average fluorescence of three readings.

The results show that GFP fluorescence decreases in a time-dependent manner when cylinder treatment is washed away. After 3 hours, the GFP fluorescence was reduced by 58 % of the control which was also left over time like this. Comparatively, under these conditions, the fluorescence of Hoechst does not decrease gradually over time. It is reduced by 56 % after 20 minutes and does not decrease further over the 3 hours (Figure 5.5A). When the cylinder remains in contact with cells, GFP fluorescence significantly decreases by 62 % and Hoechst by 60 % of the control after 20 minutes of exposure. Neither Hoechst nor GFP fluorescence decrease further over the time course (Figure 5.5B).

A

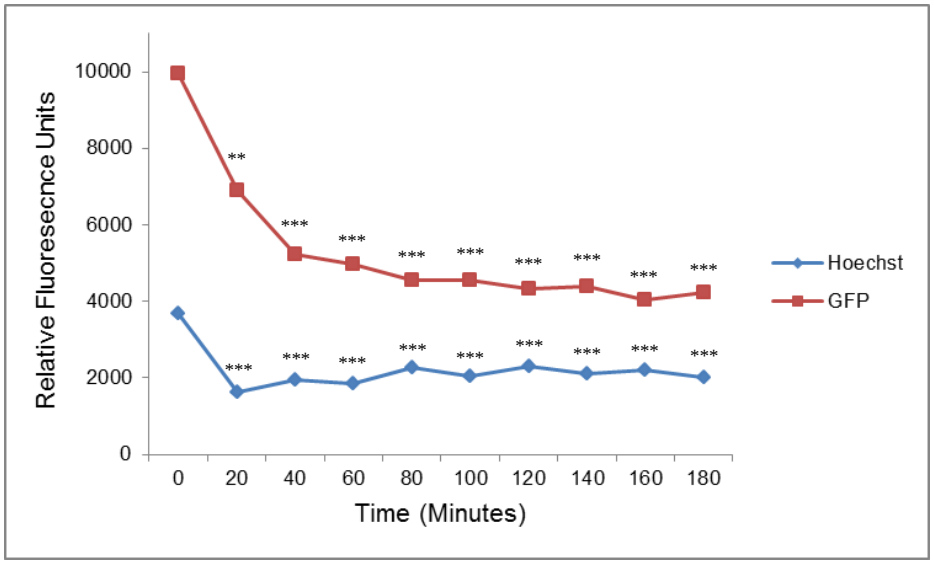

B

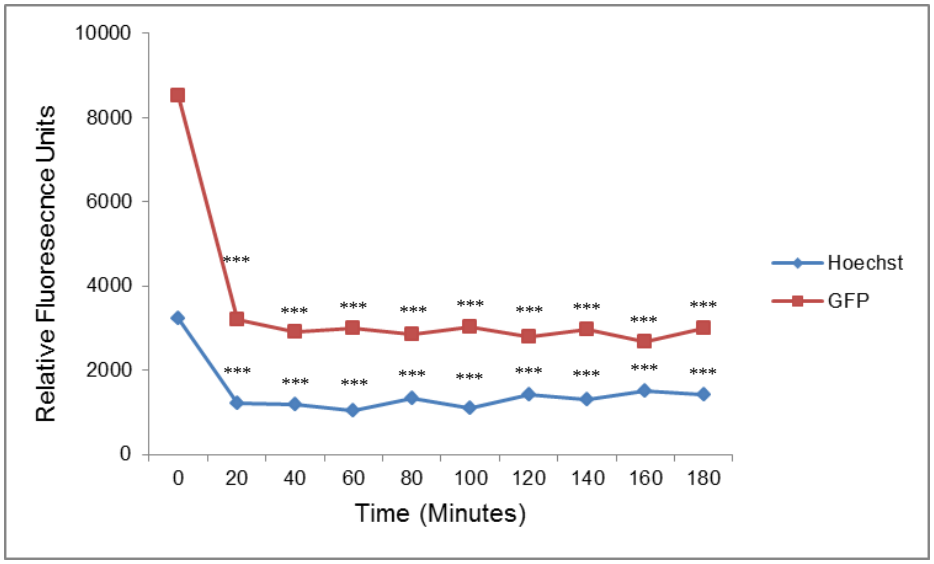

Figure 5.5. *Evaluation of Hoechst and GFP fluorescence in GFP-expressing MDAMB-231 cells exposed to 50 µM cylinder over time. Cells were treated for 20 minutes with Hoechst followed by treatment with cylinder at 37 ^{0}C.* ***A:*** *Cylinder containing media was washed away prior to measuring fluorescence via fluorimetry.* ***B:*** *Cylinder containing media remained in contact with cells and fluorescence measured via fluorimetry. Values are the mean of three separate experiments ± S.E.M. Significant difference from control, with p<0.05: *, <0.01: **, <0.001: ***. (One-way ANOVA followed by Tukey test).*

These results indicate that treatment of GFP-expressing MDAMB-231 cells with 50 µM cylinder for 20 minutes is sufficient for quenching both the Hoechst and GFP signals. As the GFP and Hoechst did not decrease further after 20 minutes of exposure to cylinder this suggests that within 20 minutes the cylinder is able to cross the cell membrane and have its effect. It is able to cross the nuclear membrane and bind to the DNA causing a displacement or quenching of Hoechst in addition to crossing the cell membrane and gaining access to the GFP chromophore causing inhibition possibly via structural changes in the protein. The results show that both Hoechst and GFP signals are quenched to similar extents (significantly reduced by around 60 % of the controls) when treated for 20 minutes with 50 µM cylinder. This data supports our previous findings where a range of concentrations of cylinder were tested over 20 minutes (Figures 5.3 and 5.4).

These results have allowed us to show that the concentration of cylinder used is far more important than the incubation period over which cells are exposed to it. 20 minutes appears to be a sufficient time point for the cylinder to have its effects. In these results, complete inhibition of GFP and Hoechst does not occur. This may be due to binding of Hoechst non-specifically to cellular targets with which the cylinder is not able to compete. Hoechst may be bound to RNA and so the signal is still present but not quenched by the cylinder. An excess of GFP may be responsible for the lack of complete inhibition of signal.

Results from Chapter 3 for MDAMB-231 cells treated with 50 μM iron cylinder for 20 minutes showed that Hoechst fluorescence was reduced by 79 % of the control. Results obtained here for the GFP-expressing MDAMB-231 cell line show a similar effect with Hoechst fluorescence reduced by 64 % under the same experimental conditions providing further support for previous findings. The cylinder may preferentially quench fluorescence from GFP than from Hoechst which could explain the greater reduction in Hoechst fluorescence seen in the non-expressing cell line.

5.2.4 Investigating Quenching of Nuclear GFP

Since the cylinder binds to DNA which is contained in the nucleus, it is of interest to investigate whether the GFP signal it appeared to quench was specifically nuclear. To test this confocal microscopy was used to image the nuclei of GFP-expressing MDAMB-231 cells. GFP-expressing MDAMB-231 cells were grown in MatTek dishes and treated with 50 μM iron cylinder for 20 minutes. Images were acquired at the beginning and the end of the cylinder treatment period. The fluorescence of the nucleus was monitored visually for changes (Figure 5.6).

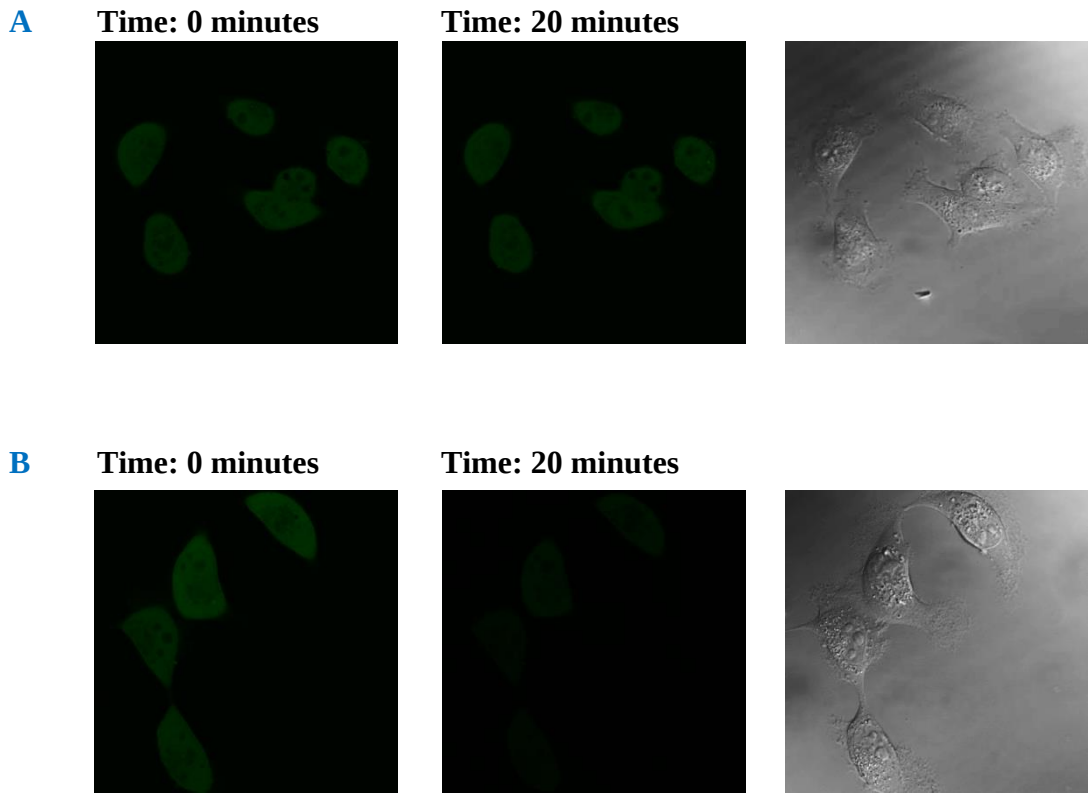

Figure 5.6. *Confocal imaging showing fluorescent and brightfield images of GFP-expressing MDAMB-231 cells treated for 20 minutes with 50 µM iron cylinder.* ***A:*** *Fluorescent and brightfield images of untreated control cells imaged at the start and end of the 20 minute period.* ***B:*** *Fluorescent and brightfield images of cells imaged immediately after cylinder treatment and 20 minutes after cylinder treatment.*

Results show a clear visual decrease in the nuclear fluorescence of cells treated with cylinder at the end of the treatment period. Comparatively, control cells which were untreated do not show any visible reduction in the fluorescence signal over the time period imaged. Bright field images reveal that the cells were intact and therefore any decrease in fluorescence can be attributed to the treatment undergone. We hypothesize

that the cylinder enters the cell, crosses the nuclear membrane and interacts with the GFP chromophore resulting in quenching of fluorescence.

5.3 Conclusions and Future Work

The results have provided evidence for the cylinder's ability to quench the green fluorescent protein, possibly from the nucleus. In order to confirm this, the cylinder's ability to quench fluorescence from the cell cytoplasm and organelles would need to be further investigated and quantified. Cellular components transfected with GFP followed by treatment with cylinder and isolation would provide further insight into the cylinder's preferential route of quenching GFP. The rate at which nuclear Hoechst is quenched by cylinder can be compared with the rate of GFP by using GFP-tagged nuclear proteins and monitoring the fluorescence over a time course at a range of cylinder concentrations. In addition, red fluorescent protein (RFP) could also be tagged and targeted to different organelles.

These results have important potential applications *in vitro* and *in vivo* for the cylinder because GFP can be stably expressed in a range of tumour cells which can be implanted into animals. Since the cylinder quenches GFP this could serve as a tool to image cylinder uptake and localization *in vivo*. It could help to further investigate the mechanism and route by which the cylinder enters cells and has its effects. GFP animal models are readily available, have stable expression and don't require additional factors to fluoresce making this protein ideal to use for tracking the progression of tumours.[1]

5.4 References

[1] Hoffman, R. (2002) Green fluorescent protein imaging of tumour growth, metastasis, and angiogenesis in mouse models. *Lancet Oncol.* 3 (9): 546-56.

[2] Mehta, S.R., Huang. R., Yang, M., Zhang, X., Kolli, B., Chang, K., Hoffman, R.M., Goto, Y., Badaro, R., Schooley, R. T. (2008) Real-Time In Vivo Green Fluorescent Protein Imaging of a Murine Leishmaniasis Model as a New Tool for Leishmania Vaccine and Drug Discovery, *Clinical and Vaccine Immunology*. 15 (12): 1764-1770.

[3] Tsien, R. Y. (1998) The Green Fluorescent Protein. *Annu. Rev. Biochem*. 67: 509–44.

[4] Bou-Abdallah, F., Chasteen, N.D., Lesser, M. P. (2006) Quenching of superoxide radicals by green fluorescent protein. *Biochimica et Biophysica Acta*. 1760 (11): 1690-1695.

[5] Zimmer, M. (2002) Green Fluorescent Protein (GFP): Applications, Structure, and Related Photophysical Behavior. *Chem. Rev.* 102 (1): 759-781.

[6] Hahn, P. J. (1993) Molecular biology of double-minute chromosomes. *Bioessays*. 15 (7): 477-484.

[7] Jung, K., Park, J., Maeng, P., Kim, H. (2005) Fluorescence Quenching of Green Fluorescent Protein during Denaturation by Guanidine. *Bull. Korean Chem. Soc.* 26 (3): 413-417.

CHAPTER 6

Investigating *In Vitro* and *In Vivo* Toxicity of Iron Cylinder

Zebrafish research was carried out at the Institute of Biomedical Research in the Medical School at the University of Birmingham. Egg collection and micro-injection was carried out by Dr. Y. Hadzhiev.

6.1 Introduction

In addition to assessing toxicity and investigating the effects of a potential anticancer agent *in vivo*, it is important to investigate toxicity *in vitro* using specific cancer cells of interest. This allows researchers to study the direct effects of the drug on mammalian cells and do so in the absence of intervening factors. Genotoxic agents induce DNA damage which can lead to mutations that can later form tumours and a number of *in vitro* methods exist to test the genetic toxicity of a drug.[1] The Comet assay is a single cell gel electrophoresis assay which provides a fast and sensitive measure of single and double stranded breaks in the DNA of cells. Two variants of the assay exist namely alkaline and neutral comet assay. It has been suggested that the variants distinguish between types of damage with the neutral assay preserving the double-stranded DNA structure and therefore only detecting double stranded breaks. Comparatively the alkaline comet assay is believed to be much more sensitive and able to detect both single and double strand DNA breaks.[1]

This assay has been used to assess the genotoxic potential of drugs such as cisplatin which despite being an effective anticancer drug, is highly cytotoxic.[2] As cisplatin is not specific in its action, genetic damage can result in unaffected tissues leading to accumulation of mutations and secondary tumors several years after cessation of treatment.[2] In addition to its genotoxicity, many tumours have also acquired resistance to this drug (see section 1.5). These drawbacks have prompted research into developing new anticancer drugs which can have their effects in the absence of genotoxicity.

An essential part of determining safe and effective dosage for novel drugs to be used in the clinic is a good understanding of the drug's performance using *in vivo* systems. Despite the fact that significant advances have been made using established cell lines, to progress further animal models are required which more closely resemble the heterogeneous nature of human tissues.[3] In comparison to cell-based systems, research using *in vivo* systems is particularly important as they provide good physiological models that more closely resemble the complex environment within the human body. Results from these studies can be used to help in the design of clinical trials and establish the likely effects a drug will have when administered to a patient.[4] The zebrafish is a popular vertebrate model organism used in medical research due to its small size and ease of culture. They offer a range of advantages including the clear visualization of complex developmental processes from embryo to adulthood with the process of embryogenesis in humans closely resembling that displayed during zebrafish development. Furthermore, the embryos are clear and develop rapidly outside the parent making it possible for researchers to visualize the embryo across developmental stages including the materialization of internal organs.[5]

In addition to these advantages, the numbers of offspring produced allows high throughput screening to be conducted relatively cheaply which would not be possible using other model organisms such as rodents. Numerous mutations have been identified in zebrafish which cause disruptions in the developing embryo. These mutants have provided accurate models for a number of human diseases including immunological disorders and cancers. Research using these models can provide information about genes

responsible for various processes in human development.[5] Furthermore, experiments on zebrafish embryos and early larvae (less than 6 days after hatching) do not require a Home Office license in the UK as The Animals Scientific Procedures Act (1986) only regulates fish from the time at which they become capable of independent feeding.[6]

In this chapter the previous *in vitro* work is moved forward to a whole organism using the *in vivo* zebrafish model. The toxicity of iron cylinder in this organism is investigated and compared with that of cisplatin. Phenotypic changes occurring in the developing embryo in response to treatment are examined and the genotoxic potential of iron cylinder is investigated in relation to cisplatin using the comet assay.

6.2 Results and Discussion

6.2.1 *In Vivo* Imaging

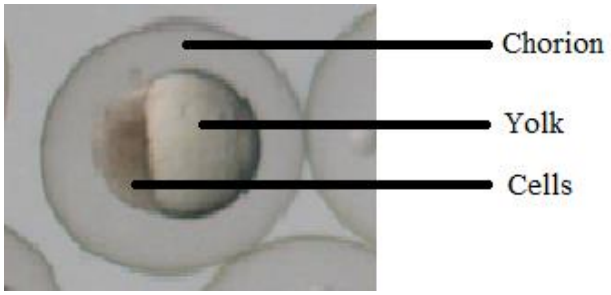

Figure 6.1. *Representative image of a zebrafish embryo 5 hours post fertilisation (hpf) obtained by bright field microscopy.*

Due to its large number of virtues, the zebrafish was chosen as a model to further investigate the iron cylinder. In chapter 3, a novel method was developed to indirectly image the non-fluorescent iron cylinder via its quenching of nuclear Hoechst fluorescence. Here, the use of zebrafish takes this work further to allow Hoechst quenching to be monitored *in vivo*. This provides a working animal model allowing direct imaging of the cylinder having its affect in an organism. This could also allow distribution of the drug to be visualized through its quenching mechanism. Initially, embryos were incubated in a range of Hoechst concentrations. However, poor penetration of the dye prevented any staining of nuclei with a range of concentrations tested.

Mature eggs of zebrafish embryos are surrounded by a protective membrane known as the chorion. The process of dechorionation carefully removes this membrane (manually using a sharp steel needle) allowing better microscopic observations as well as improving the access of an external compound to the embryonic cells. Dechorionated embryos were incubated into Hoechst solutions with the aim of improving dye penetration in the developing embryo. However, confocal microscopy revealed similar results to embryos with their chorion intact, with no penetration of dye. Higher concentrations of dye and longer incubation periods were explored (up to 100 μM for 5 hours) but the results obtained did not reveal sufficient staining. Concentrations of over 50 μM resulted in embryo death after 5 hours.

An alternative strategy was then used which involved directly micro-injecting Hoechst into the embryos. Dechorionated zebrafish embryos at one-cell stage were injected by hand with 25 µM Hoechst (final concentration) and incubated at 28 ^{0}C. Images were acquired 5 hpf using confocal microscopy (Figure 6.2)

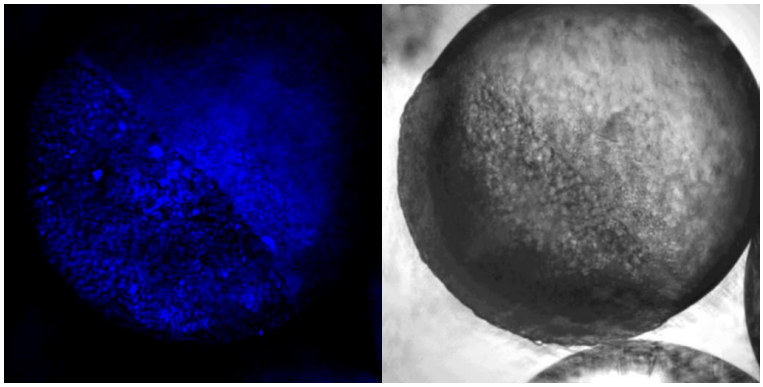

Figure 6.2. *Confocal imaging showing fluorescent and brightfield images of zebrafish embryos (5 hpf) injected with 25 µM Hoechst at one-cell stage.*

Confocal imaging results revealed a very speckled non-specific Hoechst signal which was distributed throughout the cells and the yolk. When untreated control embryos were imaged, a similar image was produced. Due to the high background UV fluorescence in the zebrafish embryos and possible trapping of the dye in the hydrophobic yolk, quenching *in vivo* upon administration of iron cylinder could not be monitored.

6.2.2 *In Vivo* Toxicity Studies

The toxicity of the cylinder in zebrafish was investigated and compared with the toxicities of Hoechst and cisplatin. This is an important part of drug development to establish therapeutic concentrations of novel drugs in a whole organism. Survival of zebrafish embryos was monitored after treatment with Hoechst, iron cylinder or cisplatin to determine a non-toxic concentration range for treatment. Embryos at one-cell stage were injected by hand with 10 or 100 μM compound and incubated at 28 ^{0}C. Survival was quantified by counting live embryos at 4 and 24 hpf. The percentages of viable embryos shown in the results were calculated using the average count of three experiments (Figure 6.3).

A

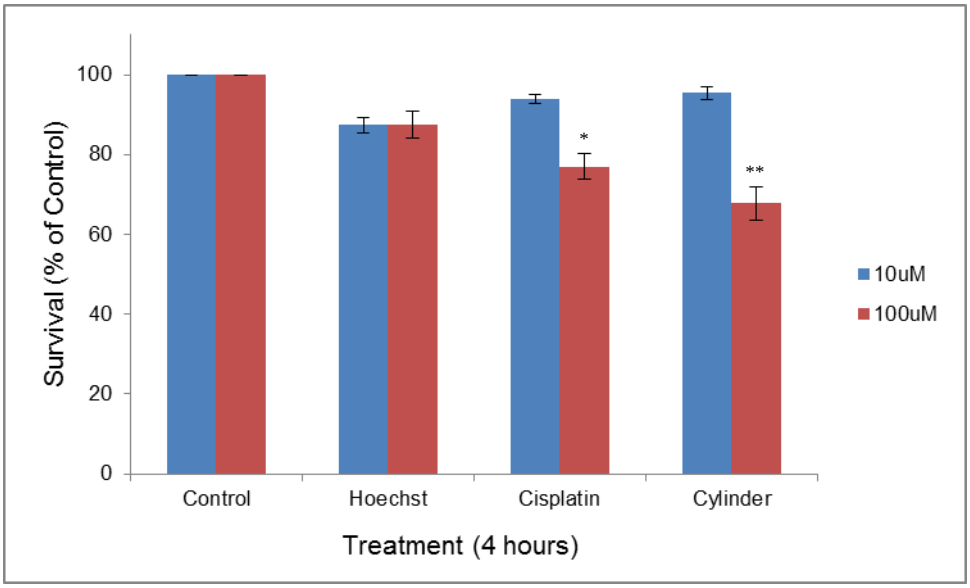

B

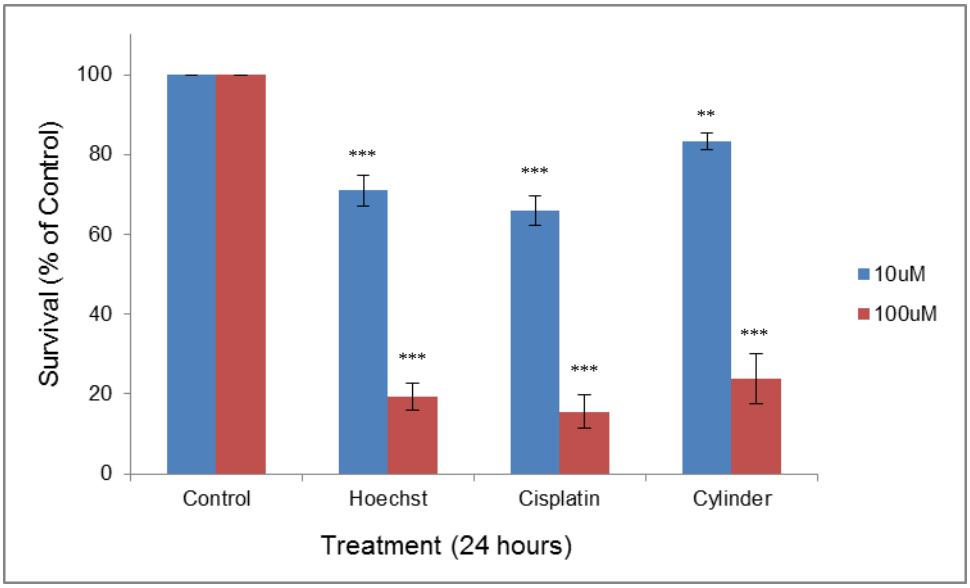

Figure 6.3. *Evaluation of toxic effects of Hoechst, Iron cylinder and Cisplatin treatment in zebrafish. Embryos were injected with compound and survival monitored by counting viable embryos over 4 hours* ***(A)*** *and 24 hours* ***(B)****. Controls were injected with phenol red. Values are the mean of three separate experiments ± S.E.M. Significant difference from control, with p<0.05: *, <0.01: **, <0.001: ***. (One-way ANOVA followed by Tukey test).*

The results show that treatment of embryos with 10 µM Hoechst, cylinder or cisplatin for 4 hours did not cause any significant decrease in survival of embryos with over 87 % remaining viable for each compound tested. Comparatively, treatment with 100 µM Hoechst, cylinder or cisplatin for 24 hours decreased survival to less than 25 % of the control with very high statistical significance ($p < 0.001$). The embryos appear to be more resistant to the effects of the cylinder as opposed to cisplatin at this time point (24 % survived cylinder treatment as opposed to 16 % for cisplatin treatment). These results indicate that concentrations of 100 µM cylinder are directly toxic to zebrafish and therefore should not be used for testing the effects of this drug *in vivo* (Figure 6.3).

Treatment of embryos with 10 µM cylinder for 24 hours reduced survival to 83 %. Comparatively, for embryos treated with 10 µM cisplatin, survival was reduced to 66 % after 24 hours. This provides a large therapeutic window for the iron cylinder over which it can be administered to have its beneficial effects without causing death to the organism (Figure 6.3). Results show that 100 µM Hoechst treatment reduced survival to 19 % after 24 hours. Hoechst toxicity data supports the earlier results where Hoechst was injected into embryos for imaging purposes with death resulting from treatment with 100 µM.

Figure 6.4 shows representative images acquired for the embryos monitored for survival. Treatment of embryos with compound resulted in a developmental delay when compared to untreated control embryos. The higher concentration (100 µM) caused abnormal cell growth with cells moving away from the yolk as opposed to spreading around it. Eventually, the cells detached from the yolk and the embryo disintegrated.

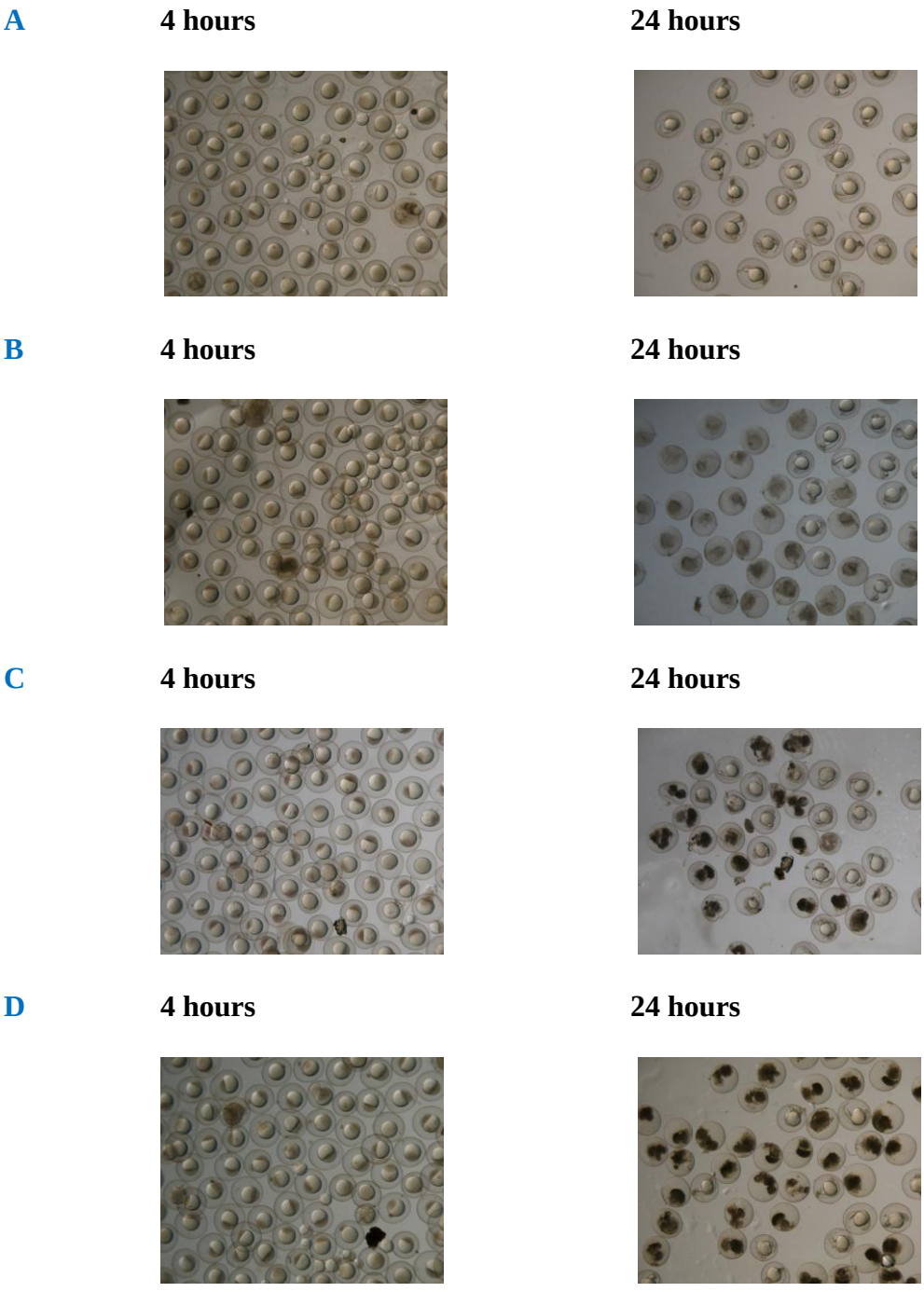

Figure 6.4. *Brightfield images showing zebrafish embryos injected at one-cell stage with 100 µM compound.* ***(A)*** *Brightfield images of untreated control embryos imaged at 4 hpf and 24 hpf,* ***(B)*** *Brightfield images of Hoechst treated embryos imaged at 4 hpf and 24 hpf,* ***(C)*** *Brightfield images of iron cylinder treated embryos imaged at 4 hpf and 24 hpf,* ***(D)*** *Brightfield images of Cisplatin treated embryos imaged at 4 hpf and 24 hpf.*

6.2.3 *In Vitro* Genotoxicity Studies

Genotoxicity is one of the major drawbacks of anticancer agents currently in use such as cisplatin. The comet assay is a single cell gel electrophoresis assay which allows sensitive detection of single and double strand breaks in the DNA. In this assay, the larger the comet tail, the greater the number of DNA strand breaks present. Neutral and alkaline conditions are two variations of the comet assay method. The prevailing view is that the neutral version detects double stranded breaks and the alkaline version detects both single and double stranded breaks in DNA.[5] However, this is the subject of some debate with some authors proposing that using a pH close to neutral does not specifically identify double-stranded breaks.[8]

Alkaline and neutral comet assays were carried out to detect DNA strand breaks in the HL60, human myeloid leukemia cancer cell line. Cells were treated with 25 μM compound for 8 hours prior to cell lysis, staining of the DNA and electrophoresis. The mean % tail intensity obtained from comets was calculated using the average of three readings (Figure 6.5).

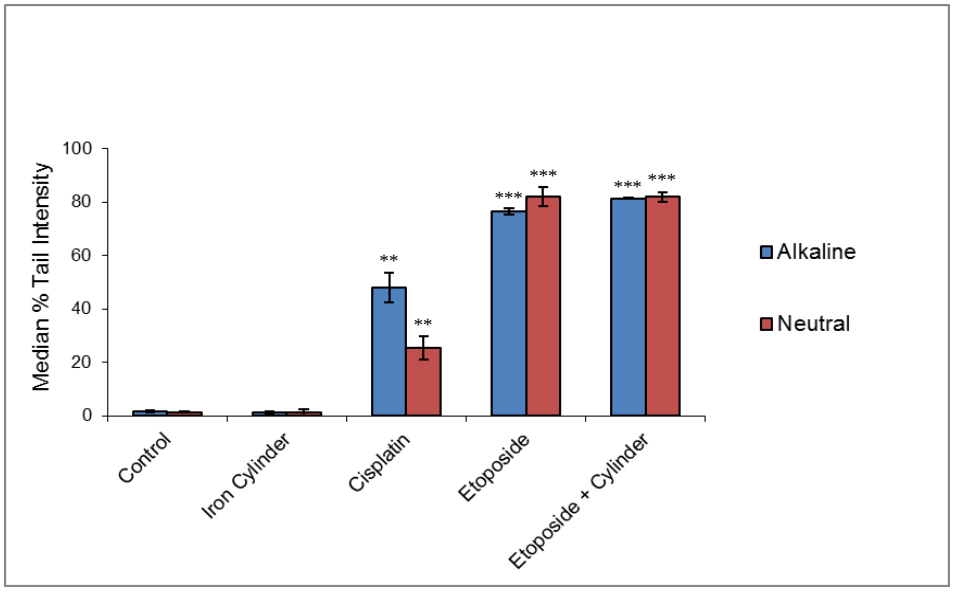

Figure 6.5. *Evaluation of genotoxic effects of treatment in HL60 cells using the comet assay. Cells were incubated with 25 µM compound for 8 hours prior to obtaining mean % tail intensity. Values are the mean of three separate experiments ± S.E.M. Significant difference from control, with p<0.05: *, <0.01: **, <0.001: ***. (One-way ANOVA followed by Tukey test).*

Results show that treatment with 25 µM cylinder for 8 hours did not cause any significant increase in mean % tail intensity (1 % of the control for both neutral and alkaline comet assays). This indicates that treatment with cylinder does not cause production of single or double strand breaks in DNA at this concentration and time point. This is positive for the potential of iron cylinder as a cancer drug as it can have its effect in cancer cells and do so in the absence of genotoxicity. Treatment of tumours with potent genotoxic drugs may result in secondary tumours occurring in patients years after treatment has ceased. Comparatively, cisplatin treatment at the same concentration and timepoint resulted in an increase to 48 % mean tail intensity under alkaline and 25 % under neutral conditions of

high statistical significance ($p < 0.01$, One-way ANOVA). These results indicate that exposure of leukemic cells to cisplatin causes single and double stranded breaks in DNA as expected.

Etoposide binds to DNA and inhibits the topoisomerase enzyme required for the unwinding of DNA. During DNA replication, strand breaks occur and trigger cell suicide mechanisms.[7] Results show that treatment with 25 μM etoposide for 8 hours increased mean % tail intensity to 76 % in the alkaline and 82 % in the neutral comet assay with very high statistical significance ($p < 0.01$, One-way ANOVA). These results are as expected with etoposide being a potent inducer of double strand breaks as indicated by results for the neutral comet assay. Similarly, treatment with cylinder and etoposide together resulted in increased % mean tail intensity (81 % and 82 % for alkaline and neutral conditions respectively). The results indicate that cylinder in the presence of etoposide does not have any protective role to reduce the DNA damage resulting from etoposide treatment. Moreover, it indicates that the cylinder's ability to coil and compact DNA is not masking the presence of strand breaks, since the etoposide tail intensity is not reduced in the presence of cylinder. This is good evidence that the cylinder is indeed not a strand break agent and that its coiling ability is not creating a false negative result in the comet assay.

6.3 Conclusions and Future Work

The results have further provided evidence for the non-genotoxic nature of iron cylinder. In comparison to the cancer chemotherapeutics, etoposide and cisplatin, the cylinder does not induce significant production of single or double strand breaks in the DNA of leukemia cells as assessed by neural and alkaline versions of the comet assay.

Treating zebrafish embryos with 100 µM cylinder for 24 hours had a similar effect to that seen with *in vitro* cell testing. HL-60 leukemia cells treated with the same concentration and timepoint resulted in direct cytotoxicity and only necrotic cells being identified.[9] Embryos injected with 10 µM cylinder for 24 hours showed a significant decrease in survival when compared to the control. Using *in vitro* cell systems, an increase in apoptotic cell numbers was observed in HL-60 cells treated for 24 hours with 10µM cylinder .[9] The *in vivo* results obtained here support data published previously for tumor cell lines. This implies that injecting 10 µM cylinder for 24 hours in zebrafish embryos induces apoptotic cell death and increasing this concentration to 100 µM causes necrotic cell death as seen by the significant decrease in embryo survival rate.

This is the first *in vivo* research conducted for the iron cylinder using the model system of zebrafish embryos. The direct micro-injection results have indicated that the concentration of cylinder tolerated in this organism is between 10 and 100 µM. This provides a large therapeutic window over which the cylinder can bring about its effect. Morphological changes in the developing embryo have been observed upon cylinder treatment which may provide further insight into its localization and distribution *in vivo*.

6.4 References

[1] Peycheva, E., Georgieva, M., Miloshev, G. (2009) Comparison between alkaline and neutral variants of yeast comet assay. *Biotechnol and Biotechnol*. 23 (1): 1090-1092.

[2] Jung, Y., Lippard, S. J. (2007) Direct cellular responses to platinum-induced DNA damage. *Chem Rev.* 107: 1387-1407.

[3] Marsden, C. G., Wright, M. J., Carrier, L., Moroz, K., Pochampally, R., Rowan, B. G. (2012) A novel in vivo model for the study of human breast cancer metastasis using primary breast tumor-initiating cells from patient biopsies. *BMC Cancer*. 12 (1): 1-16.

[4] Bjornsson, T. D., Callaghan, J. T., Einolf, H. J., Fischer, V., Gan, L., Grimm, S., Kao, J., King, S. P., Miwa, G., Ni, L., Kumar, G., Mcleod, J., Obach, R. S., Roberts, S., Roe, A., Shah, A., Snikeris, F., Sullivan, J. T., Tweedie, D., Vega, J. M., Walsh, J., Wrighton, S. A. (2003) The conduct of in vitro and in vivo drug-drug interaction studies: a pharmaceutical research and manufacturers of America (PhRMA) perspective. *Drug metabolism and disposition: the biological fate of* chemicals. 31 (7): 815-832.

[5] Blackburn, J. S., Liu, S., Raimondi, A. R., Ignatius, M. S., Salthouse, C. D., Langenau, D. M. (2011) High-throughput imaging of adult fluorescent zebrafish with an LED fluorescence macroscope. *Nat Protoc*. 6 (2): 229-241.

[6] http://www.legislation.gov.uk/ukpga/1986/14/contents

[7] Schonn, I., Hennesen, J., Dartsch, D. C. (2010) Cellular responses to etoposide: cell death despite cell cycle arrest and repair of DNA damage. *Apoptosis*. 15 (2): 162-172.

[8] Collins, A. R., Oscoz, A. A., Brunborg, G., Gaivao, I., Giovannelli, L., Kruszewski, M., Smith, C. C., Stetina, R. (2008) The comet assay: topical issues. *Mutagenesis*. 23 (3): 143-151.

[9] Hotze, A. C., Hodges, N. J., Hayden, R. E., Sanchez-Cano, C., Paines, C., Male, N., Tse, M. K., Bunce, C. M., Chipman, J. K. Hannon M. J. (2008) Supramolecular iron cylinder with unprecedented DNA binding is a potent cytostatic and apoptotic agent without exhibiting genotoxicity. *Chem Biol*. 15 (12): 1258-67.

CHAPTER 7

Conclusions and Future Work

In this thesis, the iron cylinder has been investigated as a quencher of nuclear Hoechst fluorescence in a range of cancer cell lines. Flow cytometry and fluorimetry have quantified quenching occurring in a concentration-dependent manner at the population level in a range of cancer cell types. These results provide evidence for the cylinder being able to cross the cell/ nuclear membrane and interact in close proximity of the Hoecst bound in the DNA minor groove. As the cylinder was designed to be the right size and shape to fit perfectly into the major groove spanning five base pairs, data obtained here suggests the quenching observed is due to strong binding of the iron cylinder at this location.[1] Previous studies looking at the crystal structure of the cylinder found no significant disturbances in the DNA when cylinder was bound which further supports the cylinder's perfect fit in the major groove.[2]

This work has shown that the cylinder can get into a range of tumour types within 20 minutes and is effective at concentrations as low as 10 μM. This data supports previous findings where Hoechst-loaded HL60 cells were treated with cylinder and the fluorescence spectra produced identified the displacement.[3] The work in this thesis has further expanded the current knowledge base by finding that the cylinder can penetrate the cell membrane of adherent and suspension tumour cells when administered in growth media for short periods of time. Furthermore, epifluorescence microscopy has allowed visual observations of the quenching in these cells. Ovarian cancer cells have shown a greater resistance to the cylinder's effects when compared with breast cancer and leukaemia cell lines. This finding is of interest as many ovarian cancers have developed resistance to the classic chemotherapeutic, cisplatin.[4,5] Therefore, giving the cylinder an

advantage as SKOV3 cells showed sensitivity to this compound albeit reduced when compared to the other cancer types investigated. A novel idea has been developed in this thesis which provides exciting possibilities allowing indirect fluorescent imaging of non-fluorescent compounds through the exploitation of their binding nearby a bound fluorescent stain.

Experiments were conducted to optimize the concentrations of substrates required (1 mM luciferin and 1 mM ATP) to produce luminescent signals from luciferase-expressing breast cancer cells. Once achieved, experiments were conducted using lysed cells and trypsinized cells to investigate iron cylinder's effects on light emission in the absence of cell adhesion factors. Following on from the success achieved in this work, adherent luciferase-expressing cells were used finally to confirm the results. The discovery made during this research about iron cylinder's inhibition of luciferase is unprecedented and provides new possibilities by which the location of cylinder can be tracked.

The cylinder has been shown to directly affect light emission in a concentration-dependent manner and a concentration of 10 µM cylinder has been found to be sufficient at inhibiting the emission from luciferase-modified breast cancer cells. The cylinder may be physically interacting with the ATP-luciferase complex and preventing the enzyme from accessing the substrate required for the bioluminescent reaction to proceed. Further insight was provided by investigating changes in the intensity of inhibition over time. Data obtained identified the flash kinetic nature of the enzymatic reaction as the signal produced decreased rapidly. This highlighted the importance of obtaining measurements

rapidly upon substrate addition and the need to maintain consistency across experiments to produce reliable data. The work carried out provides further opportunities for imaging by monitoring the inhibition of luminescent enzymes.

Starting with the use of purified green fluorescent protein (GFP), the idea that cylinder could quench GFP fluorescence in cells was explored further in GFP-modified breast cancer cells using fluorimetry and confocal microscopy. Results from this work identified that treatment of GFP-modified breast cancer cells with 50 μM cylinder for 20 minutes resulted in dramatic GFP quenching and the signal was not further quenched when cells were in contact with the cylinder for a longer period. These findings complement those obtained for Hoechst quenching experiments and expand on the current knowledge of the cylinder confirming that it is able to enter the nucleus and bind to the DNA within 20 minutes.

In addition to decreasing Hoechst fluorescence, iron cylinder's ability to competitively displace ethidium and propidium from DNA has previous been shown.[3] However, the discovery that iron cylinder quenches GFP fluorescence and can do so from intact cells has not previously been reported in the literature. These results are of great potential importance as the expression of the protein in tumours of could serve as a tool to image uptake and localization both *in vitro* and *in vivo.*

During the course of the experiments carried out in this thesis, the iron cylinder's genotoxicity was investigated in relation to the DNA crosslinker, cisplatin and the

topoisomerase inhibitor, etoposide. This work has supported current literature confirming that both of these widely used chemotherapeutics cause DNA single and double stranded breaks.[6,7] In contrast, the iron cylinder was found not to be genotoxic in leukemic cells. Previously, the comet assay has been carried out in ovarian and leukemic cell lines treated with cylinder for 24 hours.[3] This published data revealed no evidence of cylinder-related genotoxicity which strengthens the findings from this current research and favours its potential as an effective anticancer agent.

The work in this thesis expands the current knowledge of the cylinder's genotoxic potential as two versions of this assay have been investigated. The neutral version detects only double stranded breaks and the alkaline version is able to detect both single and double stranded structures. This research has confirmed that the cylinder is not genotoxic through either version of the comet assay. Furthermore, the novel combination of etoposide plus cylinder was tested and results showed that the presence of cylinder offered no form of protection with no reduction in damage to DNA caused by etoposide in cells. This work expanded on previously reported atomic force microscopy data showing the cylinder's ability to induce intramolecular DNA coiling.[8] Here it was confirmed that the cylinder does not cause strand breaks and its coiling is not creating a false negative result in the comet assay by masking the presence of strand breaks. The genotoxicity research could be extended to further investigate the cylinder when treated on cells with significant DNA strand breaks induced by other treatments.

Prior to the work carried out in this thesis, iron cylinder's effects in a whole organism had never been studied. In chapter six, the toxicity of iron cylinder was investigated in the model organism, zebrafish for the first time. A concentration of 10μM cylinder injected directly into embryos has been found to not kill the organism. In previously published literature, this concentration induces some (but not total population) apoptotic cell death in cancer cells *in vitro*.[3] This might explain the increased survival seen *in vivo* at 10μM when compared to 100 μM. In cancer cells, 100μM cylinder has been found to cause cell death by necrosis which may also be the mechanism causing death *in vivo* for this concentration.[3] Drugs with small therapeutic windows require close monitoring of plasma levels to maintain effective dosages in patients.[9] Therefore, the novel finding which indicates a large therapeutic window over which the cylinder can elicit its therapeutic response in the absence of toxicity is advantageous for its potential as a safe drug.

In the literature, iron cylinder has been shown to be up to five times less toxic than cisplatin in a variety of cancer cells with mitochondrial toxicity values comparable to the drug carboplatin which has fewer side effects.[3] Initial findings from the work carried out in zebrafish embryos indicate that the cylinder is less toxic than Hoechst and cisplatin over 24 hours which is in support of published *in vitro* data. Furthermore, it would be expected that the cylinder is less toxic than cisplatin *in vivo* as has already been identified *in vitro* through the use of the comet assay. However, to strengthen the zebrafish data and make the results more conclusive, further studies need to be carried out examining a greater range of concentrations and time points. A developmental delay and phenotypic

changes occurring in embryos in response to cylinder treatment have also been observed which can provide further information about its mechanism of action *in vivo*.

There is a need to carry out epifluorescence microscopy as described in chapter three but with cylinder concentrations ranging from 0 to 100 μM. Quantification of the fluorescent images produced by measuring changes in pixel intensity of nuclear Hoechst would provide further support for the data acquired. The differences observed in the uptake of cylinder between cancer cell types can be further investigated by using inhibitors of specific transporters prior to treatment. The use of *in vivo* knockout mouse models, deficient in certain drug transporters can provide further insight into the mechanism by which cylinder is absorbed across cell membranes. Further work to precisely confirm the location of iron cylinder in the nucleus should also be conducted using the synchrotron light source to carry out elemental mapping using X-ray absorption spectroscopy.

From chapter four the need arises to investigate the iron cylinder's quenching of the luminescence signal in a whole organism. Cancer cells stably expressing luciferase can be transplanted subcutaneously into a small animal such as a mouse. After supplying the substrates required for the bioluminescence reaction to occur, iron cylinder would be injected into the animal possibly through the tail vein. The absorption and distribution of the cylinder would then be tracked in the cancer cells by its inhibition of the emitted light. This system would serve as an indirect imaging tool to further investigate interactions of the cylinder in an *in vivo* system.

The data obtained from experiments carried out in chapter four was through the use of luciferase-modified breast cancer cells. Therefore, to take this research further it is important to explore ovarian cancer cells with respect to inhibition of light emission by iron cylinder. A greater resistance to the effects of cylinder when compared to breast cancer cells would be predicted and this data could further support results obtained in chapter three where increased sensitivity of breast cancer cells to fluorescence quenching by iron cylinder has been observed.

As GFP animal models are readily available, have stable expression and don't require additional factors to fluoresce, this makes this protein ideal to use for tracking the progression of tumours. The gene that encodes GFP can be inserted into zebrafish embryos to allow integration into the animal's genome. Treatment with cylinder would then occur and the cylinder could be monitored by its fluorescence quenching. This would allow changes in the distribution and accumulation of cylinder in the developing zebrafish to be studied. The same principle could be applied to GFP-mouse models.

Quenching of purified green fluorescent protein by iron cylinder should be carried out using concentrations below 10 μM as this has not been investigated. Furthermore, as GFP-quenching has only been studied in breast cancer cells during the research carried out in this thesis, it is important to make sure other cancer types are also investigated. It would be especially interesting to see how the extent of the quenching compares across ovarian and leukemic cell lines.

A cancer cell line expressing a nuclear GFP fusion protein could be used to investigate cylinder quenching GFP from the nucleus. A range of cylinder concentrations (0-100 μM) could be tested and the fluorescent images obtained through microscopy could be quantified. Analysis of nuclear GFP quenching occurring at the population level could be quantified through the use of fluorimetry and flow cytometry. The results obtained could then be compared with the same cancer cell line expressing cytoplasmic GFP. Further insight would be gained about whether the cylinder preferentially quenches nuclear or cytoplasmic GFP by testing this over a time course.

Work arising from chapter six has revealed the need for Hoechst quenching by iron cylinder to be repeated using an alternative *in vivo* model. Due to high background in the UV, zebrafish have been identified as unsuitable organisms for monitoring the quenching of this dye. An alternative dye in the red or green region of the spectrum would be better suited for use in zebrafish embryos. However the dye would first need to be identified and all the *in vitro* research carried out prior to experiments in the animal. Zebrafish can provide an interesting model to further investigate phenotypic changes occurring as a result of cylinder treatment at different embryonic stages. This can provide further details about the localization of the cylinder in specific tissues and organs.

It would be very interesting to study iron cylinder toxicity and its anticancer properties using mice as model organisms. The results would further support toxicity data obtained from the zebrafish research carried out in this thesis. A clear understanding of cylinder

concentrations that can be tolerated *in vivo* as well a sound understanding of its mechanism of action are essential to its potential for progression to the clinical trial stage.

In conclusion, progression to whole-body imaging using small animals is the next step to further the work across all chapters. In this thesis, biological and imaging studies have been carried out on the supramolecular helicate (iron cylinder) and indirect methods to image this non-fluorescent compound have been developed. The cylinder's effects on the nuclear stain, Hoechst, the enzyme luciferase and the green fluorescent protein have allowed this to be achieved. The iron cylinder's activities on luciferase and GFP can be used as a way to visualize its location as well as monitoring and visualizing the tumour *in vivo*. This work has concluded that bioluminescent and fluorescent imaging can provide sensitive and quantifiable data for the rapid evaluation of cylinder efficacy.

This thesis has also pioneered the first *in vivo* research relating to the iron cylinder. Using zebrafish embryos as model organisms, the toxicity of the cylinder in relation to the classic anticancer drug, cisplatin has been investigated and results show promising novel evidence for its use in clinic in the near future. Development of a fluorescent version of the iron cylinder would provide a much enhanced imaging tool. However, its synthesis may pose challenges which highlight the need to develop methods to indirectly image the cylinder such as those developed in this thesis.

7.1 References

[1] Moldrheim, E., Hannon, M. J., Meistermann, I., Rodger, A., Sletten, E. (2002) Interaction between a DNA oligonucleotide and a dinuclear iron(II) supramolecular cylinder; an NMR and molecular dynamics study. *J. Biol. Inorg. Chem*. 7 (7-8): 770-780.

[2] Hannon, M. J. (2007) Metal-based anticancer drugs: From a past anchored in platinum chemistry to a post-genomic future of diverse chemistry and biology. *Pure Appl Chem.* 79 (12): 2243-61.

[3] Hotze, A. C., Hodges, N. J., Hayden, R. E., Sanchez-Cano, C., Paines, C., Male, N., Tse, M. K., Bunce, C. M., Chipman, J. K. Hannon M. J. (2008) Supramolecular iron cylinder with unprecedented DNA binding is a potent cytostatic and apoptotic agent without exhibiting genotoxicity. *Chem Biol*. 15 (12): 1258-1267.

[4] Koberle, B., Tomicic, M. T., Usanova, S., Kaina, B. (2010) Cisplatin resistance: preclinical findings and clinical implications. *Biochim Biophys Acta* 1806 (2): 172-182.

[5] Siddik, Z. H. (2003) Cisplatin: mode of cytotoxic action and molecular basis of resistance. *Oncogene*. 22 (47): 7265-7279.

[6] Schonn, I., Hennesen, J., Dartsch, D. C. (2010) Cellular responses to etoposide: cell death despite cell cycle arrest and repair of DNA damage. *Apoptosis*. 15 (2): 162-172.

[7] Hannon, M. J. (2007) Metal-based anticancer drugs: From a past anchored in platinum chemistry to a post-genomic future of diverse chemistry and biology. *Pure Appl Chem.* 79 (12): 2243-61.

[8] Meistermann, I., Moreno, V., Prieto, M. J., Moldrheim, E., Sletten, E., Khalid, S., Rodger, P. M., Peberdy, J. C., Isaac, C. J., Rodger, A., Hannon, M. J. (2002) Intramolecular DNA coiling mediated by metallo-supramolecular cylinders: differential binding of P and M helical enantiomers. *Proc. Natl. Acad. Sci*. 99 (8): 5069-5074.

[9] Begg, E. J., Barclay, M. L., Kirkpatrick, C. M. J. (2001) The therapeutic monitoring of antimicrobial agents. *Br. J. Clin. Pharmacol.* 52 (1): 35-43.